WHITE DWARFS

Thesis by

Henry Longfellow Shipman

In Partial Fulfillment of the Requirements

for the Degree of

Doctor of Philosophy

California Institute of Technology

Pasadena, California

1971

(Submitted May 17,1971)

ACKNOWLEDGEMENTS

Thanks to my thesis advisor, Dr. J. B. Oke, for teaching me how to observe astronomical objects and advice on all aspects of this thesis. Special thanks to him for the observing program which formed the basis of this work.

Thanks to Dr. Jesse Greenstein, who as father-confessor and teacher has gone far beyond the call of duty in helping me.

Thanks to Drs. Peter Goldreich and Jim Gunn for discussions on magnetic white dwarfs.

Thanks to the astrometrists of the world for doing their thing, which I never appreciated until I did this thesis.

Thanks to Gary Tuton and Jim Dittman for stimulating conversations.

Thanks to Peter Foukal for being at Caltech.
Thanks to Ward and Alice Davidson for numerous invitations to Tucson.

Thanks to Pierre Demarque for giving me a job.

Thanks to the taxpayers of America, who, through the National Science Foundation, have given me financial support.

PREFACE

Portions of this thesis have appeared or will shortly appear in print elsewhere, to wit:

The more reliable model atmospheres in Chapter 2 (e.g., the hydrogen-rich models with $T_{eff} \geq 12{,}000^{\circ}K$) will appear, along with some other models, in the June 15,1971 issue of the Astrophysical Journal.

Chapter 7 will appear in its entirety in the July 1,1971 issue of the Astrophysical Journal.

Preliminary results on the masses and radii of a few white dwarfs were presented in a paper by J.B. Oke and the present author, which was read at the I.A.U. Symposium on White Dwarfs, August, 1970, by Jesse L. Greenstein.

ABSTRACT OF THESIS

The aim of this thesis is to use model-atmosphere techniques and intermediate-band photoelectric scans to determine the properties of white dwarfs. Model atmospheres have been calculated with $6{,}000^{\circ} \leq T_{eff} \leq 50{,}000^{\circ}$ for solar composition, and $6{,}000^{\circ} \leq T_{eff} \leq 22{,}000^{\circ}$ for helium-rich (Y=1) models. Photoelectric scans of some 37 white dwarfs are the observational basis of the thesis.

The essential results for the program stars are that the DA stars have a mean radius of .013 $R_{\odot}$. With one or two exceptions, the program stars are on the upper sequence of the white dwarfs. The median mass is 0.58 $M_{\odot}$. One of the DA,F stars in the program, L 870-2, has a radius of .04 $R_{\odot}$. The DA stars cover a wide range of effective temperature; the DB stars, with the exception of HZ 29, have $12{,}000^{\circ} \leq T_{eff} \leq 18{,}000^{\circ}$K. The DA stars contain very little helium ($\sim$ 0.8% by number); and the DB stars contain very little metals. It is possible to interpret the spectrum of the one DC star in the program (L 1363-3) as a cooled-off DB star, since the helium lines fade out at $T_{eff}=11{,}000^{\circ}$.

The spectrum of Sirius B is analyzed; the hydrogen line profiles, combined with the mass of 1.02 $M_{\odot}$ (van den Bos 1960) and the visual magnitude of 8.29 (Lindenblad 1970) yield an effective temperature of $32{,}000^{\circ}$K and a surface gravity of 8.65, corresponding to a radius

of 0.0078 $R_\odot$. These values are consistent with the measured gravitational redshift of +88 km/sec.

Using the program stars, I then define a U-V versus T_{eff} relation for DA stars and for the DB and DC stars. Using this relation, and the m_1-indices as measured by Graham (1969), I compute masses and radii for a much larger sample of white dwarfs than the program stars - those with known distances. The median radius of these stars, which include quite a few on the lower sequence, is 0.0095 $R_\odot$. Using these data, I find that the atmospherically derived masses of white dwarfs are in reasonable agreement with the mass-radius relation for degenerate stars and with the gravitational redshifts measured by Greenstein and Trimble (1967).

The effective temperatures of all the stars in the lists of Eggen and Greenstein were computed for the purpose of testing the convection-accretion theory of Strittmatter and Wickramasinghe (1971) which purports to account for the formation of DB stars. The results here contradict their prediction that there should be a shortage of DA stars with $15{,}000^\circ \leq T_{eff} \leq 18{,}000^\circ$K. I propose a modification of their theory which explains the existence of both the DA and the DB stars in the temperature ranges in which they are observed. This modification also explains the DC stars, and suggests a possible explanation for the 4670 stars.

The wavelength dependence of the circular polarization of Grw+70°8247 for $3000 < \lambda < 8000$ Å is explained in the context of radiative transfer theory.

TABLE OF CONTENTS

CHAPTER I

INTRODUCTION

White dwarfs are luminous objects of stellar masses and planetary dimensions. Current theory indicates that they are the end products of stellar evolution, and they are therefore of considerable interest in interpreting stellar-evolution theory. They are also of interest because of their relevance to the theory of degenerate matter - in fact, the explanation of white dwarfs as bodies supported by the degeneracy pressure of a Fermi gas by Fowler (1926) was an early achievement of Fermi-Dirac statistics. The discovery of pulsars in 1967 raised several problems about the interpretation of late stages of stellar evolution. This discovery added to the interest in the evolution of white dwarfs, since, unlike neutron stars, it is possible to derive a fair amount of information about them from optical observations.

Several reviews on the subject of white dwarfs have appeared in recent years (Weidemann, 1958; Greenstein 1958, 1960). This chapter will therefore consist of a very brief overview of the problem, including a discussion of some of the more recent discoveries. The chapter ends with a general discussion of the approach and content of the thesis.

The spectra of white dwarfs have been examined mainly by Greenstein (Eggen and Greenstein 1965a,1965b,

Maanen 2); these stars are classified DF (Ca II), DG (Fe I, Ca II), or DM (Ca II, weak Ca I). There is one star (Grw+70°8247) in which the main feature of the spectrum is an unidentified broad line (or band) at 4135 Å; subsequent investigation has shown that this star also shows He I lines. The light from Grw+70°8247 is circularly polarized; more will be said about this later (Chapter 7).

The luminosities of the hydrogen-rich stars (hereafter simply called DA) are fairly well determined in about 30 cases, either from trigonometric parallaxes or from cluster membership. Unfortunately only one unreliable trigonometric parallax exists for a DB star (L930-80), although it is possible to estimate the luminosity of two other DB stars from their membership in binary systems. Although the astrometric data are not as extensive as one would wish, there are indications that more parallaxes will become available in the near future.

The existing data suggest that the white dwarfs form two sequences, as was first suggested by Parenago (1946) and later by Greenstein (cf. EG I). The reality of these two sequences has been disputed by Weidemann (1968), who has used a theoretical mass-radius relation combined with equivalent widths from EG to derive effective temperatures and luminosities. It is my belief

(cf. Eggen 1969) that the two sequences really exist, as Weidemann's method for determining masses and radii uses uncertain data (the equivalent widths of EG are sometimes based only on 180 Å/mm plates from the nebular spectrograph at Palomar and are quite uncertain). Consequently Weidemann's luminosity-radius diagram is complicated by a lot of noise which tends to obscure the two sequences.

The masses of white dwarfs are not at all well known. Three white dwarfs (40 Eri B, Sirius B, and Procyon B) are members of binary systems and the masses have been astrometrically determined to be 0.43 $M_\odot$, 1.03 $M_\odot$, and 0.63 $M_\odot$, respectively. Unfortunately, from the point of view of spectroscopy, only one of these three stars is easily observable - observation of Procyon B is impossible because of the proximity of the first-magnitude A component, and observation of Sirius B is extremely difficult. Thus the use of these known masses to test the accuracy of model-atmosphere techniques is only possible in the case of 40 Eri B, although a spectrum of Sirius B has been obtained by Oke and Greenstein and will be analyzed in Chapter 5. Weidemann (1963) and Terashita and Matsushima (1969) have attempted to calculate masses from model-atmosphere techniques, but they have been hampered by the difficulties of relating model-atmosphere energy distributions to UBV colors. One of the main aims of this thesis is to calculate masses from intermediate-band spectrum

scans.

Masses have also been derived by Greenstein and Trimble (1967) from measurements of the gravitational redshift of white dwarfs. Unfortunately these measurements are extremely difficult to make, as one is looking for a shift of about an Ångstrom in a line which has a halfwidth of 40-50 Ångstroms or more. Furthermore, one needs to know the radius of the star as the redshift is proportional to M/R. This extremely difficult job has been done for a fair number of stars, and Greenstein and Trimble derive a median mass of 0.73-0.98 $M_\odot$, depending on which temperature scale is adopted.

Theoretical work on the structure and evolution of white dwarfs has been summarized by Mestel (1965). If one assumes that the pressure of the Fermi gas in the interior of a white dwarf is independent of the temperature, one can calculate a unique model for each value of the central density. This was first done by Chandresekhar (1939) and subsequently by Hamada and Salpeter (1961) using a modified equation of state in which ion-electron interactions were included. However, Hubbard and Wagner (1970) have shown that the inclusion of temperature-dependent terms arising from Coulomb interactions at a finite temperature modifies the zero-temperature results appreciably. The zero-temperature calculations lead to a unique mass-radius relation in which a star of a given mass and chemical composition has a unique radius;

the finite-temperature calculations modify this mass-radius relation by an amount that depends on the luminosity of the star. These modifications are considerable if the star has a small mass and an extensive hydrogen envelope.

It has long been thought that white dwarfs evolve by cooling along lines of constant radius (cf. Schwarzschild 1958, pp. 240-244). The star radiates its thermal energy, which is principally locked up in the ions, while its structure is determined by the degeneracy pressure of the electrons. If one assumes that the heat capacity of the non-degenerate ion gas is constant, the rate at which a star moves along a line of constant radius in the H-R diagram will only be a function of its luminosity.

It has been realized fairly recently (Mestel and Ruderman 1967, van Horn 1968) that the interior of a white dwarf will crystallize at some point during the white dwarf stage of evolution. The time-scale of a star's evolutionary path will depend greatly on the nature of the phase change that takes place. Van Horn assumes that this phase change is a first-order phase change, in which latent heat is given off during the crystallization process. A white dwarf undergoing a first-order phase change in its interior will remain at the same point in the H-R diagram for an appreciable time since its luminosity, which is determined by the internal temperature through its influence

on the opacity of the outer envelope, will not change. Van Horn claims that this phenomenon is able to explain the existence of the two sequences in the H-R diagram as two crystallization sequences corresponding to internal compositions of elements heavier than S^{32} (for the upper sequence) and elements such as C^{12} (for the lower sequence). Mestel and Ruderman, however, assume that crystallization is a second-order phase change with no release of latent heat, and consequently they do not predict the existence of two crystallization sequences. There is no way, a priori, to decide between the two theoretical pictures; observations are needed.

The origin of the white dwarf is an unanswered question. Clearly they represent the end products of stellar evolution, but one still has to ascertain what kinds of stars will become white dwarfs, as opposed to becoming neutron stars or black holes. It is clear that mass loss must take place - the existence of Sirius B, with a mass of 1 $M_\odot$, in a binary system with a main sequence star of mass 2.31 $M_\odot$, as well as the existence of white dwarfs in the Hyades, where the mass of stars at the main sequence turnoff is approximately 2 $M_\odot$, is a persuasive argument for the existence of mass loss (Jones 1970).

An attractive idea is to suppose that white dwarfs originated from planetary nebulae, since the emission of the nebular shell involves a considerable quantity of

mass loss. However, Weidemann (1968) contends that the planetary nuclei cannot have substantial hydrogen shells, and he thus contends that the DA stars cannot have originated as planetary nuclei. Another possible mechanism for mass loss is mass exchange in close binaries, which has been invoked as an explanation for the existence of stars lying magnitudes above the horizontal branch in globular clusters by Strom and Strom (1970). The possible importance of noncatastrophic mass loss must also be considered.

One further problem in white dwarf evolution is the explanation of the existence of both hydrogen-rich and hydrogen-poor white dwarfs at approximately the same temperature. This may be related to events in the pre-white dwarf evolutionary phase of the star, or may be soley a function of the properties of the white dwarf phase itself. Strittmatter and Wickramasinghe (1971) have attempted to relate this phenomenon to the presence of convection zones in the outer layers of white dwarfs, which would mix the surface material with the material of the interior. I will show in Chapter 6 that a suitable modification and extension of the Strittmatter and Wichramasinghe mechanism can account for the existence of DA, DB, DC, and λ4670 stars in the appropriate temperature ranges.

One of the most interesting developements in the white dwarf field has been the discovery of two unusual

phenomena: light variability and circular polarization. Four white dwarfs (out of 29 which have been looked at) are known to be variable (Ross 548, G 44-32, HZ 29, and HL Tau 76; cf. Lasker and Hesser 1971 and earlier references cited therein, although HZ 29 may not be a white dwarf). The periods in all four cases are on the order of several hundreds of seconds. These variations have not been adequately explained as yet; although Vila (1971) has contended that adiabatic pulsations driven by deuterium burning may be the source of the pulsations of HL Tau 76, he does not provide a convincing place in any evolutionary scheme for his model of a low-mass, subluminous condensed hot star which has not gone through a normal main-sequence phase (in which all the deuterium would be used up).

The recognition of pulsars as rotating neutron stars with magnetic fields of 10^{12} gauss stimulated a search for magnetic fields of the order of 10^{7} gauss in white dwarfs. Preston (1970) tried to look for such magnetic fields in DA stars by looking for a Zeeman shift in the hydrogen lines, and found no visible fields. However, Kemp et. al. (1970) found circularly polarized light coming from the peculiar white dwarf GRW+70°8247, which he explains as arising from a magnetic field of 10^{7} gauss. The wavelength dependence of this polarization will be explained in Chapter 7. At the time of this writing, three such

white dwarfs have been found (the others are G195-19, and G99-37), and in one of them (G99-37) the polarization has been found to be variable with a period of about I I/2 days.

The model atmospheres used as the basis of this thesis are presented in Chapter 2. The observations are given in Chapter 3. In Chapter 4 the effective temperatures, surface gravities, and (in some cases) radii and masses of the program stars are derived, and in Chapter 6 the significance of these results are discussed in terms of the broader questions pertaining to the structure and evolution of white dwarfs. In Chapter 5, I discuss the case of Sirius B, and in Chapter 7 the wavelength dependence of the circular and linear polarization of GRW+70°8247 explained by means of radiative transfer theory.

CHAPTER 2

MODEL ATMOSPHERES FOR WHITE DWARFS

In this chapter I discuss the physical theory underlying models for white dwarf-type stars. The models themselves are then presented, and comparisons with the results of other workers are made. The temperature range covered by the hydrogen-rich models is $6{,}000 \leq T_{eff} \leq 50{,}000^{\circ}K$ and by the helium-rich models is $6{,}000 \leq T_{eff} \leq 22{,}000^{\circ}K$.

General Assumptions

Model atmospheres for the white-dwarf temperature-density range present a few problems not encountered in main sequence stars. Hydrogen convection zones exist at higher effective temperatures in white dwarfs than in main sequence stars because of the changed ionization equilibrium of hydrogen. Pressure ionization becomes important. For the helium-rich models for DB stars, the main source of opacity is He^-, an opacity source whose properties are uncertain.

The computer program used for these calculations is the program ATLAS, written by R. Kurucz of the Harvard College and Smithsonian Observatories. (For a description see Kurucz 1969a,b .) Opacity sources included in all models were H,He,C, N, O, Ne, Mg, Si in appropriate stages of ionization; He^-, H^-, electron and Rayleigh

scattering. The He^- opacity subroutine was that of Gingerich et. al.(1966); all others are described by Kurucz (1969b). Hydrogen line blanketing was included in all of the DA models with $T_{eff} \leq 25{,}000^{\circ}K$; its effects are unimportant at higher temperatures. The effect of helium line blanketing are not terribly important for the DB models, as was confirmed by numerical experiment using the broadening theories described in section 4 and with a hydrogen-like broadening theory for the helium lines with no known broadening theory. Helium line blanketing was therefore neglected. The models are all in local thermodynamic equilibrium.

Pressure ionization was taken into account with a Debye-shielding approach:

$$\Delta E = \frac{e^2}{\lambda_D} \; ; \; \lambda_D = \left[\frac{kT}{4\pi (n_i + n_e)} \right]^{1/2} \qquad (2\text{-}1)$$

where ΔE is the change in ionization potential, λ_D the Debye length, and the other symbols have their usual meaning. At $T=20{,}000^{0}$, equation (2-1) corresponds to

$$6 \log n = 21.64 - \log n_e \qquad (2\text{-}2)$$

where n is the quantum number of the highest bound state. the constant in equation (2-2) agrees with the values given by Kolesov (1964) and Schatzman (1958).

II. CONVECTION

Energy transport by convection was taken into account

only for the DB models. While the hydrogen-rich models with $T_{eff} \leq 12{,}000^{\circ}K$ are convectively unstable, in view of the uncertainty in fitting models to observations (see Chapter 4) convection was ignored for the sake of computational simplification. In this temperature range, the uncertainty in choosing an appropriate model for a particular star overshadows the errors due to the neglect of convection. All of the DB models calculated here with $T_{eff} \geq 14{,}000^{\circ}K$ were convectively unstable, and convective energy transport was included. At $T_{eff} \leq 10{,}000^{\circ}K$ the top of the convection zone is below $\tau=3$, and consequently, convection was neglected.

An adequate treatment of convection in the DB models is made somewhat difficult because of the peculiar nature of helium absorption. In the classical formulation of the mixing-length theory, one assumes that the mixing length is small compared to other lengths of interest in the atmosphere. In a helium-rich atmosphere where convection typically sets in at about $\tau=0.1$, however, the onset of convection coincides with the onset of bound-free absorption from He I. Consequently the transition from $\tau=0.1$ to $\tau=100$ corresponds to a very small increase in geometrical height in the atmosphere, because the atmosphere has suddenly become much more opaque. One cannot assume, as one does in the classical mixing-length theory, that a blob of material which starts to rise from, say, $\tau=1$, will keep rising for a

distance equal to one mixing length, for it will stop rising after it has reached the top of the convective zone, which is, in general, less than one mixing length away from $\tau=1$. One therefore has an effective mixing length of approximately 0.3 times the pressure scale height. Since the convective flux is proportional to the square of the mixing length, the flux is different by a factor of 9 from an atmosphere in which a mixing-length/scale height ratio of 1 is assumed.

Because of the above difficulties, I have revised the treatment of convection in ATLAS to follow explicitly the motion of a blob as it travels through the convective layer. This treatment is similar to that of Böhm and Stückl (1967), except that the integrals of Equns. 2-3,2-4, and 2-5 are carried out explicitly here. The flux carried by a blob of unit volume moving from h_1 to h_2 is (cf. Schwarzschild 1958, pp. 44-50)

$$H(h_1,h_2)=\left[T(h_1)-T(h_2)-\int_{h_1}^{h_2}\left(\frac{dT}{dx}\right)_{ad}dx\right]c_p(h_2)\rho(h_2)v(h_1,h_2) \qquad (2\text{-}3)$$

where $(dT/dx)_{ad}$ is the adiabatic temperature gradient, c_p the heat capacity, ρ the density, and v the convective velocity defined by

$$v(h_1,h_2)=\int_{h_1}^{h_2}(-g)\left[\rho(x)-\left(\frac{P(h_1)}{P(x)}\right)^{1/\Gamma_1}\rho(h_1)\right]dx \qquad (2\text{-}4)$$

where g is the acceleration of gravity, P the pressure, and Γ_1 the first adiabatic index of Chandresekhar(1939).

One then obtains the total convective flux at depth h_2 by averaging over depth:

$$H_{tot}(h_2) = \frac{\int H(h_1, h_2)\, dh_1}{\int dh_1} \qquad (2\text{-}5)$$

where the integrals are carried out over all depths h_1 from which blobs can move to h_2. In the calculations, I assumed that the blobs would move no farther than one pressure scale height. I also extended the atmosphere calculations deep enough into the star so that the deepest point was at least one mixing length from $\tau = 1$. This procedure ensured that the representation of the convective flux at $\tau = 1$ was not affected by any artificial cutoff in the integration of equations (2-4) and (2-5).

The calculation of the convective flux by equation (2-5) is still quite approximate, for numerous complications have been ignored. Viscous forces, which would decrease the convective efficiency, have been ignored; the high convective velocities (about 10^6 cm/sec) lead to problems with convective overshoot, which has been neglected. These velocities are just below the velocity of sound; the problems and possibilities of supersonic convection need to be considered. A most serious complication is that the convective flux calculated by Eq. (2-5) carries a very sizeable fraction (60-70%) of the total flux, even above $\tau = 1$. I have assumed, in following the classical mixing-length theory, that blobs rise adiabatically during convection; in fact, a blob moving at $\tau = 1$ will lose a considerable

amount of energy radiatively. Its path in the pressure-density diagram as it rises or falls may be quite nonadiabatic. Such radiative cooling would markedly decrease the convective efficiency.

These considerations would, in general, reduce the convective efficiency and cause the real star to be more like a radiative model. If the convective efficiency were zero and the star were completely radiative, the effective temperatures derived from the models at the end of this chapter would be too high by 1,000° to 2,000°, according to the calculations of Wickramasinghe and Strittmatter (1971). This change is comparable to the observational uncertainties. Nevertheless, these defeciencies in the theory of convection emphasize the tentative nature of the models for the DB stars presented here. More work needs to be done on the theory of convection before better models can be obtained.

III. FLUX CONSTANCY

In the hydrogen-rich models, flux constancy of a few tenths of one percent was acheived at all optical depths. For the DB models, convergence was extremely difficult to obtain, and iteration was terminated when flux constancy of a few percent was obtained. Flux errors considerably greater than this were tolerated in two places : at the top of the convective layer, where

the computation of the total flux was extremely sensitive to very small changes in temperature, and at the bottom of the atmosphere ($\tau \sim 10^3$). Because of the considerable uncertainties in DB models (the convective flux is not known to an accuracy of 30%, at least, and the value of the He^- absorption coefficient, which is the main component of the opacity, is uncertain to about 15%) it was felt that better flux constancy would be meaningless. Flux constancy of a few tenths of a per cent from one layer to the next is irrelevant when the present state of the art produces uncertainties in all the fluxes of 20-30%. In the cooler ($T_{eff} \leq 10{,}000^\circ K$) hydrogen-poor models, a further uncertainty is the possible influence of molecular absorption in the infrared - an unknown quantity which is responsible for many frustrations in calculating models for main sequence M stars. Consequently the DB models should be regarded as provisional.

These uncertainties do not apply to the DA models, in which the absorption coefficient (due to hydrogen) is extremely well known, and the abundance of other possible atmospheric constituents is irrelevant. In the DA models, flux constancy of a few tenths of a per cent (the usual model atmosphere criterion) was obtained without too much difficulty.

IV. LINE BROADENING

The hydrogen line broadening theory used in the calculations was that of Griem (1964), which, according

to D. Peterson (private communication) is the most accurate theory for main-sequence B stars. At white dwarf densities, the difference between the Griem theory and the Edmonds, Schluter, and Wells (1967) semi-empirical broadening theory is negligible, as densities in a white dwarf atmosphere are fairly close to densities in the laboratory. For He I λ4471 the broadening theory of Barnard, Cooper, and Shamey (1969) was used, and for He I λ4388 the theory of Shamey (private communication) was supplemented by that of Gieske and Griem (1969) for low electron densities.

V. THE MODELS

The set of models divides itself, like Gaul, into three parts. The DA models cover $6{,}000^{\circ} \leq T_{eff} \leq 25{,}000^{\circ}$, with log g=7 and 8; all these models are hydrogen-line blanketed and convection was neglected. The high temperature DO and sdO models have $30{,}000^{\circ} \leq T_{eff} \leq 50{,}000^{\circ}$, with log g=6 and 8; neither hydrogen line blanketing nor convection is important here, The DB models have $6{,}000^{\circ} \leq T_{eff} \leq 22{,}000^{\circ}$ with log g=8 and $T_{eff}=14{,}000^{\circ}$ and $17{,}000^{\circ}$ for log g=7. Two sets of DB models were computed--one having a metals/He ratio of 1/10 that of the sun and one having no metals at all, except for $T_{eff} \leq 10{,}000^{\circ}$, where the no metal models were omitted. The metal abundance is unimportant in determining the structure of DA stars, since hydrogen is the primary source of both opacity and electrons, but in DB stars the metal abundance

is quite important, since the metals are an important source of both opacity and electrons.

The emergent fluxes H_ν for the models are given in Tables 1-6, normalized so that $\int H_\nu d\nu = \sigma T_e^4/(4\pi \times 10^4)$. The notation under "model" corresponds to [$T_{eff}/10^2$, log g; metals/GMA, N(He)/(N(He)+N(H))], where GMA refers to the solar abundances determined by Goldberg, Müller, and Aller (1960). The ratio metals/GMA is given in terms of metals/total number of atoms. Hγ profiles, equivalent widths, and the parameter D(0.2) (the full width of the line profile where the line depth = 0.2) are presented in Tables 7-10. In all the models the residual intensity was set to 1.0 at $\Delta\lambda$ =100 Å; while this procedure cuts off part of the line for the DA models, a consistent definition of "continuum" was obtained. When the scanner observations were analyzed, model flux and stellar flux were treated in a self-consistent way (see Chapter 4). Helium line profiles and equivalent widths are presented in Tables 11-13; the residual intensity was set equal to 1.0 at $\Delta\lambda$=50 Å for the high-temperature models, $\Delta\lambda$=110 Å for the DA models, and $\Delta\lambda$ =150 Å in the DB models.

VI. DISCUSSION

Models for DA stars for $T_{eff} \geq 12{,}000^\circ$K have been computed previously by Terashita and Matsushima (1966, 1969; Matsushima and Terashita 1969a,1969b) and by Strittmatter and Wickramasinghe (1971). The hydrogen lines lines computed by Terashita and Matsushima (hereafter

referred to as TM) are weaker than those presented here because TM did not take the effects of pressure ionization into account when solving the Saha equation for the electron density. As a result, their electron densities are too low by a factor of about 2 at $\tau_{5000}=1$. The hydrogen lines computed by Strittmatter and Wickramsinghe (SW) are somewhat stronger than those presented here, because in Table 2 the equivalent width integration has been artificially cut off at $\Delta\lambda=100$Å, and also because SW have used a higher helium abundance, thereby increasing the effects of Stark broadening. There is no appreciable difference in the emergent fluxes computed here and those of TM.

The DA models for $T_{eff} \geq 12{,}000^{\circ}$K present no surprising features - the Balmer discontinuity becomes smaller and the hydrogen lines get weaker in much the same way as in main sequence stars. However, in the cooler DA stars the absorption of radiation by H^- is much more important than in main sequence stars of the same temperature. In the $T_{eff}=10{,}000^{\circ}$, log g=4 model of Carbon, Gingerich and Kurucz (1969) (hereafter CGK), H^- is only 12% of the total opacity at $\lambda=4000$ Å and $\tau=1$, whereas in my $10{,}000^{\circ}$ log g=8 model, H^- contributes 50% of the total opacity at the same wavelength. At $T_{eff}=8{,}000^{\circ}$ the corresponding figures are 50% for the main sequence

model and 90% for the white dwarf model. The importance of H^- explains some of the peculiar features of the spectra of cool DA stars.

In the white dwarf models, the hydrogen lines weaken surprisingly fast as the effective temperature decreases, as is shown in Figure 1 where the equivalent width of $H\gamma$, $W(H\gamma)$, is plotted against the effective temperature for main sequence models (log g=4) and log g=8. The main sequence points were taken from CGK for $T_{eff} \leq 15{,}000^{o}K$ and for $T_{eff} \geq 15{,}000^{o}K$, the models of Peterson (Schild, Peterson, and Oke 1971; Peterson and Scholz, 1971; in some cases the hydrogen line strengths were calculated by the author.) What happens is that as the effective temperature decreases, the continuum absorption increases much faster in white dwarfs because of H^-. Thus the ratio of line absorption to continuum absorption decreases, and the hydrogen line strengths weaken much faster than in main sequence stars. In some cases, (eg. at $T_{eff}=8{,}000^{o}K$), the continuum absorption coefficient increases faster than the line absorption coefficient with increasing gravity, and $H\gamma$ actually <u>weakens</u> as the gravity increases. Such a situation occurs when the line is sufficiently weak that doppler broadening is still somewhat important, so that the line absorption coefficient increases slower than n_e^{1}, while the continuum absorption coefficient varies as n_e^{1} (as is the case for H^-.) The rapid weakening of the hydrogen lines explains the observed abrupt decrease

in W($H\gamma$) for U-V -0.2 (cf. Greenstein 1960.)

The high-temperature DO and sdO models do not seem to contain any surprising results-again the hydrogen lines weaken in more or less the usual way. It is noteworthy that the hydrogen lines persist for temperatures as hot as 50,000°; in fact an extrapolation of the 50,000° temperature distribution indicated that hydrogen lines would still be visible at T_{eff}=100,000°, although a more accurate model atmosphere might indicate otherwise.

The DB models have previously been calculated by Bues (1969,1970) and SW (1971). Bues' models did not include the effects of convection, and consequently the temperatures of her models at points within the convective zone are too high. As a result, the equivalent widths she computes are higher than those presented here. SW included convection, but used the classical mixing-length theory without the modifications described above. A precise comparison of models is difficult because of the difference in metal abundance between the SW models and mine, but the equivalent widths computed by both of us seem to be in fairly good agreemant.

The one major difference between the results of SW and the results here is that SW predict the appearance of a forbidden component of He I λ4471 at λ=4517 Å. This line corresponds to the 2^3P-4^3P transition, and has been predicted by Griem (1968), whose broadening theory

was used by SW. The theory of Barnard, Cooper, and Shamey (1969) , which was used for my λ4471 calculations, does not predict the existence of a forbidden component at 4517 Å; they claim (Cooper, private communication) that this transition is unlikely to be of importance in astrophysical situations. Until the existence of this forbidden component is confirmed by observation, it would seem best to ignore it in theoretical calculations as I have done.

There is a great difference between the metal-rich and zero-metal DB models. The metals are an extremely important source of opacity in the ultraviolet, and in the cooler models they are an important source of electrons, since helium, with its ionization potential of 24.51 eV, is so hard to ionize. Consequently the He^- absorption is increased in the metal rich models, since there are more electrons and more He^- is formed. As a result, the metal-rich models have a steeper temperature gradient. One would thus expect that a metal-rich model would look hotter than a zero-metal model with the same effective temperature, and this is indeed the case. An additional reason that the metal-rich models have a somewhat (about 20%) higher value for the absolute flux emitted in the visual region of the spectrum is that the absorption of radiation in the ultraviolet by ionized metals causes more radiation to emerge from the star in the visual

region of the spectrum.

Furthermore, the metal-rich models have stronger helium lines than the zero-metal models, as one would expect from the higher temperatures. The one exception occurs at $T_{eff}=22,000^{o}$, where He I $\lambda 4471$ is so strong and so heavily broadened by Stark broadening that the cutoff of the line at $\Delta\lambda=150$ Å cuts off a considerable part of the equivalent width and the line seems weaker in the metal-rich model. One further anomaly in the helium line strengths is that He I $\lambda 4471$ decreases in equivalent width as the gravity is increased from log g=7 to log g=8 in some cases; the reason is that the continuum absorption coefficient is increasing faster than the line absorption coefficient in the same way as in the $T_{eff}=8,000^{o}$ hydrogen-rich models.

VII. CONCLUSION

The model atmospheres for the DA stars presented in this chapter are probably quite reliable, since the relevant physics is fairly well known. The importance of H^{-} as an absorber in the cooler DA models explains the anomalous behavior of hydrogen line strengths which has been observed by Greenstein. The models presented in this chapter cover most of the temperature range in which white dwarfs with hydrogen lines in their spectra have been observed.

The models for the DB stars are considerably less reliable, because of the uncertain value of the He^{-}

absorption coefficient, the uncertainties in the theory of convection, and the uncertain value of the metal abundance. It will probably be some time before these problems are cleared up, and so these models will have to do as a first approximation for the analysis of the DB stars.

FIGURE CAPTION

Figure 1. The behavior of the equivalent width of Hγ versus effective temperature in main-sequence stars and white dwarfs. The source of the main-sequence points is explained in the text.

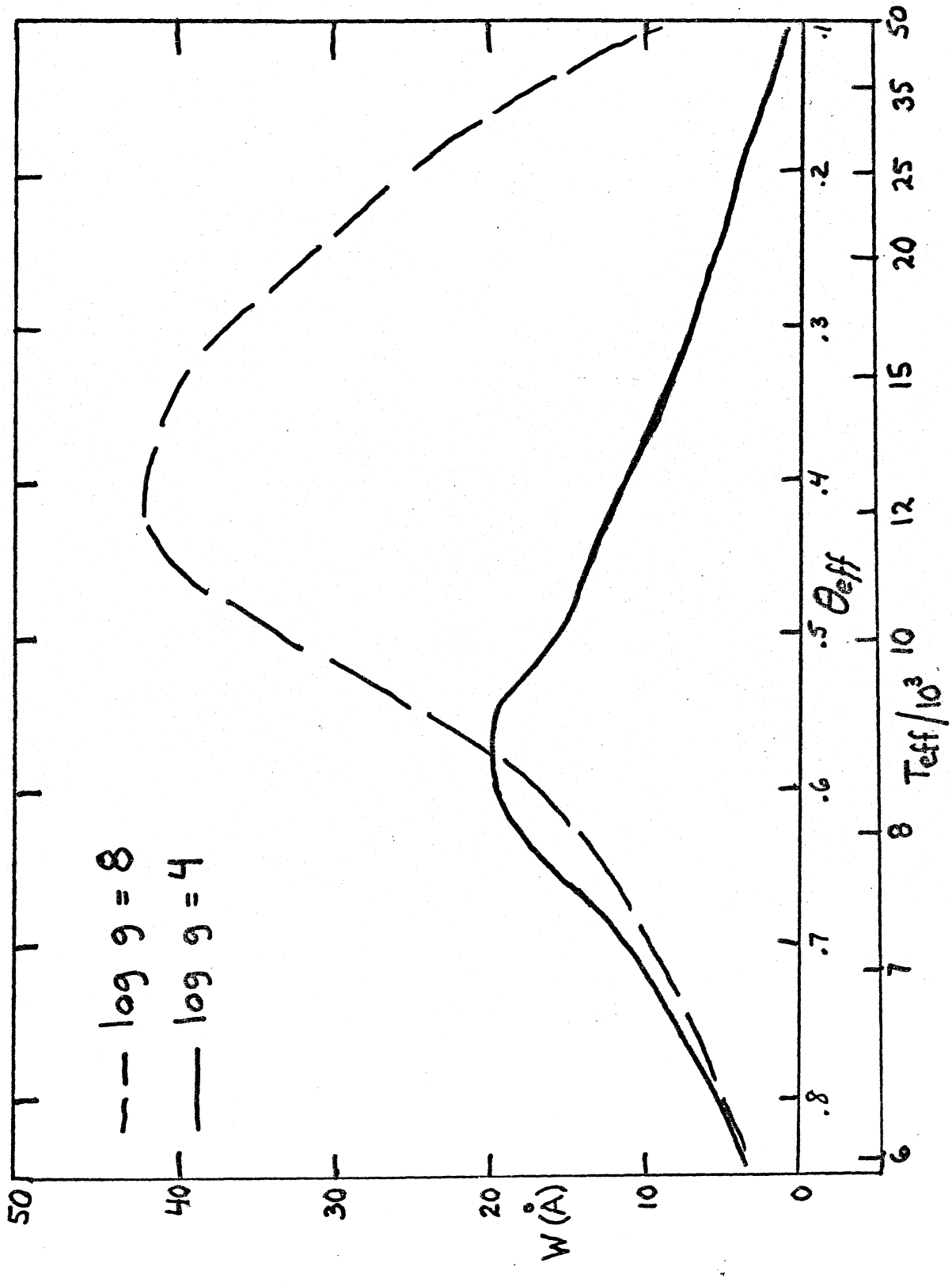
log g = 8
log g = 4
W (Å)
50
40
30
20
10
0
θeff
.8
.7
.6
.5
.4
.3
.2
.1
Teff/10³
6
7
8
10
12
15
20
25
35
50

TABLE 1- EMERGENT FLUXES FOR COOL DA MODELS

Model / λ(Å)	6, 7 1, 0.1	8, 7 1, 0.1	10, 7 1, 0.1	6, 8 1, 0.1	8, 8 1, 0.1	10, 8 1, 0.1
3122	.026	.104	.229	.026	.113	.268
3364	.030	.114	.239	.031	.123	.278
3647	.036	.125	.249	.036	.134	.287
4058	.045	.175	.422	.044	.164	.384
4102	.033	.072	.160	.037	.076	.165
4148	.047	.179	.431	.046	.168	.393
4219	.048	.187	.488	.047	.175	.445
4292	.049	.183	.434	.048	.172	.399
4340	.037	.081	.173	.039	.078	.175
4393	.051	.186	.438	.050	.175	.465
4521	.053	.194	.498	.052	.182	.459
4656	.055	.196	.488	.054	.184	.406
4800	.057	.193	.431	.056	.182	.330
4861	.048	.100	.197	.047	.094	.197
4927	.059	.195	.430	.058	.184	.443
5242	.064	.202	.460	.063	.191	.426
5600	.068	.203	.439	.067	.192	.407
6010	.072	.202	.415	.071	.192	.361
6485	.076	.198	.370	.075	.189	.314
6563	.069	.128	.220	.068	.124	.222
6646	.077	.198	.364	.076	.188	.359
7611	.082	.191	.337	.081	.184	.295
8206-	.083	.185	.312	.082	.178	.331
8206+	.083	.187	.342	.082	.179	.295
10504	.084	.162	.257	.083	.156	.212

TABLE 2- EMERGENT FLUXES FOR DA MODELS

MODEL / λ(Å)	12, 7 1, 0.1	16, 7 1, 0.1	20, 7 1, 0.1	25, 7 1, 0.1
3122	.43	1.11	2.07	3.66
3364	.44	1.07	1.94	3.36
3647-	.44	1.03	1.81	3.08
4058	.75	1.50	2.29	3.43
4102	.28	.64	1.09	1.86
4148	.76	1.50	2.26	3.36
4219	.88	1.60	2.35	3.43
4292	.76	1.45	2.17	3.21
4340	.29	.64	1.06	1.73
4393	.76	1.43	2.12	3.12
4521	.87	1.50	2.16	3.10
4656	.84	1.44	2.07	2.96
4800	.71	1.29	1.89	2.73
4861	.32	.64	1.01	1.58
4927	.71	1.26	1.83	2.63
5242	.75	1.23	1.74	2.45
5600	.68	1.13	1.57	2.20
6010	.64	1.02	1.41	1.96
6485	.54	.88	1.23	1.70
6563	.32	.55	.81	1.17
6646	.53	.86	1.18	1.63
7611	.47	.72	.97	1.31
8206-	.43	.64	.86	1.16
8206+	.49	.72	.93	1.22
10504	.33	.48	.61	.79

TABLE 3- EMERGENT FLUXES FOR DA MODELS

MODEL / λ(Å)	12, 8 1, 0.1	16, 8 1, 0.1	20, 8 1, 0.1	25, 8 1, 0.1
3122	.48	1.16	2.14	3.80
3364	.48	1.11	2.00	3.48
3647-	.48	1.06	1.86	3.17
4058	.64	1.30	2.06	3.20
4102	.28	.64	1.12	1.90
4148	.65	1.31	2.06	3.17
4219	.79	1.55	2.32	3.44
4292	.66	1.30	2.01	3.05
4340	.29	.62	1.05	1.72
4393	.66	1.29	1.98	2.99
4521	.83	1.52	2.19	3.17
4656	.81	1.46	2.10	3.02
4800	.65	1.20	1.80	2.67
4861	.31	.61	.97	1.51
4927	.64	1.18	1.76	2.58
5242	.74	1.26	1.78	2.51
5600	.69	1.15	1.60	2.25
6010	.64	1.04	1.43	2.00
6485	.52	.85	1.20	1.69
6563	.31	.53	.78	1.12
6646	.51	.83	1.16	1.63
7511	.48	.73	.98	1.34
8206-	.44	.65	.87	1.18
8206+	.49	.73	.95	1.25
10504	.34	.48	.62	.80

TABLE 4- EMERGENT FLUXES FOR DO MODELS

Model / λ (Å)	30, 6 0,0.01	37.5,6 0,0.01	50,6 0,0.01	30, 8 0,0.01	37.5,8 0,0.01	50, 8 0,0.01
3122	5.43	10.4	16.6	5.31	10.6	16.8
3265	5.12	9.68	15.4	5.00	9.35	15.6
3531	4.62	8.58	13.6	4.51	8.82	13.7
3647-	4.41	8.16	12.9	4.31	8.38	13.0
3647+	5.72	9.29	13.8	5.65	9.55	13.9
4037	4.85	7.83	11.5	4.79	8.03	11.6
4472	4.85	7.83	9.66	4.05	6.73	9.73
5011	3.40	5.40	7.88	3.35	5.52	7.93
5699	2.73	4.31	6.25	2.69	4.40	6.28
6726	2.06	3.20	4.61	2.03	3.26	4.61
8026-	1.45	2.23	3.20	1.43	2.27	3.21
8026+	1.52	2.28	3.23	1.50	2.32	3.24
10503	.97	1.43	2.03	.95	1.46	1.03

TABLE 5- EMERGENT FLUXES FOR DB MODELS

Model / λ (Å)	14, 7 0, 1	17, 7 0, 1	14, 8 0, 1	17, 8 0, 1	22, 8 0, 1	6, 8 1, 1
3122-	1.04	1.44	.96	1.57	2.71	.049
3122+	1.04	1.46	.96	1.59	2.76	.049
3265	1.04	1.43	.97	1.56	2.64	.052
3422-	1.03	1.40	.97	1.52	2.52	.054
3422+	1.10	1.71	1.00	1.73	3.19	.054
3530	1.10	1.67	1.00	1.69	3.08	.055
3680-	1.08	1.61	.99	1.64	2.94	.057
3680+	1.10	1.72	1.00	1.70	3.17	.057
4038	1.05	1.59	.97	1.57	2.85	.061
4472	.98	1.43	.93	1.43	2.50	.062
5011	.90	1.26	.86	1.27	2.14	.064
5699	.79	1.08	.78	1.10	1.77	.063
6726	.66	.88	.66	.89	1.37	.058
8206	.51	.67	.52	.68	1.00	.051
10504	.36	.46	.37	.46	.67	.042

TABLE 6- EMERGENT FLUXES FOR DB MODELS

MODEL / λ(Å)	10, 8 1, 1	14, 7 1, 1	17, 7 1, 1	14, 8 1, 1	17, 8 1, 1	22,8 1, 1
3122-	.40	1.20	1.83	1.24	1.89	3.12
3122+	.40	1.21	1.85	1.25	1.92	3.17
3265	.40	1.20	1.81	1.24	1.87	3.03
3422-	.41	1.18	1.77	1.22	1.81	2.93
3422+	.41	1.31	2.16	1.30	2.18	3.55
3530	.41	1.29	2.10	1.27	2.12	3.43
3680-	.41	1.26	2.03	1.25	2.04	3.28
3680+	.41	1.30	2.20	1.26	2.16	3.52
4038	.41	1.22	1.91	1.18	1.97	3.15
4472	.40	1.13	1.80	1.16	1.76	2.76
5011	.40	1.02	1.58	.99	1.54	2.36
5655	.38	.90	1.35	.87	1.31	1.96
6726	.34	.74	1.08	.72	1.05	1.52
8206	.28	.57	.82	.58	.79	1.12
10504	.21	.40	.55	.39	.54	.75

TABLE 7- Hγ PROFILES FOR COOL DA STARS

Model / Δλ(Å)	6. 7 1, 0.1	8, 7 1,0.1	10, 7 1,0.1	6, 8 1,0.1	8, 8 1,0.1	10, 8 1,0.1
0.0	385	335	289	401	355	317
1.0	698	413	353	713	427	387
3.0	862	562	412	862	579	445
5.0	918	654	459	917	673	487
10.0	968	779	557	966	796	582
20.0	990	885	697	990	897	719
30.0	996	932	788	996	941	804
40.0	998	958	851	998	964	861
50.0	999	973	896	999	977	903
60.0	1000	983	930	999	985	933
70.0	1000	989	955	1000	991	957
80.0	1000	994	974	1000	995	974
90.0	1000	997	989	1000	998	989
100.0	1000	1000	1000	1000	1000	1000
D(0.2)	3.9	22.0	63.4	3.7	20.6	62.6
W(Å)	3.23	15.36	33.54	3.04	14.10	31.53

TABLE 8- Hγ PROFILES FOR DA STARS

Model / Δλ (Å)	12, 7 1, 0.1	16, 7 1, 0.1	20, 7 1, 0.1	25, 7 1, 0.1
0.0	267	388	433	496
1.0	330	405	460	518
3.0	386	461	520	578
5.0	422	499	560	619
10.0	500	581	644	702
20.0	627	718	775	823
30.0	730	818	862	897
40.0	810	885	916	940
50.0	869	928	949	965
60.0	914	956	970	979
70.0	946	974	982	988
80.0	970	986	991	994
90.0	988	994	996	998
100.0	1000	1000	1000	1000
D(0.2)	77.4	55.6	45.0	35.5
W(Å)	39.5	28.9	23.5	18.9

TABLE 9 - Hγ PROFILES FOR DA STARS

Model / Δλ(Å)	12,8 1,0.1	16,8 1,0.1	20,8 1,0.1	25,8 1,0.1
0.0	274	373	419	467
1.0	353	399	456	506
3.0	412	445	501	550
5.0	444	475	532	584
10.0	511	537	596	650
14.0	621	641	700	751
20.0	711	730	784	828
30.0	783	804	849	885
40.0	841	862	897	924
50.0	887	907	933	952
60.0	925	941	959	971
70.0	955	967	977	984
90.0	980	986	990	993
100.0	1000	1000	1000	1000
D(0.2)	84.8	78.4	64.2	52.0
W(Å)	42.0	38.4	31.6	27.1

TABLE 10 - Hγ PROFILES FOR DO MODELS

Model / Δλ(Å)	30,6 0,.01	37½,6 0,.01	50,6 0,.01	30,8 0,.01	37½,8 0,.01	50,8 0,.01
0.0	516	710	809	510	705	812
1.0	583	731	827	563	733	840
3.0	672	782	858	604	743	844
5.0	729	826	887	640	761	853
10.0	828	901	938	707	806	879
14.0	880	936	961	749	838	898
20.0	929	965	980	800	877	924
30.0	968	985	992	866	924	954
40.0	984	993	996	912	954	973
50.0	991	996	998	944	972	984
60.0	995	998	999	965	983	991
70.0	997	999	999	979	990	995
90.0	999	1000	1000	995	998	999
100.0	1000	1000	1000	1000	1000	1000
D(0.2)	16.8	8.0	0	40.0	19.0	0
W(Å)	10.0	5.8	3.6	21.09	12.7	7.7

TABLE 11 - HELIUM LINE STRENGTHS (in milliangstroms)

Model	W(4471) He=0.1	W(4471) He=.03	Model	W(4471) He=0.01	W(4388) He=0.01
16,7,1,0.1	1774	897	30,6,0,0.01	992	229
20,7,1,0.1	5124	2906	37½,6,0,.01	499	89
25,7,1,0.1	7838	5345	50,6,0,0.01	146	17
16,8,1,0.1	909	475	30,8,0,0.01	1276	120
20,8,1,0.1	3368	1475	37½,8,0,.01	634	55
25,8,1,0.1	8367	4252	50,8,0,0.01	264	21

TABLE 12- HE I λ4471 PROFILES

Model / Δλ (Å)	14, 7 0, 1	17, 7 0, 1	14, 8 0, 1	17, 8 0, 1	22, 8 0, 1
-150	1000	1000	1000	1000	1000
-125	990	989	990	988	980
-85	986	981	987	979	950
-75	984	978	985	975	937
-60	981	967	983	966	920
-40	970	935	978	946	974
-20	948	869	964	890	780
-10	896	780	926	808	702
-5	821	693	867	720	650
0	506	420	493	480	608
5	842	713	885	745	662
10	908	795	937	830	720
20	950	879	966	906	807
30	968	933	976	944	871
40	974	950	978	954	891
60	978	966	980	962	910
80	981	979	981	976	947
100	982	987	982	984	973
150	1000	1000	1000	1000	1000
W(Å)	6.71	14.70	5.01	13.12	24.78

TABLE 13- HE I λ4471 PROFILES

Model / Δλ(Å)	10, 8 1, 1	14, 7 1, 1	17, 7 1, 1	14, 8 1, 1	17, 8 1, 1	22, 8 1, 1
-150	1000	1000	1000	1000	1000	1000
-125	999	990	991	988	982	990
-85	999	986	982	982	966	971
-75	999	984	978	980	950	957
-60	998	978	969	974	945	940
-40	994	967	950	960	914	905
-20	991	929	892	926	843	853
-10	987	856	764	865	765	794
-5	981	767	684	795	696	766
0	977	524	574	632	578	746
5	982	791	700	816	715	772
10	987	874	789	885	785	808
20	998	930	887	940	864	865
30	991	958	932	961	914	907
40	991	968	952	966	929	921
60	994	976	969	970	942	936
80	998	982	983	977	965	964
100	1000	984	991	980	979	983
150	1000	1000	1000	1000	1000	1000
W(Å)	1.08	9.16	15.33	8.82	18.11	17.84

CHAPTER 3-THE OBSERVATIONAL MATERIAL

Summary

The photoelectric observations which are analyzed in this thesis are presented in tables 1-6.

The bulk of the observations used in this thesis are multichannel observations by Oke. The multichannel spectrometer has been described by Oke (1969). With this instrument it is possible to observe almost any white dwarf with a spectral resolution of some tens of Angstroms, since it is possible to measure the flux in 18 wavelength regions simultaneously. The observing program included 36 white dwarfs of which 17 were of type DA, 2 of type DAwk (DA stars with weak lines), 3 of type DO and sDO, 6 of type DB, 2 of type DA,F; 2 of type DF, 1 of type DG, and 3 peculiar objects.

The scans from the original observing program covered the spectral range from about 3200 Å to about 10,000 Å. Below 5800Å the spectral resolution was generally 80Å, and above 5800Å it was 160Å. After this thesis began, Oke and Shipman obtained some higher resolution scans with the 200" multichannel spectrometer for stars of known distances; these scans covered (with some gaps) the spectral region from 3100Å to 7200 Å the resolution was 20Å in the blue region ($\lambda <$ 5800 Å)

and 40 Å for longer wavelengths. The resolution of the latter scans is adequate for the purpose of measuring hydrogen line profiles, whereas the lower-resolution scans can merely provide less accurate values of the equivalent widths. Line profiles for two of the stars in the program were measured one night at the Cassegrain scanner of the Mount Wilson 60" by Shipman. These measurements covered a very limited spectral range ($4190 \leq \lambda \leq 4550$Å) and were made solely for the purpose of measuring $H\gamma$ profiles.

The observations made by Oke for the observing program will be published along with the data at the end of this chapter in the Astrophysical Journal Supplements. Tabulated at the end of this chapter, in tables 1-6, are the stars which were observed by Oke and Shipman with the 200" multichannel as well as the stars observed at Mount Wilson. The standard deviations listed at the bottom of each table (or in some cases in Table 6) are based solely on counting statistics; the actual errors are somewhat larger. The energy distributions are presented as a list of magnitudes per unit frequency interval, AB ($AB=-2.5 \log F_\nu + \text{const.}$)

One comment should be made on the observations: there appears to be a diffuse feature located at $\lambda = 5030$Å and of halfwidth $W \sim 50$Å in many of the high-resolution scans(20Å). This feature is probably not real for the following reasons: (1) The apparent equivalent width of this feature is roughly constant from one star to another, and

(2) The feature generally shows up in one channel only. Observations at λλ 5010, 5030, 5050, and 5070 were made with channel 13, and observations at 5050, 5070, and longer wavelengths were made with channel 14 of the multichannel spectrometer. The feature did not appear in the observations made with channel 14, so I am inclined to believe that this feature is an instrumental artifact.

The other observations referred to in this thesis are in the literature; they are mainly in the papers of Greenstein and collaborators. The observations pertaining to Sirius B will be discussed separately (Chapter 5).

TABLE 1- MULTICHANNEL OBSERVATIONS

λ	HZ 4	+70° 5824	SA29 -130	HZ 7	HZ 2	LB 1240	LB 227
3210	14.66	12.63	13.56	13.77	13.68	14.09	15.17
3230	14.72	12.65	13.61	13.82	13.69	14.13	15.28
3250	14.73	12.70	13.74	13.84	13.75	14.11	15.30
3270	14.53	12.68	13.59	13.93	13.76	14.14	15.19
3290	14.63	12.71	13.68	13.89	13.75	14.12	15.38
3310	14.66	12.71	13.59	13.93	13.84	14.20	15.37
3330	14.66	12.78	13.70	13.97	13.79	14.18	15.27
3350	14.69	12.75	13.59	13.91	13.74	14.17	15.51
3370	14.68	12.76	13.54	13.97	13.85	14.25	15.28
3390	14.70	12.75	13.51	13.93	13.84	14.18	15.29
3410	14.74	12.78	13.67	13.98	13.88	14.19	15.37
3430	14.69	12.78	13.68	13.95	13.83	14.20	15.37
3450	14.63	12.80	13.60	13.93	13.79	14.20	15.29
3470	14.67	12.82	13.61	13.99	13.87	14.18	15.38
3490	14.74	12.81	13.64	13.96	13.82	14.22	15.39
3510	14.73	12.84	13.57	14.02	13.85	14.23	15.42
3530	14.65	12.85	13.52	14.00	13.88	14.23	15.35
3550	14.72	12.87	13.60	14.03	13.86	14.17	15.38
3570	14.79	12.83	13.70	13.99	13.85	14.16	15.36
3590	14.70	12.88	13.66	14.05	13.87	14.20	15.45
3610	14.64	12.87	13.63	14.03	13.85	14.22	15.36
3630	14.70	12.85	13.63	14.04	13.89	14.21	15.40
3650	14.76	12.85	13.68	14.03	13.91	14.20	15.39
3670	14.74	12.85	13.64	14.04	13.89	14.17	15.48
3690	14.74	12.89	13.61	14.02	13.94	14.19	15.50
3710	14.80	12.90	13.64	14.05	13.97	14.23	15.40
3730	14.84	12.94	13.73	14.11	13.95	14.23	15.37
3750	14.77	12.94	13.74	14.08	13.96	14.21	15.47
3770	14.80	12.99	13.68	14.15	13.98	14.28	15.47
3790	14.81	13.03	13.73	14.18	14.06	14.36	15.54
3810	14.83	13.01	13.79	14.19	14.02	14.28	15.52
3830	14.82	13.07	13.81	14.18	14.00	14.31	15.52
3850	14.76	13.00	13.62	14.11	14.01	14.22	15.51
3870	14.82	13.08	13.68	14.19	14.07	14.24	15.50
3890	14.97	13.12	13.96	14.26	14.14	14.42	15.65
3910	14.67	13.04	13.56	14.12	13.97	14.23	15.46
3930	14.62	12.83	13.40	14.05	13.84	14.14	15.34
3950	14.72	12.91	13.59	14.12	13.88	14.18	15.42
3970	14.94	13.04	13.80	14.25	14.11	14.41	15.58

TABLE 1-MULTICHANNEL OBSERVATIONS (cont)

λ	HZ 4	+70° 5824	SA 29 -130	HZ 7	HZ 2	LB 1240	LB 227
3990	14.66	12.90	13.42	14.14	13.96	14.09	15.40
4010	14.52	12.77	13.18	14.02	13.85	13.97	15.32
4030	14.49	12.75	13.17	13.90	13.79	13.85	15.18
4050	14.54	12.78	13.32	13.93	13.79	13.93	15.16
4070	14.62	12.91	13.47	14.04	13.89	14.10	15.29
4090	14.96	13.15	13.79	14.31	14.12	14.44	15.58
4110	14.85	13.11	13.63	14.33	14.20	14.38	15.59
4130	14.64	12.88	13.41	14.06	13.93	14.02	15.37
4150	14.51	12.82	13.21	13.99	13.80	13.87	15.21
4170	14.38	12.74	13.10	13.90	13.73	13.81	15.11
4190	14.37	12.72	13.09	13.90	13.77	13.78	15.07
4210	14.38	12.72	13.17	13.86	13.76	13.78	15.05
4230	14.34	12.78	13.15	13.90	13.75	13.75	15.04
4250	14.36	12.79	13.19	13.94	13.77	13.84	15.08
4270	14.48	12.85	13.23	14.01	13.80	13.87	15.17
4290	14.63	12.94	13.40	14.10	13.94	14.00	15.29
4310	14.80	13.12	13.60	14.22	14.05	14.16	15.39
4330	15.10	13.40	13.90	14.50	14.33	14.52	15.73
4350	14.98	13.27	13.70	14.43	14.34	14.40	15.69
4370	14.78	13.02	13.51	14.23	14.04	14.07	15.38
4390	14.53	13.05	13.33	14.06	13.92	13.93	15.26
4410	14.46	12.85	13.22	14.03	13.80	13.87	15.18
4430	14.36	12.83	13.17	13.98	13.79	13.81	15.12
4450	14.36	12.77	13.18	13.94	13.75	13.76	15.10
4470	14.34	12.82	13.12	13.94	13.79	13.73	15.06
4490	14.30	12.77	13.10	13.94	13.80	13.72	15.00
4510	14.34	12.80	13.10	13.95	13.82	13.74	15.02
4530	14.35	12.79	13.17	13.98	13.82	13.75	15.02
4550	14.29	12.83	13.17	13.95	13.80	13.72	15.04
4570	14.29	12.79	13.12	13.98	13.77	13.74	15.03
4590	14.28	12.80	13.16	13.98	13.82	13.73	15.04
4610	14.36	12.79	13.19	13.98	13.81	13.75	15.09
4630	14.34	12.83	13.15	13.99	13.81	13.74	15.07
4650	14.33	12.81	13.13	13.97	13.84	13.76	15.05
4670	14.39	12.83	13.17	14.01	13.90	13.76	15.10
4690	14.40	12.86	13.19	14.03	13.87	13.77	15.07
4710	14.34	12.86	13.23	13.99	13.86	13.75	15.09
4730	14.38	12.85	13.18	14.03	13.77	13.79	15.11
4750	14.43	12.87	13.22	14.06	13.82	13.81	15.16

TABLE 1- MULTICHANNEL OBSERVATIONS (cont)

λ	HZ 4	+70° 5824	SA29 -130	HZ 7	HZ 2	LB 1240	LB 227
4770	14.48	12.88	13.30	14.07	13.88	13.85	15.19
4790	14.56	12.95	13.32	14.14	13.92	13.91	15.25
4810	14.66	13.02	13.38	14.15	14.04	13.97	15.38
4830	14.90	13.15	13.58	14.29	14.17	14.06	15.46
4850	15.22	13.42	13.96	14.53	14.40	14.43	15.76
4870	14.99	13.34	13.77	14.53	14.38	14.40	15.76
4890	14.78	13.12	13.53	14.33	14.11	14.15	15.49
4910	14.63	13.03	13.40	14.24	14.05	14.03	15.41
4930	14.63	12.98	13.37	14.16	14.00	13.95	15.32
4950	14.54	13.00	13.32	14.18	13.99	13.91	15.27
4970	14.49	12.97	13.24	14.13	13.99	13.88	15.21
4990	14.52	12.96	13.28	14.09	13.98	13.89	15.20
5010	14.56	12.98	13.36	14.13	13.99	13.90	15.26
5030	14.51	13.02	13.38	14.20	14.04	13.90	15.25
5050	14.53	13.01	13.34	14.22	14.01	13.93	15.24
5070	14.47	13.04	15.25	14.21	13.98	13.89	15.16
5090	14.44	13.00	13.31	14.15	13.99	13.83	15.20
5110	14.50	13.02	13.31	14.17	13.95	13.83	15.23
5130	14.43	13.00	13.20	14.09	14.01	13.83	15.16
5150	14.49	13.03	13.26	14.18	14.02	13.81	15.17
5170	14.52	13.04	13.31	14.17	13.99	13.88	15.14
5190	14.41	13.03	13.35	14.10	14.97	13.83	15.21
5210	14.46	13.02	13.28	14.14	14.00	13.85	15.21
5230	14.45	13.02	13.32	14.18	13.98	13.88	15.26
5250	14.47	13.01	13.34	14.18	14.02	13.87	15.21
5270	14.51	13.05	13.33	14.20	14.03	13.85	15.26
5290	14.46	13.03	13.29	14.12	14.05	13.89	15.20
5310	14.54	13.07	13.34	14.22	14.06	13.87	15.22
5330	14.55	13.08	13.35	14.23	14.08	13.86	15.28
5350	14.52	13.08	13.38	14.19	14.11	13.98	15.26
5370	14.51	13.08	13.38	14.24	14.05	13.95	15.22
5390	14.46	13.10	13.38	14.23	14.06	13.92	15.28
5410	14.62	13.09	13.38	14.21	14.10	13.89	15.29
5430	14.54	13.10	13.42	14.26	14.06	13.91	15.24
5450	14.53	13.15	13.38	14.20	14.06	13.91	15.27
5470	14.55	13.15	13.43	14.32	14.18	13.93	15.23
5490	14.58	13.15	13.44	14.30	14.15	13.99	15.31
5510	14.61	13.15	13.46	14.27	14.15	13.91	15.39
5530	14.52	13.20	13.41	14.31	14.10	13.94	15.35

TABLE 1- MULTICHANNEL OBSERVATIONS (cont)

λ	HZ 4	+70° 5824	SA29 -130	HZ 7	HZ 2	LB 1240	LB 227
5550	14.56	13.23	13.42	14.29	14.08	13.94	15.30
5570	14.57	*	13.43	14.28	14.10	13.94	15.28
5590	14.58	*	13.37	14.34	14.16	13.94	15.28
5610	14.55	*	13.36	14.34	14.17	13.95	15.37
5630	14.63	*	13.43	14.33	14.21	13.94	15.32
5650	14.66	*	13.42	14.33	14.19	13.97	15.40
5670	14.62	13.13	13.47	14.35	14.19	13.97	15.35
5690	14.57	13.14	13.47	14.38	14.19	13.97	15.41
5700	14.61	13.16	13.47	14.35	14.17	13.95	15.36
5740	14.64	13.21	13.44	14.40	14.20	13.98	15.38
5780	14.62	13.21	13.43	14.40	14.26	14.01	15.43
5820	14.65	13.20	13.46	14.41	14.25	13.98	15.41
5860	14.70	13.22	13.52	14.38	14.26	14.00	15.39
5900	14.66	13.27	13.52	14.40	14.27	14.02	15.46
5940	14.65	13.28	13.54	14.44	14.30	14.03	15.48
5980	14.71	13.28	13.51	14.44	14.26	14.04	15.45
6020	14.64	13.30	13.52	14.44	14.23	14.08	15.42
6060	14.73	13.28	13.58	14.46	14.25	14.05	15.48
6100	14.71	13.35	13.55	14.55	14.29	14.06	15.52
6140	14.69	13.27	13.54	14.44	14.33	14.07	15.47
6180	14.74	13.33	13.59	14.51	14.34	14.07	15.51
6220	14.75	13.35	13.57	14.48	14.29	14.05	15.50
6260	14.70	13.37	13.63	14.49	14.38	14.09	15.54
6300	14.74	13.40	13.66	14.51	14.37	14.11	15.54
6340	14.77	13.38	13.61	14.55	14.37	14.12	15.57
6380	14.77	13.39	13.63	14.56	14.34	14.15	15.54
6420	14.84	13.36	13.68	14.62	14.38	14.16	15.60
6460	14.90	13.46	13.69	14.58	14.41	14.20	15.72
6500	14.98	13.48	13.77	14.66	14.51	14.32	15.81
6540	15.26	13.67	14.05	14.81	14.72	14.56	16.04
6580	15.31	13.68	14.08	14.93	14.75	14.58	16.05
6620	15.01	13.57	13.83	14.77	14.54	14.32	15.78
6660	14.90	13.52	13.77	14.66	14.53	14.24	15.75
6700	14.91	13.47	13.75	14.73	14.53	14.24	15.69
7060	14.94	13.58	13.79	14.74	14.52	14.26	15.72
7100	14.94	13.61	13.80	14.74	14.59	14.29	15.74
7140	14.97	13.58	13.81	14.77	14.59	14.25	15.80
7180	15.00	13.58	13.81	14.78	14.53	14.27	15.78
7220	14.97	13.62	13.78	14.78	14.62	14.31	15.84

Bandwidth=20(3210-5690), 40 (5700-7220). *-Unreliable.

TABLE 2- HZ 14

λ	AB	λ	AB	λ	AB	λ	AB
3230	13.11	4070	13.50	4850	14.01	5650	13.95
3250	13.13	4090	13.71	4870	14.04	5670	13.96
3270	13.17	4110	13.75	4890	13.87	5690	13.96
3290	13.26	4130	13.57	4910	13.77	5700	13.98
3310	13.29	4150	13.47	4930	13.75	5740	13.99
3330	13.31	4190	13.42	4950	13.74	5820	14.01
3350	13.21	4210	13.42	4970	13.71	5860	13.98
3390	13.32	4230	13.45	4990	13.70	5900	14.05
3410	13.28	4250	13.49	5010	13.72	5940	14.01
3430	13.30	4270	13.58	5030	13.78	5980	14.06
3450	13.28	4290	13.63	5050	13.79	6020	14.13
3470	13.33	4310	13.71	5070	13.79	6060	14.12
3490	13.33	4330	13.95	5090	13.78	6100	14.12
3510	13.33	4350	13.90	5110	13.76	6180	14.08
3550	13.33	4370	13.68	5130	13.75	6220	14.07
3570	13.35	4390	13.60	5150	13.74	6260	14.13
3590	13.35	4410	13.55	5170	13.75	6300	14.16
3610	13.41	4430	13.54	5190	13.75	6340	14.21
3630	13.40	4450	13.50	5210	13.77	6380	14.26
3650	13.43	4470	13.51	5230	13.75	6420	14.23
3670	13.41	4490	13.52	5250	13.82	6460	14.25
3710	13.43	4510	13.51	5270	13.81	6540	14.44
3730	13.44	4530	13.50	5310	13.80	5680	14.52
3750	13.51	4550	13.50	5330	13.81	6620	14.33
3770	13.54	4570	13.55	5350	13.84	6660	14.28
3790	13.58	4590	13.55	5370	13.84	7060	14.44
3810	13.57	4610	13.59	5390	13.85	7100	14.45
3830	13.57	4630	13.59	5410	13.87	7140	14.43
3870	13.55	4670	13.59	5430	13.87	7180	14.41
3890	13.60	4690	13.56	5470	13.87	7260	14.44
3910	13.51	4710	13.58	5490	13.90	7300	14.44
3930	13.49	4730	13.61	5510	13.94	7340	14.45
3950	13.55	4750	13.62	5530	13.91	7380	14.43
3970	13.67	4770	13.64	5550	13.94	7420	14.43
3990	13.56	4790	13.65	5570	13.96		
4030	13.40	4810	13.68	5540	13.93		
4050	13.40	4830	13.79	5630	13.93		

Standard Deviation=.02(3230-3810), .01(3810-5050, .02(5050-7420). Bandwidth=20(3230-5690),40(5690-7420).

TABLE 3- L 1512-34B

λ	AB	λ	AB	λ	AB	λ	AB
3210	13.14	3990	13.12	4770	12.82	5550	12.93
3230	13.20	4010	12.95	4790	12.90	5570	12.91
3250	13.19	4030	12.86	4810	12.97	5590	12.92
3270	13.11	4050	12.90	4830	13.11	5690	12.93
3290	13.20	4070	13.01	4850	13.50	5630	12.94
3310	13.19	4090	13.34	4870	13.40	5650	12.98
3330	13.22	4110	13.34	4890	13.12	5670	12.94
3350	13.17	4130	13.00	4910	13.00	5690	12.96
3370	13.17	4150	12.88	4930	12.93	5700	12.96
3390	13.19	4170	12.77	4950	12.90	5740	12.98
3410	13.23	4190	12.76	4970	12.85	5780	13.02
3430	13.18	4210	12.75	4990	12.84	5820	13.01
3450	13.17	4230	12.74	5010	12.88	5860	13.04
3470	13.16	4250	12.78	5030	12.89	5900	13.03
3490	13.15	4270	12.86	5050	12.88	5940	13.05
3510	13.22	4290	12.98	5070	12.85	5980	13.04
3530	13.13	4310	13.18	5090	12.80	6020	13.02
3550	13.17	4330	13.51	5110	12.83	6060	13.05
3570	13.22	4350	13.37	5130	12.84	6100	13.07
3590	13.22	4370	13.12	5150	12.78	6140	13.07
3610	13.18	4390	12.93	5170	12.85	6180	13.07
3630	13.17	4410	12.83	5190	12.87	6220	13.09
3650	13.17	4430	12.78	5210	12.83	6260	13.08
3670	13.19	4450	12.72	5230	12.84	6300	13.12
3690	13.19	4470	12.70	5250	12.85	6340	13.11
3710	13.22	4490	12.71	5270	12.85	6380	13.15
3730	13.25	4510	12.70	5290	12.85	6420	13.17
3750	13.25	4530	12.73	5310	12.89	6460	13.23
3770	13.24	4550	12.68	5330	12.90	6500	13.29
3790	13.29	4570	12.71	5350	12.89	6540	13.52
3810	13.25	4590	12.71	5370	12.87	6580	13.66
3830	13.30	4610	12.72	5390	12.88	6620	13.35
3850	13.21	4630	12.72	5410	12.88	6660	13.30
3870	13.26	4650	12.74	5430	12.90	6700	13.23
3890	13.44	4670	12.75	5450	12.91	7060	13.23
3910	13.14	4690	12.77	5470	12.90	7100	13.25
3930	13.01	4710	12.76	5490	12.96	7140	13.25
3950	13.15	4730	12.77	5510	12.93	7180	13.25
3970	13.38	4750	12.81	5530	12.92	7220	13.28

Standard Deviation=.03(3210-7220).
Bandwidth=20(3210-5690), 40(5700-7220).

TABLE 4 -MULTICHANNEL OBSERVATIONS

λ	L 870-2	R 627	LDS 749B	λ	L 870-2	R 627	LDS 749B
3210	13.58	15.06	14.76	3990	13.14	14.51	14.51
3230	13.56	14.77	14.48	4010	13.12	14.47	14.63
3250	13.52	14.56	14.46	4030	13.10	14.38	14.60
3270	13.56	14.73	14.41	4050	13.10	14.46	14.50
3290	13.54	14.75	14.63	4070	13.09	14.43	14.45
3310	13.54	14.76	14.56	4090	13.23	14.57	14.47
3330	13.53	14.69	14.48	4110	13.15	14.46.	14.53
3350	13.49	14.75	14.48	4130	13.09	14.50	14.56
3370	13.50	14.93	14.59	4150	13.07	14.46	14.55
3390	13.50	14.72	14.46	4170	13.06	14.43	14.60
3410	13.43	14.71	14.50	4190	13.05	14.41	14.54
3430	13.40	14.77	14.58	4210	13.06	14.37	14.56
3450	13.40	14.66	14.47	4230	13.04	14.39	14.54
3470	13.36	14.63	14.51	4250	13.06	14.40	14.55
3490	13.39	14.73	14.51	4270	13.07	14.44	14.56
3510	13.40	14.74	14.47	4290	13.11	14.54	14.55
3530	13.41	14.64	14.50	4310	13.12	14.47	14.59
3550	13.42	14.78	14.49	4330	13.32	14.68	14.59
3570	13.42	14.61	14.51	4350	13.14	14.50	14.57
3590	13.32	14.67	14.52	4370	13.05	14.36	14.57
3610	13.34	14.65	14.54	4390	13.03	14.40	14.58
3630	13.36	14.69	14.54	4410	13.02	14.36	14.60
3650	13.32	14.68	14.55	4430	13.00	14.34	14.60
3670	13.30	14.72	14.49	4450	12.98	14.37	14.68
3690	13.29	14.64	14.56	4470	13.00	14.33	14.80
3710	13.29	14.63	14.55	4490	12.99	14.35	14.64
3730	13.27	14.66	14.54	4510	12.96	14.41	14.60
3750	13.29	14.61	14.49	4530	12.98	14.32	14.60
3770	13.31	14.61	14.57	4550	12.93	14.28	14.60
3790	13.34	14.76	14.61	4570	12.95	14.29	14.59
3810	13.28	14.66	14.67	4590	12.94	14.30	14.59
3830	13.32	14.71	14.65	4610	12.96	14.34	14.59
3850	13.25	14.67	14.63	4630	12.97	14.34	14.60
3870	13.24	14.67	14.64	4650	12.94	14.30	14.61
3890	13.35	14.68	14.72	4670	12.94	14.31	14.63
3910	13.21	14.59	14.57	4690	12.93	14.32	14.58
3930	13.15	14.47	14.50	4710	12.92	14.27	14.65
3950	13.14	14.44	14.51	4730	12.90	14.27	14.60
3970	13.24	14.58	14.48	4750	12.91	14.29	14.60

Bandwidth=20

TABLE 4 -MULTICHANNEL OBSERVATIONS (cont)

λ	L 870-2	R 627	LDS 749B	λ	L 870-2	R 627	LDS 749B
4770	12.89	14.31	14.63	5550	12.82	*	14.76
4790	12.90	14.38	14.55	5570	12.83	*	14.76
4810	12.88	14.31	14.60	5590	12.81	*	14.78
4830	12.89	14.33	14.61	5610	12.80	*	14.75
4850	13.08	14.50	14.63	5630	12.83	*	14.81
4870	13.00	14.40	14.63	5650	12.82	*	14.79
4890	12.89	14.28	14.65	5670	12.78	*	14.81
4910	12.89	14.23	14.71	5690	12.81	*	14.71
4930	12.88	14.29	14.69	5700	12.81	14.23	14.84
4950	12.89	14.32	14.68	5740	12.81	14.26	14.81
4970	12.86	14.29	14.67	5780	12.81	14.24	14.85
4990	12.87	14.30	14.69	5820	12.81	14.24	14.84
5010	12.88	14.24	14.76	5860	12.80	14.17	14.98
5030	12.91	14.29	14.74	5900	12.81	14.21	14.89
5050	12.90	14.25	14.70	5940	12.81	14.24	14.86
5070	12.90	14.21	14.73	5980	12.83	14.22	14.86
5090	12.89	14.28	14.68	6020	12.81	14.18	14.89
5110	12.86	14.24	14.75	6060	12.78	14.22	14.86
5130	12.88	14.24	14.72	6100	12.78	14.23	14.88
5150	12.88	14.26	14.67	6140	12.79	14.21	14.88
5170	12.84	14.21	14.73	6180	12.76	14.19	14.89
5190	12.83	14.19	14.72	6220	12.77	14.20	14.88
5210	12.82	14.22	14.70	6260	12.77	14.17	14.86
5230	12.83	14.20	14.68	6300	12.78	14.16	14.90
5250	12.84	14.28	14.69	6340	12.79	14.17	14.90
5270	12.84	14.24	14.70	6380	12.77	14.19	14.89
5290	12.85	14.28	14.71	6420	12.79	14.20	14.92
5310	12.85	14.24	14.71	6460	12.78	14.20	14.92
5330	12.85	14.21	14.71	6500	12.80	14.23	14.87
5350	12.82	14.21	14.73	6540	12.93	14.36	14.92
5370	12.82	14.23	14.73	6580	13.04	14.36	14.93
5390	12.83	14.24	14.74	6620	12.77	14.25	14.98
5410	12.82	14.24	14.74	6660	12.77	14.22	15.03
5430	12.83	14.23	14.70	6700	12.78	*	15.00
5450	12.82	14.26	14.75	7060	12.77	14.20	15.13
5470	12.83	14.17	14.81	7100	12.79	14.20	15.05
5490	12.85	14.19	14.80	7140	12.79	14.23	15.06
5510	12.85	14.21	14.77	7180	12.78	14.21	15.04
5530	12.82	14.19	14.75	7220	12.79	14.21	15.10

Bandwidth=20(4770-5690), 40(5700-7220)
* - Observations Unavailable

TABLE 5 - 60" OBSERVATIONS

λ	He 3	W 485	λ	He 3	W 485
4190	11.72	12.15	4390	11.85	12.42
4210	11.68	12.09	4410	11.78	12.21
4230	11.70	12.08	4430	11.81	12.10
4250	11.72	12.12	4450	11.73	12.16
4270	11.73	12.19	4470	11.75	12.10
4290	11.78	12.29	4490	11.74	12.07
4310	11.92	12.54	4510	11.69	12.06
4330	12.18	12.77	4530	11.73	12.08
			4550	11.71	12.12

Points at λλ 4350 and 4370 are omitted because the night-sky line of mercury reduces the signal/noise ratio to about 1/10, from 3/1 at other points.

Standard deviation=.015 (He 3), .02 (W 485)

TABLE 6 - STANDARD DEVIATIONS FOR STARS IN TABLES 1 AND 4

Table	Star	Standard deviations and wavelengths
1	HZ 4	.04 (3210-3570), .02(3570-7220).
1	+70°5824	.02 (3210-3530), .01(3530-7220).
1	SA 29-130	.03 (3210-3570), .01(3590-5570), .02 (5570-7220).
1	HZ 7	.03(3210-3390), .02(3390-7220)
1	HZ 2	.03(3210-3550), .01(3570-5900), .02 (5940-7220).
1	LB 1240	.03(3210-3650), .01(3670-7220)
1	LB 227	.03(3210-3810), .02(3830-6020), .03 (6060-7220).
4	L 870-2	.02(3210-3690), .01(3710-7220)
4	R 627	.08(3210-3370), .05(3390-3730), .02 (3750-7220)
4	LDS 749B	.04(3210-3370), .02(3390-7220)

CHAPTER 4-

ATMOSPHERIC PARAMETERS, MASSES, AND RADII OF WHITE DWARFS

Abstract

Effective temperatures and surface gravities are derived for the program stars, and luminosities and radii are determined for those stars whose distances are known. I find that the median radius for DA stars is 0.0129 $R_\odot$. Masses are then determined for the DA stars in the sample; the median mass is 0.57 $M_\odot$. Three cool white dwarfs (L870-2, L745-46A, Ross 640) have radii substantially greater than the median.

I. Procedure

The determination of masses and radii for white dwarfs provides an important and interesting check on the theory of degenerate matter and the measurement of gravitational redshifts. Previous attempts (Weidemann 1963, Terashita and Matsushima 1969 , Matsushima and Terashita 1969a,b) have suffered from a lack of precise observational data. The use of intermediate and narrow-band spectrum scans makes it possible to determine effective temperatures by matching the observed and theoretical energy distributions over a wide range of wavelength without going through transformation formulae for broad-band filters. It is also possible in some cases to measure the surface gravity from line profiles. Effective temperature, surface gravity and abundance

are the only parameters which can be computed from an analysis of the stellar spectrum alone. However, if the distance to the star is known, masses and radii can be calculated.

The usual method for computing the radius of a star, once the effective temperature is known, is to compute the bolometric magnitude by assuming a value for the bolometric correction, and then by using the definition of effective temperature.

$$L=4\pi R^2 \sigma T_{eff}^4 \qquad (4-1)$$

to compute the radius. In this paper, however, I will calculate the radius from visual magnitudes only, eliminating the uncertainties of the bolometric correction (except when luminosities are determined). From the model atmospheres, the emergent flux in the V filter can be read from Tables 1-7 of Chapter 2, if one assumes an effective wavelength of 5480 Å for the V filter (Allen 1963). Then, through using the normal definitions of magnitudes, we find

$$2 \log R/R_\odot = -\log H_V - 2 \log \pi - m_V/2.5 - 1.221 \qquad (4-2)$$

where the logarithms are taken to base 10, H_V is the flux at 5480 Å as normalized on page 18, π the parallax, and m_V the observed visual magnitude of the star. The absolute flux calibration was that of Oke and Schild (1970). A plot of log H_V versus log T_{eff} is shown in Figure 4-1, where

$T_4=(T_{eff}/10^4)$. It is apparent that the differences in the emergent fluxes for models with different chemical compositions are only moderately important. In practice, it turns out in most cases that the major uncertainty in applying equation (4-2) is the uncertainty in the parallax.

A thorough discussion of the parallax determinations for white dwarfs is given by Eggen (1969). There are quite a few parallaxes in the literature, although a distressingly large number of these are determinations by only one observatory with fairly low weight. Table 1 summarizes the parallaxes and visual magnitudes that were used in this chapter to derive masses and radii. I have given each parallax a rating, which is quite subjective, based largely on the size of the parallax, the quoted probable error, and the number of different observatories which have measured the particular parallax. Parallaxes rated A have an estimated uncertainty of 10% or less; those rated B, 10% to 25%; those rated C, 25% to 50%; and those rated D are sufficiently inaccurate to be of academic interest only. A listing of the individual parallax determinations from the Yale catalogue is given by Eggen (1969). Comments on specific parallaxes are given in the notes to Table 1.

For the Hyades, I haved used the value of $m-M = 3.03$ magnitudes, determined by the moving cluster method by Wayman et. al. (1965). This value has been questioned recently, on several grounds (for a discussion, see van Altena 1969). Because the question is unsettled, I have

provisionally adopted the old value. The distance modulus of any individual star is uncertain by about 0.3 mag, because of the depth of the Hyades cluster. This uncertainty is about comparable to the change in m-M suggested by van Altena (he gives m-M = +3.23). If van Altena's value for the distance modulus is adopted, the radii of the Hyades stars become larger by 0.04 in the logarithm, and the masses larger by 0.08 in the log. Even with this uncertainty, the radii of the Hyades white dwarfs are considerably better determined than the radii of most of the white dwarfs. The uncertainty in the mass due to any possible error in the distance modulus is swamped by the uncertainties in the determination. In Table 1 I have assumed HZ 2 is a mamber of the Hyades cluster, although van Altena (1969) contends that it is not a member on the basis of only one measurement of the proper motion. In this determination I follow the arguments of Eggen(1969).

Once the radius of a white dwarf is known from equation 4-2, the luminosity is computed from the equation

$$\log L/L_\odot = 2 \log R/R_\odot + 4 \log T_4 + .944. \quad (4-3)$$

If the surface gravity of the star is known, the mass can be determined:

$$\log M/M_\odot = \log g - 2 \log R/R_\odot - 4.44. \quad (4-4)$$

The values of T_{eff} and log g determined for each star in the program are tabulated in Table 2, and the masses and radii are listed in Table 3. The rest of the

chapter consists of a description of the methods of, and uncertainties in, determining the quantities which appear in Tables 2 and 3. The general techniques applicable to each type of star are described, and comments on individual cases are made where appropriate.

II. DA STARS

The DA stars are the simplest to analyze of all the white dwarf types. This fact, combined with the well-established nature of the basic physics used in constructing the models for DA stars, means that the atmospheric parameters are determined with a high degree of accuracy.

The effective temperatures of DA stars are found by comparing the observed energy distributions with predictions from model atmospheres. The two features which change with changing effective temperature are the Balmer discontinuity and, to a lesser degree of importance, the slope of the Paschen continuum (which remains almost constant for $T_{eff} \geq 16{,}000^{\circ}K$). To a large extent, the determination of the effective temperature of a given star was made simply by fitting the scans and the models by eye. In order to facilitate interpolation, however, I also used a color index Δm to determine T_{eff}, where

$$\begin{aligned} \Delta m &= AB\ (1/\lambda = 1.8) - AB\ (1/\lambda = 2.8) \\ &= AB\ (\lambda = 5560\ ) - AB\ (\lambda = 3600) \end{aligned} \qquad (4\text{–}5)$$

where $AB = -2.5 \log F_{\nu} + \text{const.}$ as defined in Chapter 3.

This index is analogous to -(U-V) in the UBV system, while the scans eliminate the uncertainties in knowing the proper transformation formulae from fluxes to the UBV system. This uncertainty is one of the major difficulties in trying to compare directly UBV observations and model atmospheres. A plot of Δm against reciprocal effective temperature is shown in Figure 2.

From the color index Δm, as well as from eye estimates of fitting scans to models, the effective temperature of a DA star can be determined with an uncertainty of about 5%. In each individual case, an estimate of the uncertainty was made on the basis of goodness of fit. Typical comparisons of the models and the observations are made in Figures 3 and 4 for Grw+73°8031 and Hertzsprung 3 respectively. The shape of the energy distributions is almost independent of surface gravity. Only for the coolest stars ($T_{eff} \leq 14{,}000°K$) did the surface gravity assumed in the fitting of energy distributions make any difference in the resulting effective temperature, and here the difference is only about 500°K, as is apparent from Figure 2.

Once the effective temperature is known, the surface gravity was determined from fitting both Hβ and Hγ profiles to the observations. In order to eliminate as much as possible the systematic error inherent in the uncertainty in locating the continuum, a self-consistent

treatment of models and observations is needed. What the scanner does in looking at a star is to count all the photons with

$$\lambda_c - \frac{B}{2} < \lambda < \lambda_c + \frac{B}{2} \qquad (4\text{-}6)$$

where λ_c is the central wavelength of the scanner observation, B the bandpass, and λ the wavelength of the photon. I therefore synthesized a set of theoretical scanner observations for each model by folding the theoretically calculated profile with a rectangular instrumental profile of the appropriate width. The central wavelengths of the rectangular bandpasses were chosen to correspond with the wavelengths of the observations, and then the resulting fluxes were converted to magnitudes. The continuum was defined as a straight line (on a magnitude scale) drawn through the observations at specified wavelengths, and the theoretical continuum was defined in the same way. The continuum wavelengths were $\lambda\lambda$4190,4210,4230, and 4250 on the blue side of H_γ and $\lambda\lambda$4510,4530 and 4550 on the red side. For H_β the wavelengths were $\lambda\lambda$4690,4710,4730, 4750,5110,5130,5150. These wavelengths were chosen so that any possible influence on the location of the continuum from He I λ4471 or He I λ5015 would be eliminated, even though these lines were not detected.

Once an observed and theoretical line profile was calculated in a self-consistent way, the surface gravity

was determined by fitting theory and observation. Highest weight was given to the points at 30 and 50 Å from line center. In this way it was possible to determine surface gravities with uncertainties of about .2 in the logarithm, although the uncertainty in each individual case varied from 0.15 to 0.3. In the one case where the derived surface gravity was 9.1, it was determined by extrapolating plots of log W versus log g for both Hβ and Hγ. This determination (for GD 185) is somewhat uncertain.

For those stars which were not observed at high resolution, the calculation of equivalent widths provided less certain surface gravities. With bandpasses of 40 Å some comparison of detailed profiles was possible, while with bandpasses of 80 Å the equivalent widths had to suffice. In all cases, however, the equivalent widths and profiles were calculated from the models using the folding procedure described above to minimize (hopefully) the influence of systematic errors. The uncertainties were, naturally, somewhat greater here (e.g., upwards of 0.3 in the log). In the cases where the determination of the surface gravity rested on only one or two observed points, the uncertainty was determined by the probable errors of those points, which could be estimated from counting statistics and the smoothness of the neighboring continuum. The error estimates in Tables 2 and 3 are intended to be generous estimates of the probable error.

Some sample profiles are plotted in Figures 5 and 6. The 40 Eri B profile in Figure 5 is that of Oke (1963); for comparison, the profile of Greenstein (1960) is also plotted. It is evident that the fit between theory and observation is quite good because the data for this star are highly reliable. The value of log g obtained here, by interpolation, is 7.75. Figure 6 shows the observations of HZ 2, and the appearance of this profile is typical of most of the profiles observed. Considering the errors in the observations, the fit is not too bad. The asymmetry in the observations is probably due to errors in guiding ($\sim$1-2 Å) or to velocity shifts, and should not be regarded as real. The value of log g found here was 8.0. It is evident from Figure 6 that attainable accuracy is only moderately good, largely because of observational problems.

It is impossible to determine the abundance of elements other than hydrogen in DA stars, because lines of other elements are not seen. However, from the absence of He I lines in DA spectra, it is possible to set an upper limit on the helium abundance. The most reliable upper limit comes from the scans rather than the photographic spectra, since photoelectric scans are better able to detect broad, shallow features like He I λ4471. The model-atmosphere results predict a λ4471 strength of 4.25 Å for T_{eff}=25,000°, log g=8 model with

a helium abundance of 3% of the total (by number). Assigning an upper limit of 1 Å from the scans (which for a 20 Å bandwidth corresponds tp a depression of 0.05 magnitudes, or more than three times the error from counting statistics) results in a helium abundance of less than 0.2% by number on the assumption that He I λ4471 is on the square-root part of the curve of growth, as is probable. If it is on the linear part of the curve of growth, the upper limit is 0.75%. At any rate, there is very little if any helium in the atmospheres of DA stars.

It is not possible to set very stringent limits on the metal abundance. Strittmatter and Wickramasinghe (1971) have calculated equivalent widths for some of the stronger metal lines such as C II λ4267, and they found that the maximum strength is about 0.4 Å for a normal metal abundance. Greenstein (1958) has estimated that a line of equivalent width 0.5 Å would have been detected in the spectrum of 40 Eri B, but the interesting metal lines are not very strong at this temperature. The spectra of the hotter stars have not been taken at the high dispersion necessary to place such stringent upper limits on the line strengths. I believe that all one can say is that DA atmospheres have twice the solar abundance of metals or less.

The absence of helium in the DA stars means that the surface gravities derived directly from the spectra have to be increased by 0.1 in the log to account for

the fact that the model atmospheres were calculated with an assumed helium abundance of 10% by number (cf. Matsushima and Terashita 1969a). This is due to the fact that increasing the helium abundance increases the pressure of a stellar atmosphere without changing the opacity or the temperature structure. The gravities given in Table 2 were determined directly from the spectra, and were increased by 0.1 in the log before the masses in Table 3 were computed.

A few stars deserve special comments. If LB 1240 is assumed to be in the Hyades cluster, the derived radius is 1.92×10^{-2} $R_\odot$, which is considerably larger than the radii of most other white dwarfs; the distance given by the U.S. Naval Observatory parallax (Riddle 1970) seems accurate. LB 227 is certainly a Hyades member and certainly has a smaller radius than most of the other DA stars, which have a median radius of about 1.3×10^{-2} $R_\odot$. The case of HZ 14 is a particularly interesting one; the surface gravity was determined as an average of that derived from the scan and derived from the m_1-index measured by Graham (1969, see Chapter 6). The m_1-index is an indicator of the strength of Hδ. HZ 14 is quite similar to Sirius B (Chapter 5).

Two possible high-mass white dwarfs are the DAn stars GD 140 and GD 185. The determined surface gravity of GD 185, 9.1, is extremely uncertain because the only scan had a slit width of 80 Å. However, if this gravity

is assumed to be correct, then the mass-radius relation implies a mass barely under the Chandresekhar limit, and a radius of 0.004 $R_\odot$, and a parallax of 0".03, again just barely measureable. If GD 140 has a radius of 1.3×10^{-2} $R_\odot$, the mean for upper-sequence white dwarfs, then it has a mass of 1.2 $M_\odot$ and a parallax of 0".04. However, again the surface gravity is uncertain because 80 Å scans were used. If the radius is less, then the parallax will be correspondingly greater. It would be interesting to measure the parallax of these two stars. The surface gravity and mass of W 485A determined here are consistent with the m_1-index as measured by Graham(1969, see Chapter 6).

The case of 40 Eri B offers a unique opportunity to test the essential accuracy of the model-atmosphere technique in that the mass is known from an analysis of the orbit (van den Bos 1960) and the radius can be measured from a measurement of the gravitational red shift. The surface gravity is sufficiently low so that the gravitational red shift measurement is unaffected by Stark shifts (see Chapter 6). The mass determined from the model-atmosphere analysis is 0.45 ± 0.13 $M_\odot$, and the dynamical mass is $0.43 \pm 0.04 M_\odot$. A further check on the analysis is permitted because the gravitational red shift has been measured by Popper (1954) from high-dispersion spectra. My calculations predict a shift of +22 km/sec, and Popper's results give $+21 \pm 4$ km/sec. I regard this agreement as excellent. Although it must be admitted that the

observational data which are the basis of the model-atmosphere analysis are much more accurate for 40 Eri B than for any of the other white dwarfs in this study, the good agreement between the model-atmosphere values for the mass and radius, and the values determined by other methods lends confidence to the idea that systematic errors in the model-atmosphere approach are small. Further comparisons with gravitational red shift results will be made in Chapter 6.

III. DB STARS

Unfortunately the astrometric data for the DB stars is much more limited than is the case for the DA stars. It is also unfortunate the the DB spectra do not permit an accurate determination of the surface gravity, since the helium line strengths are not very strongly dependent on the surface gravity. Still, it is possible to come to a few conclusions.

The effective temperatures of the DB stars were determined by fitting the energy distributions to the predictions of models. The principal temperature-dependent feature is the slope of the continuum in the visual region of the spectrum. Unfortunately, this slope is also dependent on the metal abundance, because increasing the metal abundance increases the electron density, which increases the He^- absorption. Consequently, the continuum in the red is lowered and the star looks hotter. It was also possible to use the size of the discontinuity around

3600 Å, which is a combination of the discontinuities arising from the n=2 levels of helium (at 3422 and 3680Å), for the one hotter DB star in the program. A sample comparison between observations and various theoretical models is shown in Figure 7. The continuum between $1/\lambda = 2.5$ and $1/\lambda = 2.9$ ($3480 \leq \lambda \leq 4000$ Å) is depressed by the presence of overlapping He I lines.

Since the helium line equivalent widths are only slowly dependent on the surface gravity, they can be used as another indication of temperature. I measured equivalent widths for unblended helium lines from the scans, and the results are tabulated in Table 4. The measurements of the line strengths are somewhat uncertain because the lines are weak and broad. In all cases the temperature determined from He I λ4471 line strengths was consistent with the continuum temperature.

One can attempt to guess the surface gravity of a DB star by examining the shape of the He I lines, because the lines become broader (though not stronger) as the surface gravity increases. Unfortunately it is not possible to make a very accurate determination, and any conclusions about the masses of DB stars must be given very low weight. When this was done, the same self-consistent treatment of observations and theory was used as was used for the DA stars.

The abundance of elements other than helium is easier to determine than in the case of DA stars because

the opacity is much reduced. Bues (1970) has estimated metal abundance (relative to the total number of atoms) of DB stars is 1/10 to 1/50 that of the sun. The calculations of Strittmatter and Wickramasinghe (1971) indicate that the equivalent width of the H and K lines of ionized calcium is 10 Å at T_{eff}=14,000°, log g=8 for a metals/total ratio 1/5 that of the sun. On the assumption that the H and K lines are on the square-root part of the curve of growth (which is certainly true for W=10 Å but may not be valid for weaker lines) calcium is underabundant by a factor of 500 relative to the sun, and certainly by at least a factor of 50. In view of the inaccuracies of the broadening theory, as well as the inaccuracies of the model atmospheres, I do not feel that more detailed calculations of the metal line strengths are warranted. The hydrogen abundance must be less than 10^{-4} of the total, according to the calculations of Bues (1970).

The effective temperature listed for the DB stars in Table 2 represent a mean of the values obtained from fitting metal-rich (where metals/total equals the solar value) and metal-poor models to the observations. The uncertainty in the temperature determination arising from the fitting of a set of models with a given metal abundance to the observations is about 1000°, which is approximately equal to the uncertainty produced by the indeterminacy of the metal abundance. It should be pointed out that the models themselves are somewhat inaccurate owing

to the indeterminacy of the He^- absorption coefficient and to the problems of convection. Because of all the difficulties, both theoretical and observational, involved in the analysis of DB stars, it is not possible at this time to compute any masses that are at all reliable, so the masses in Table 3 are only correct to within a factor of 10 or so. The radii are somewhat better determined, but more accurate distances are needed, since only two of the DB stars have reasonably accurate distances. In particular, another measurement of the large parallax of L 930-80 is needed.

IV. HOT WHITE DWARFS

The group of hot stars (DO,sdO,DAwk) analyzed here is quite heterogeneous. There are two stars which are definitely white dwarfs (HZ 43 and HZ 21), two which may be white dwarfs (F 24 and G 191), and one subdwarf (HZ 44). This particular group of stars has T_{eff}=50,000° or hotter. The effective temperatures are quite indeterminate, because the slope of the Paschen continuum is only moderately dependent on T_{eff}. The error in θ_{eff}(=5040/T_{eff}) for any individual determination is about 0.02, only twice that for cooler stars, but at high temperatures (small θ) this error corresponds to a very large error in T_{eff} and consequently a large error in the radius. The size of the Balmer discontinuity was used as a provisional indicator of temperature, and this method should only run into

trouble if there is a sizeable abount of helium in the atmosphere of the star being considered. The temperatures listed in Table 2 are, in some cases, merely lower limits caused by the absence of any visible Balmer discontinuity.

The subdwarf HZ 44 was also analyzed by V. Peterson (1969), who found T_{eff}=40,000°, log g=5.7, with a helium abundance of 40% by number. The reason that I have assigned it a higher effective temperature is on the basis of a small Balmer discontinuity, and if there is a substantial ammount of helium in the atmosphere the effective temperature I have assigned will be too high, and the gravity will consequently be too high as well.

The star HZ 43 is the only star in this part of the H-R diagram which has a measured parallax (Wagman 1967). Its radius is the same as that of the DA stars on the upper sequence. Its mass is very uncertain, largely because the indeterminacy of T_{eff} causes a large indeterminacy in log g (because of the strong temperature dependence of the hydrogen line strengths). Figure 8, which illustrates the energy distribution of this star, also illustrates the difficulties of analyzing this type of star. All that can be said about the program stars here is that there are two genuine white dwarfs with very high temperatures.

V. COOL DA STARS

In the list of program stars, there are two representatives of the class DA,F (L870-2 and Ross 627). Effective temperatures for these stars can be determined

fairly accurately by comparing observed and model energy distributions, as the maximum of the energy distribution is shifting into the visual region of the spectrum. The model atmospheres are fairly reliable, as the absorption cross section of hydrogen is well known, and no molecular bands are present. Unfortunately, the hydrogen line strengths are almost completely independent of surface gravity, and there is thus no way to compute the mass of these objects.

It is possible to set quite stringent limits on the metal abundance of the DA,F stars because of the expected strengths of the Ca II K line. I expect that the equivalent width of Ca II K will be more or less independent of surface gravity, since on the square-root part of the curve of growth $W \propto \sqrt{NfF/K}$ where N is the abundance, f the f value, Γ the damping constant and K the continuum absorption coefficient. Almost all of the calcium in the atmospheres of these stars is singly ionized as is evident from the absence of Ca I λ4227. Since most of the absorption in this temperature range is from H^-, K is linearly proportional to the electron density N_e. However, Γ is also linearly proportional to N_e, and the N_e-dependence of the equivalent width vanishes, in this approximation. On the basis of line strengths from Wright et. al.(1964), one would expect a line strength of about 10 Å for the K line at a temperature of about 6,000°. The K-line strength is 1 Å in Ross 627, and the K line is not observed in L 870-2. Consequently calcium is underabundant

in these stars by a factor of at least 10 and probably a factor of 100. In view of the inaccuracies in the calculated damping constants, I do not believe that more accurate results can be obtained from detailed model calculations.

The radius of Ross 627 is in general agreement with the mean upper-sequence radius. However, the radius of L 870-2 is much larger and deserves some comment. If L 870-2 were to have the same radius as the upper-sequence white dwarfs, either the effective temperature would have to be increased to 14,000° or the parallax would have to be increased to 0".18. I believe that either of these is beyond the bounds of possible error, and I therefore conclude that the radius of L 870-2 is indeed considerably larger than the radius of upper-sequence DA stars.

VI. PECULIAR TYPES

The remainder of the program stars to be analyzed in this section, are peculiar white dwarfs - there are two DF stars, two λ4670, one DC, and one λ4135. The analyses of all of these stars are quite uncertain, because the chemical composition of the atmospheres is unknown. Furthermore, the possible influence of molecular opacity is a major problem, especially in the cases of the λ4670 stars. However, it is possible to determine very rough effective temperatures for most of these stars.

I have assigned temperatures to these stars on the assumption that the major constituent of the atmospheres

of these stars is helium. This assumption is probably valid for the DC stars, on the basis of two arguments: first, if these stars are the evolutes of DB stars (as is perhaps reasonable to suppose, see Chapter 6), then their atmospheres will contain mostly helium, and second, helium is one of the few elements that could exist in a stellar atmosphere and give no sign of its existence. All of the helium lines in the visible part of the spectrum arise from levels that are approximately 20 eV (or more) above the ground state, and in cool stars, the Boltzmann factor is very small, and consequently the populations of the excited levels is quite small. Most other possible constituents of white dwarf atmospheres would give some sign of their presence (e.g. by showing lines such as C I λ4711, N I λ4151, O I λ3947, λ4368, etc.). The validity of the assumption for the DF stars is somewhat more doubtful, and the λ4670 stars may well have carbon as the main constituent of their atmospheres. In order to decide the composition of these stars, model atmospheres which have as their principal constituent some element such as C, Ne, O, or maybe Ca.

Apart from the compositional difficulties, the major uncertainty in the effective temperatures of these stars is the extremely non-grey character of He^- absorption coefficient. As a result, the energy distribution from a $T_{eff}=6000^o$ He-rich model resembles an 8000^o black-body curve (see figure 9). The amount of He^- absorption is influenced by the metal abundance assumed in the model,

and the assumed metal abundance is probably too high, although it varies from one star to another. In Tables 2 and 3 I have derived temperatures and radii for these stars, both on the assumption that they are He-rich and on the assumption that they radiate as black bodies. The truth should lie somewhere in between the two results obtained in these different ways, since reducing the metal abundance will reduce the effect of He^- absorption and will consequently make the star radiate more like a black body.

The metal abundance of Ross 640, L 1363-3, and L 745-46A are quite peculiar. As is evident from Figure 9, Ross 640 and L 1363-3 have almost identical energy distributions, although Ross 640 has a Ca-K line strength of 19.7 Å (Greenstein 1960) and L 1363-3 has no K-line visible which means $W_K < 1$ Å). Calculating a K-line strength using the same curve-of-growth approach outlined in the previous section, while taking into account the difference in absorption coefficient in main sequence stars and He-rich white dwarfs yields a K-line strength of 100 Å for the 6000^o model. One can tentatively say that the abundance of Ca (relative to the total number of atoms as before) is less than in main sequence stars by a factor of from 5 to 25 in Ross 640 and by a factor of at least 100 in L 1363-3 (or 10^4 if, as is more likely, the square-root part of the curve of growth is applicable). As was mentioned above, the He-rich assumption is considerably more

reasonable for L 1363-3; it may well be that the atmospheres of L 745-46A and Ross 640 are pure Ca, although it is difficult to imagine an evolutionary sequence which would result in such a state of affairs. L 745-46A is somewhat cooler than Ross 640 and L 1363-3, and has a K-line strength of 4.2 Å (Greenstein 1960). I therefore regard it as an intermediate case, being underabundant by a factor of between 30 and 900 with respect to main-sequence stars. In all of these cases, all of the Ca in the atmosphere is Ca II, as is evident by the absence of Ca I λ4227.

The effective temperatures of G 47-18 and G 99-37 are very uncertain owing to the probable influence of molecular absorption (the main feature of the spectra of these stars are the Swan bands of C^2 and the bands of CH). As is shown in chapter 6, it is quite probable that the λ4670 stars may have atmospheres of pure carbon. Consequently, the black-body temperatures may well be more reliable than the temperatures deduced from the helium-rich model. A model-atmosphere study of these stars by Kumar is in progress. Clearly more work needs to be done on these stars, especially since one of them, G 47-18, shows circular polarization (Angel and Landstreet 1971).

The magnetic white dwarf Grw+70°8247 was originally classified λ4135, because the strongest line in this star's spectrum is a still unidentified feature at 4135 Å, which was first noticed by Minkowski (1937). However, the

remaining spectral features can be very tentatively identified as lines of neutral helium. The ratios of line strengths are not at all in accord with what one expects for helium-rich white dwarfs (for example, λ6678 is absent). Furthermore, the existence of any lines at all in a star with a surface field of 10^7 gauss in the region which causes the polarization of the continuum is a puzzle. If the interpretation of these features as helium lines is correct, one can tentatively say that the equivalent width of He I $\lambda\lambda$4471 and 5015 is consistent with an effective temperature of 14,000°, while the continuum scan indicates a temperature of 10,000°. I have very tentatively adopted an effective temperature of 12,000° for the purpose of calculating the radius; the interpretation of the spectrum of this peculiar star needs much more work.

VII. SUMMARY

Clearly, work on the peculiar, cooler white dwarfs is only beginning. The spectra of the DA stars have proved to be readily amenable to a straightforward interpretation, and the data indicate a mean radius of 1.3×10^{-2} $R_\odot$ and a median mass of 0.6 solar masses for the DA stars under study in this chapter. The DB stars are somewhat more difficult to interpret because of theoretical uncertainties and the lack of astrometric data, but the radii do not seem to differ drastically from the radii of the DA stars. The DO and sdO stars are quite a heterogeneous group, and are not too easy to analyze because they are so hot. The

DA,F stars are simply cool DA stars with a small admixture of calcium in their atmospheres; the weakness of their hydrogen lines is a consequence of the influence of H^- absorption. There is at least one DA,F star (L 870-2) with a radius twice as large as the radii of other upper-sequence white dwarfs. The peculiar white dwarfs are an extremely mixed group of objects with a wide range of chemical abundances. Further remarks based on the analyses in this chapter will be found in Chapter 6.

TABLE 1 - PARALLAXES AND MAGNITUDES

Star	π (".001)	Qual., Total Wt.	Source	M_V	Source
HZ 4	025±03	B	Hyades	14.47	H
LB 1240	036 03	C(20)	USNO	13.80	60(3)
LB 227	025 03	B	Hyades	15.35	100(1)
HZ 2	025 03	B	Hyades	13.86	H
40 Eri B	202 04	A(67)	Yale	9.52	200(2)
HZ 7	025 03	B	Hyades	14.18	H
HZ 14	025 03	B	Hyades	13.83	200(2)
He 3	060 10	B(35)	Yale	12.10	60(2)
SA 29-130	032 03	C(28)	Yale,USNO	13.30	H
L 970-30	046	C	EG I	12.92	100(3)
W 485 A	062 06	B(31)	Yale,USNO	12.30	100(3)
+70°5824	027 12	D(7)	Yale	12.79	H
W 1346	072 10	B(59)	Yale*	11.54	H
+73°8031	045 10	D(9)	Allegheny	12.88	H
L1512-34B	069 15	C	Allegheny*	12.90	200(3)
LDS 235B	011	C	EG I	15.55	200(2)
LDS 749B	021 03	C(16)	USNO	14.73	100(3)
L 930-80	052 15	D-	Gliese*	14.80	100(1)
HZ 43	021 11	D(10)	Allegheny	12.86	H
L 870-2	061 13	C(6)	Yale	12.84	H
L745-46A	146 07	B(15)	Yale	12.98	100(2)
R 627	074 10	C(23)	Yale,USNO	14.24	H
R 640	056 07	C(15)	Allegheny	13.86	100(2)
+70°8247	081 10	B(24)	Yerkes	13.19	H
L 1363-3	074 04	C(17)	USNO	13.23	100(3)
G 47-18	056	C	E69	15.18	100(1)

Notes

The sources are: Hyades - Wayman et.al.(1965;see text); Yale= Jenkins (1963; General Catalogue of Stellar Parallaxes); Allegheny=Wagman (1967); USNO=Riddle (1970); Gliese= Gliese (1969; Catalogue of Nearby Stars); Yerkes=van Altena (1971); EG I=Eggen and Greenstein (1965a); E69= Eggen (1969); H=Harris (1956). Parallaxes from EG I or E69 are based on proper-motion companions. The numbers in column 6 indicate the size of the Hale Observatories telescope and the number of observations used for photometry.

W 1346 - In addition to the parallaxes cited by Jenkins, Wagman gives π=.072.

L 1512-34B - Wagman (1967) gives π=.057, while EG I give π=.080 from the luminosity of L 1512-34A. I have used the mean.

Notes to Table 1 (continued)

L 930-80 - This value is very doubtful as it leads to a rather small radius for this star. Furthermore, Gliese (1969) gives no source for his value, which makes it very difficult to evaluate this parallax.

TABLE 2 - ATMOSPHERIC PARAMETERS

EG No.	Star	T_{eff}	log g	Spectrum
26	HZ 4	15,300± 400	8.1 ±0.30	DA
28	LB 1240	13,800 500	7.5 0.30	DA
29	LB 227	16,500 500	8.5 0.30	DA
31	HZ 2	22,500 500	8.0 0.20	DA
33	40 Eri B	17,000 500	7.75 0.15	DA
39	HZ 7	23,000 500	7.9 0.20	DA
42	HZ 14	34,000 1000	8.5 0.40	DA
50	He 3	25,000 700	8.1 0.15	DA
67	SA 29-130	14,500 500	8.0 0.30	DA
76	L 970-30	16,000 500	7.9 0.20	DA
184	GD 140	23,000 800	8.2 0.50	DAn
99	W 485 A	15,500 500	8.5 0.30	DA
102	+70° 5824	21,000 1000	7.7 0.30	DA
192	GD 185	19,000 500	9.1 0.50	DAn
139	W 1346	20,000 700	7.3 0.30	DA
144	+73°8031	16,000 500	7.7 0.30	DA
162	L 1512-34B	14,000 300	7.9 0.30	DA
63	LDS 235B	15,000 1000	8.0:	DB
77	Ton 573	14,000 1000		DB
193	GD 190	18,000 2000	8.5 ±1.0	DB
133	L 1573-31	15,000 1000		DB
145	LDS 749B	14,000 1000	7.5 ±0.6	DB
149	L 930-80	16,500 1000	8.0 ±0.5	DB
20	F 24	50,000+	6.6+	DAwk
	G 191	50,000+	6.0+	sdO
86	HZ 21	70,000+	~8	DO
98	HZ 43	50,000±5000	8.8±1.0	DAwk
	HZ 44	50,000 5000	6.5 1.0	sdO
11	L 870-2	6,500 500		DA
54	L745-46A	5,000 (1)		DF
54	L 745-46A	7,000 (2)		DF
79	R 627	7,000±500		DA,F
119	R 640	6,000 (1)		DF
119	R 640	8,000 (2)		DF
248	G 99-37	5,000(1)		DGp(CH)
248	G 99-37	7,000(2)		DGp(CH)
182	G 47-18	10,000(1)		λ4670
182	G 47-18	12,000(2)		λ4670
129	+70°8247	12,000±1000		λ4135
148	L 1363-3	6,000(1)		DC
148	L 1363-3	8,000(2)		DC

NOTE FOR TABLE 2

For L 745-46A, R 640, G 99-37, G 47-18, and L 1363-3, effective temperatures denoted by (1) are derived under the assumption that the star is helium-rich and those denoted by (2) are derived by fitting black-body curves to the scans.

TABLE 3 - MASSES, RADII AND LUMINOSITIES

Star	log $M/M_\odot$	log $R/R_\odot$	log $L/L_\odot$
HZ 4	$-.09\pm.30$	$-1.92\pm.06$	$-2.09\pm.12$
LB 1240	$-.80\ .30$	$-1.92\ .05$	$-2.36\ .10$
LB 227	$-.28\ .30$	$-2.12\ .06$	$-2.43\ .12$
HZ 2	$-.20\ .15$	$-1.92\ .06$	$-1.46\ .12$
40 Eri B	$-.35\ .15$	$-1.88\ .02$	$-1.90\ .10$
HZ 7	$-.44\ .20$	$-2.00\ .06$	$-1.47\ .12$
HZ 14	$-.02\ .40$	$-2.04\ .06$	$-1.01\ .12$
He 3	$-.24\ .22$	$-2.00\ .07$	$-1.36\ .14$
SA 29-130	$+.06\ .40$	$-1.80\ .10$	$-1.99\ .30$
L 970-30	$-.27\ .30$	$-1.91\ .10$	$-2.05\ .20$
W 485 A	$+.37\ .30$	$-1.90\ .07$	$-2.09\ .14$
$+70^\circ5824$	$-.11\ .50$	$-1.74(+.26,-.15)$	$-1.23\ .40$
W 1346	$-.83\ .15$	$-1.89\pm.07$	$-1.64\ .14$
$+73^\circ8031$	$-.40\ .35$	$-1.88\ .08$	$-2.00\ .16$
L 1512-34B	$-.49\ .35$	$-2.03\ .07$	$-2.52\ .14$
LDS 235B	0.0:	$-1.78\ .05$	$-1.80\ .20$
LDS 749B	$-.60\pm.60$	$-1.83\ .10$	$-2.12\ .20$
L 930-80	-1.12:	-2.34:	-2.80:
HZ 43	$+.60\pm1.0$	$-1.83(+.28,-.23)$	$-0.02\pm.40$
L 870-2		$-1.41\pm.15$	$-2.63\pm.40$
L 745-46A		-1.45(1)	-3.16(1)
L 745-46A		-1.92(2)	-3.30(2)
R 627		$-1.86\pm.07$	$-3.46\pm.40$
R 640		-1.53(1)	-3.00(1)
R 640		-1.80(2)	-3.16(2)
G 47-18		-1.94(1)	-2.94(1)
G 47-18		-2.07(2)	-2.90(2)
$+70^\circ8247$		$-2.08\pm.10$	$-2.90\pm.30$
L 1363-3		-1.50(1)	-2.94(1)
L 1363-3		-1.67(2)	-2.81(2)

Note: Radii and Luminosities denoted by (1)are calculated on the assumption that the star is He-rich, and those denoted by (2) on the assumption that the star radiates like a black body.

TABLE 4 - HELIUM LINE STRENGTHS (in Ångstroms)

Star	+70° 8247	LDS 235B	GD 190	L1573 -31	LDS 749B	L930 -80
He I λ						
4026	< 3	blend	blend	14.2	4.7	9.6
4471	6.5	22.7	32.6	16.2:	6.0	22.0
4922	< 2	14.2	24.3	14.2	5.1	17.6
5015	6.3				4.8	
5876	11.7	39	22.8	12.4	6.2	13.6

The resolution in the scans used for determining these equivalent widths was 20 Å (LDS 749B), 40 Å (+70°8247), and 80 Å (LDS 235B, GD 190, L 1573-31, L 930-80).

FIGURE CAPTIONS

Figure 1. Emergent fluxes at λ=5480 Å as a function of effective temperature from model atmospheres, where H_V= the flux at 5480 Å and $T_4=T_{eff}/10^4$ °K.

Figure 2. The monochromatic color index $\Delta m=(m_{5560}-m_{3570})$ as a function of inverse effective temperature.

Figure 3. Observed and theoretical energy distributions for Grw+73°8031, a DA star.

Figure 4. Observed and theoretical energy distributions for Hertzsprung 3, a DA star.

Figure 5. Observed and theoretical H_γ profile for 40 Eri B.

Figure 6. Hydrogen line profiles for HZ 2. The ordinate is in magnitudes.

Figure 7. Observed and theoretical energy distributions for L 930-80, a DB star.

Figure 8. Observed and theoretical energy distributions for HZ 43, a DAwk star.

Figure 9. Observed and theoretical energy distributions for L 1363-3 (spectral type DC) and Ross 640 (spectral type DF). The hydrogen-rich model (solid line) is for comparison only; these stars are not hydrogen-rich.

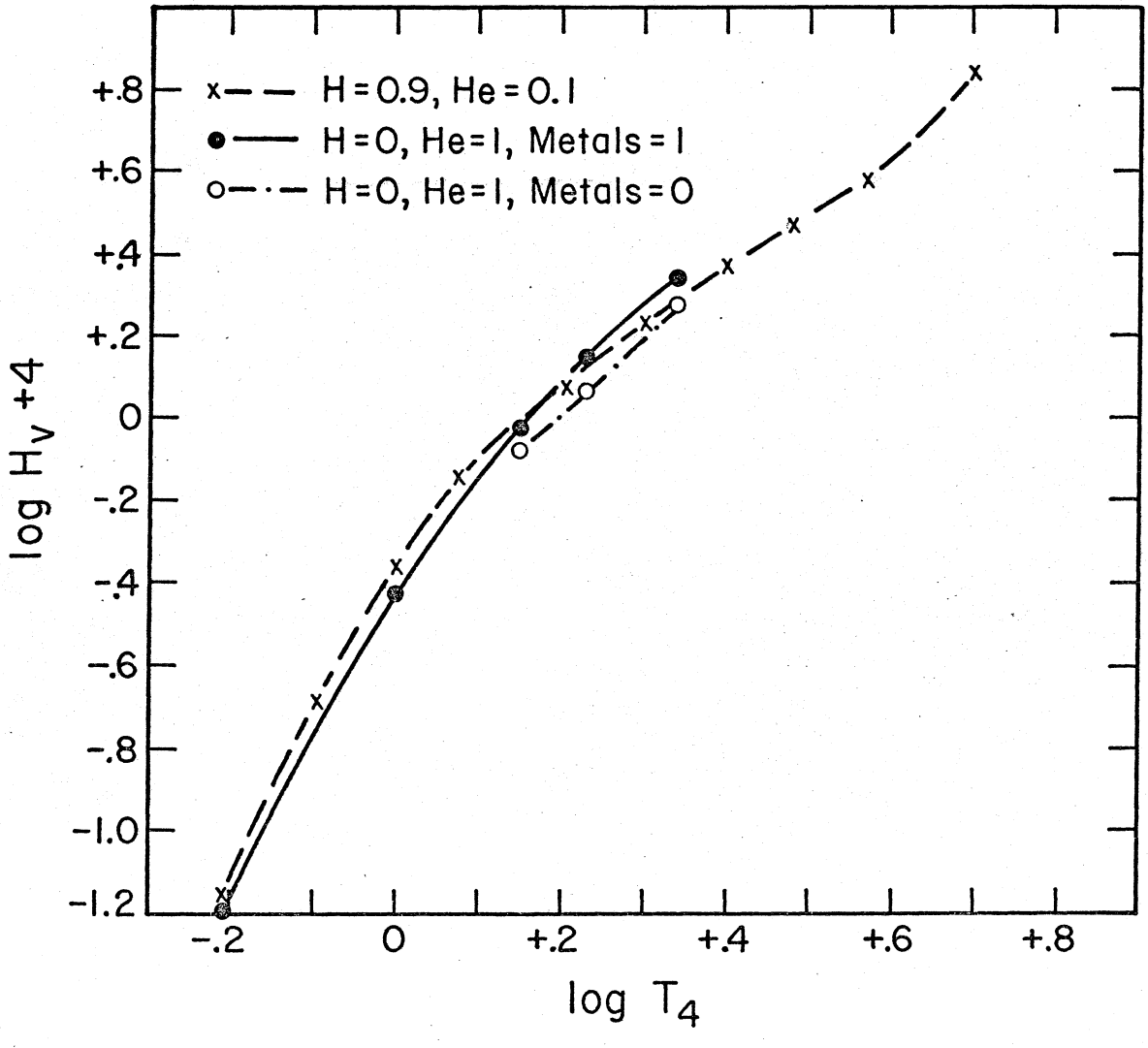
x— — H=0.9, He=0.1
●—— H=0, He=1, Metals=1
○—·— H=0, He=1, Metals=0
+.8
+.6
+.4
+.2
0
-.2
-.4
-.6
-.8
-1.0
-1.2
log H_v +4
-.2
0
+.2
+.4
+.6
+.8
log T_4

Figure 1.

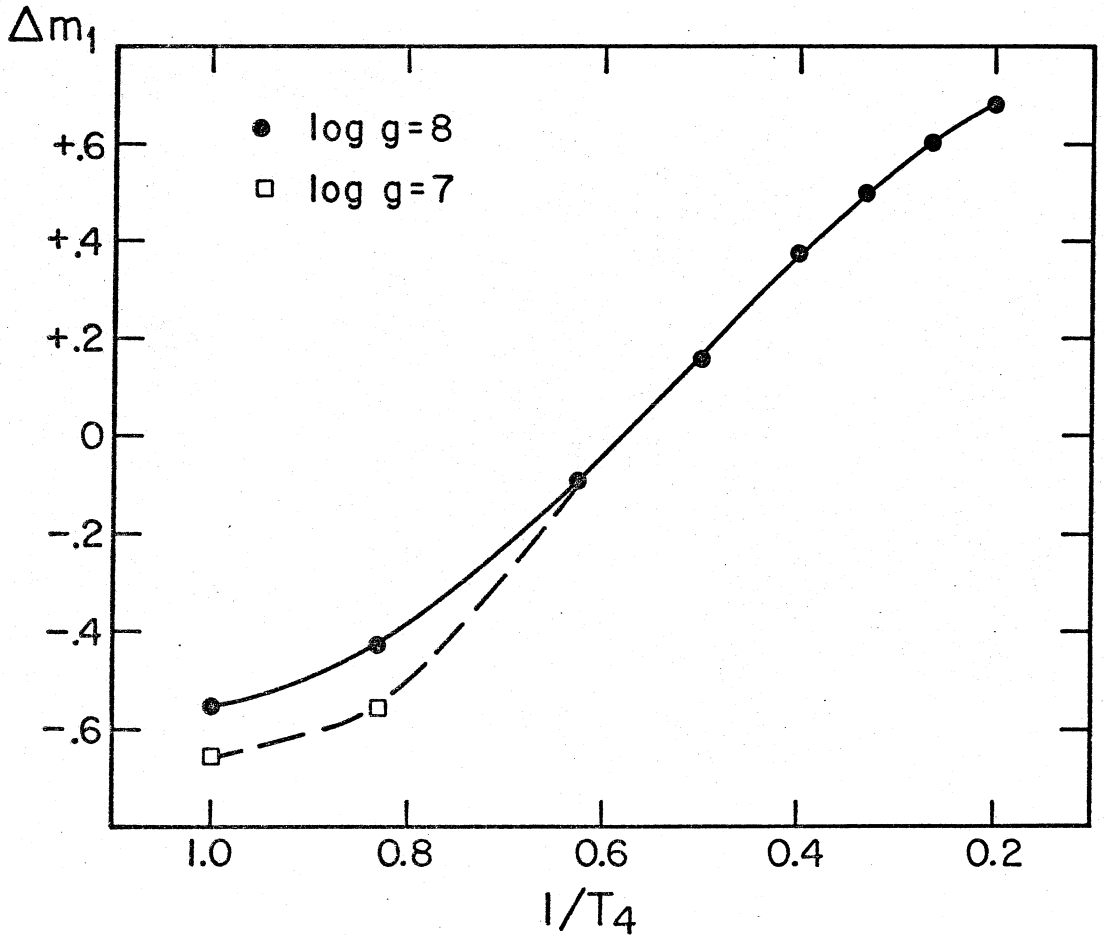

Figure 2.

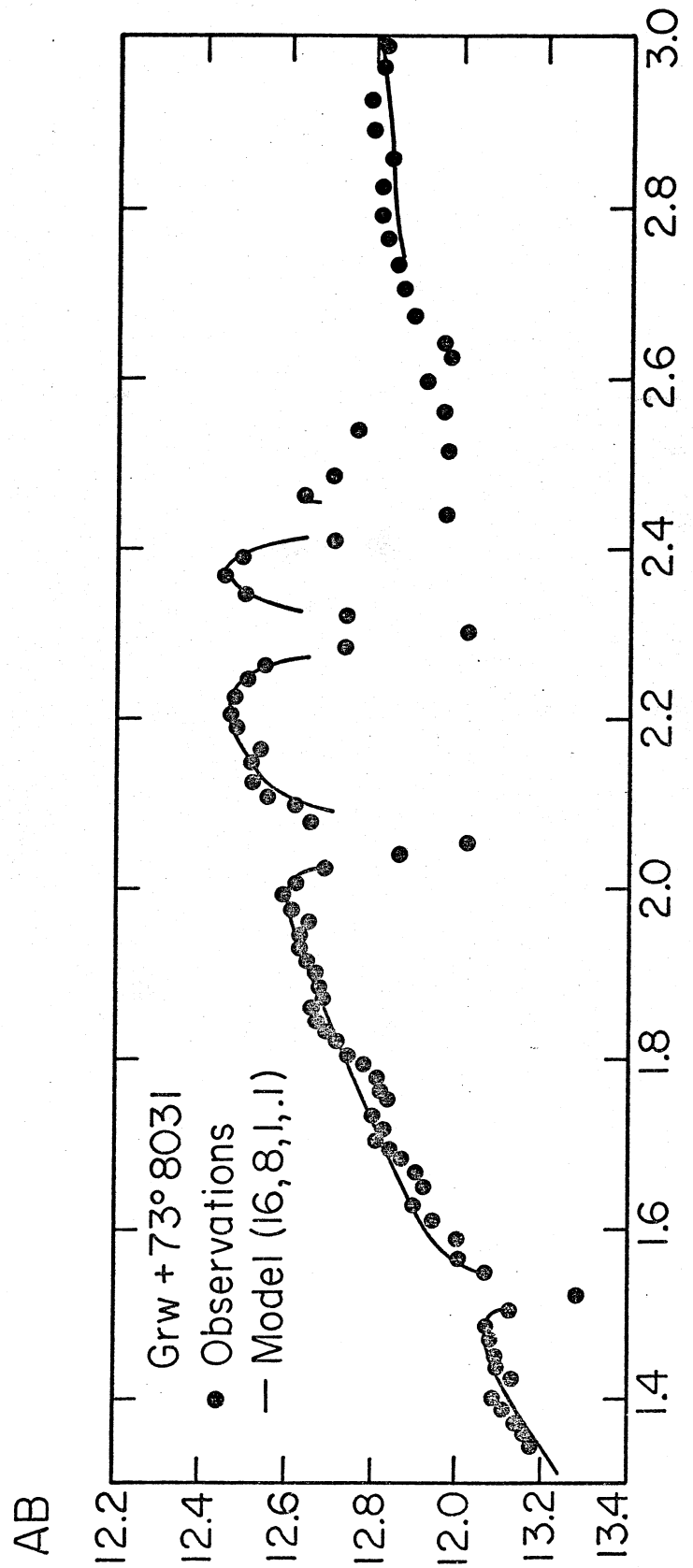
AB
Grw +73° 8031
Observations
Model (16,8,1,.1)
12.2
12.4
12.6
12.8
12.0
13.2
13.4
1.4
1.6
1.8
2.0
2.2
2.4
2.6
2.8
3.0
1/λ (μ⁻¹)

Figure 3.

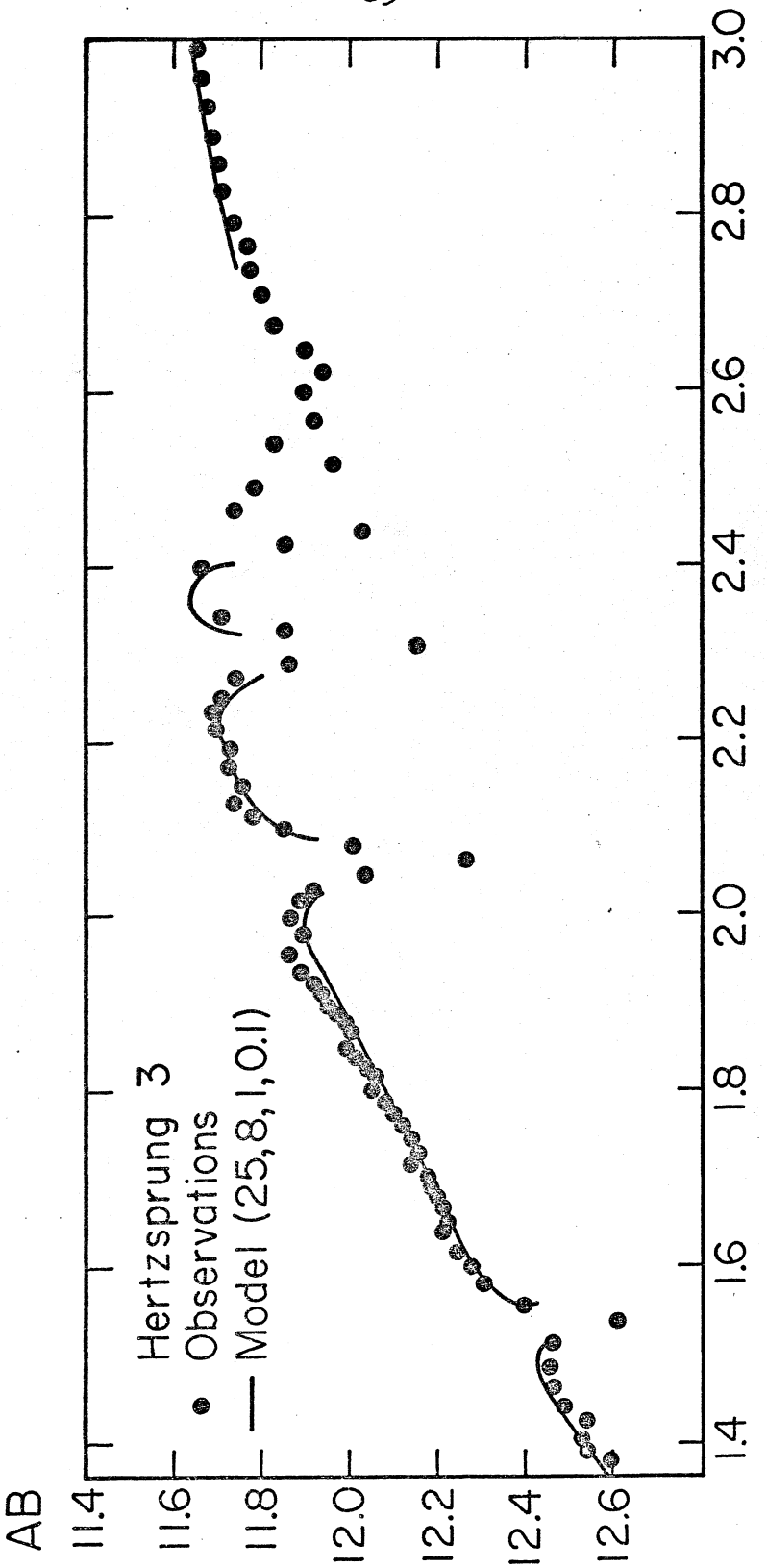
Hertzsprung 3
Observations
Model (25,8,1,0.1)
AB
11.4
11.6
11.8
12.0
12.2
12.4
12.6
1.4
1.6
1.8
2.0
2.2
2.4
2.6
2.8
3.0
1/λ (μ⁻¹)

Figure 4.

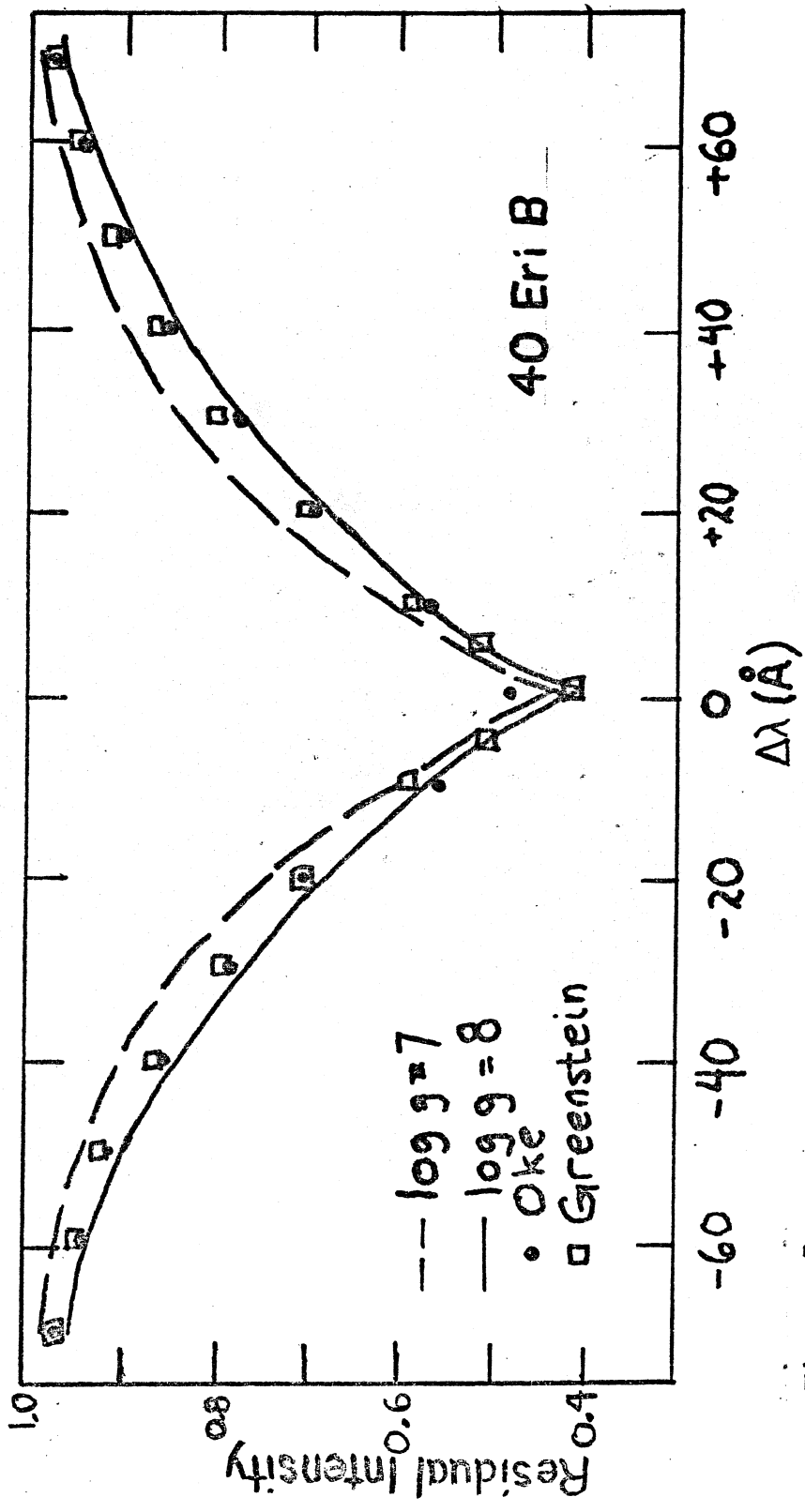
40 Eri B
log g = 7
log g = 8
Oke
Greenstein
Residual Intensity
1.0
0.8
0.6
0.4
-60
-40
-20
0
+20
+40
+60
Δλ (Å)

Figure 5.

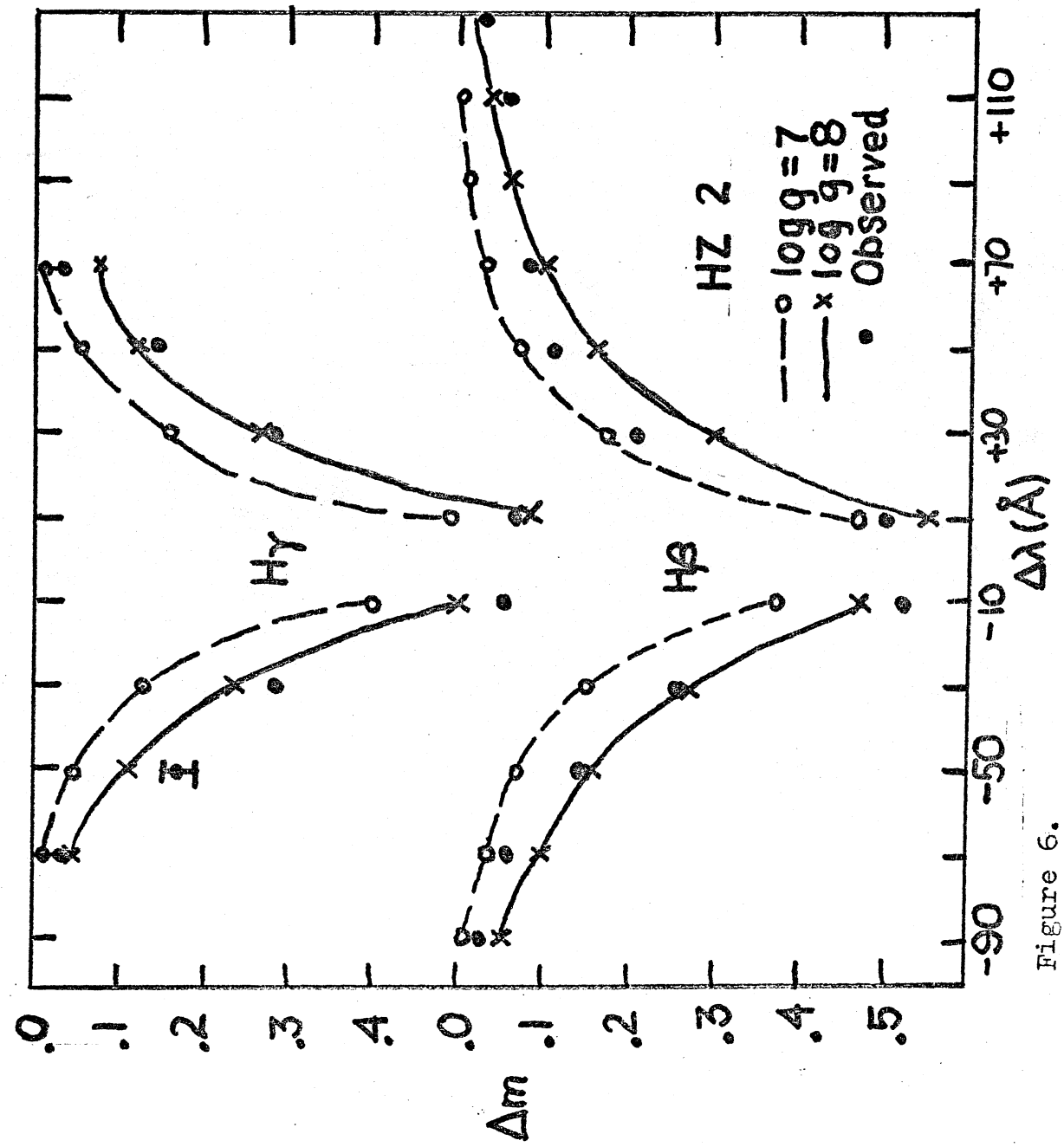
HZ 2
o log g=7
x log g=8
• Observed
Hγ
Hβ
Δm
Δλ (Å)
0.
.1
.2
.3
.4
.5
-90
-50
-10
+30
+70
+110

Figure 6.

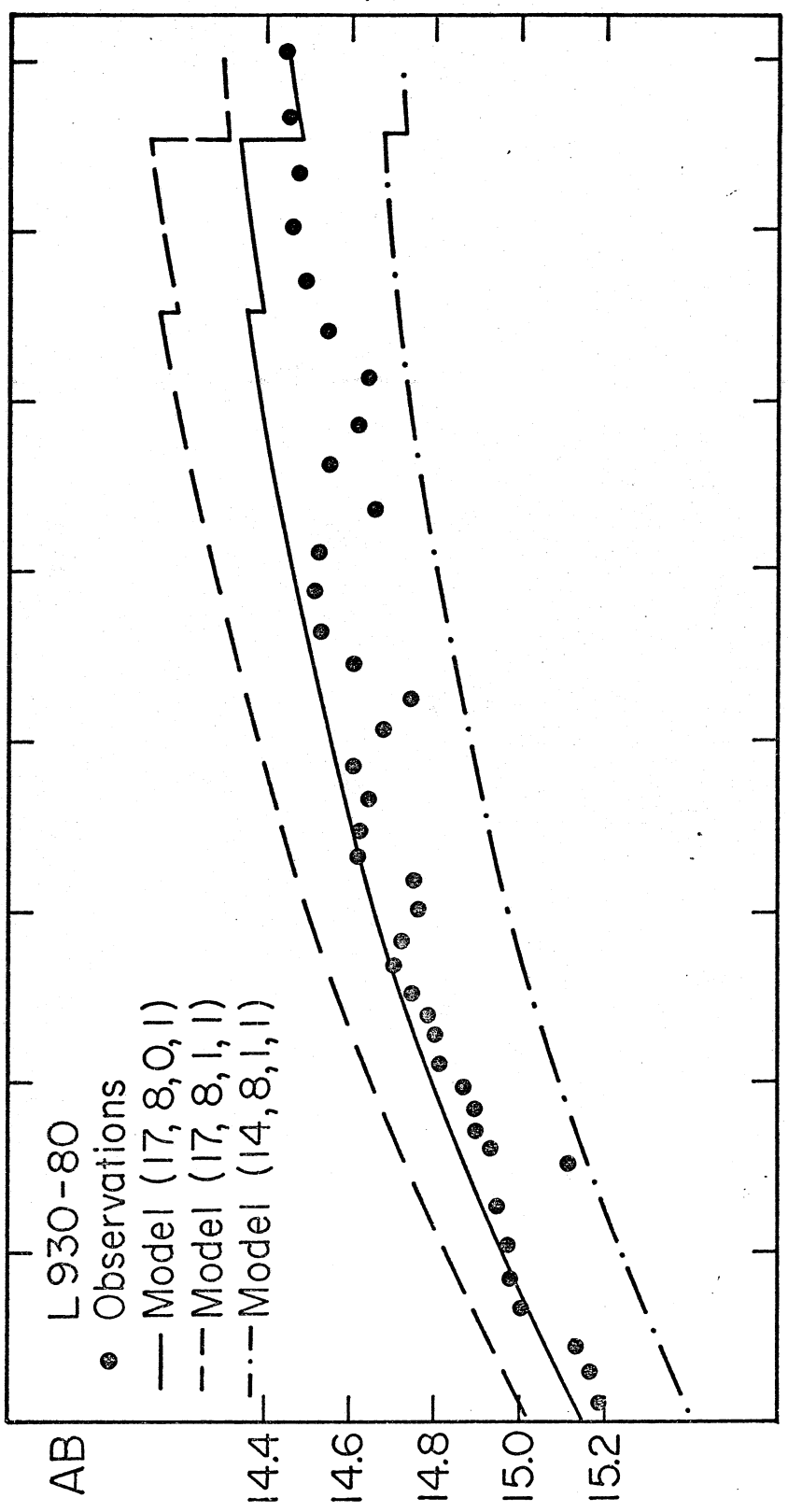
L930-80
Observations
Model (17, 8, 0, 1)
Model (17, 8, 1, 1)
Model (14, 8, 1, 1)
AB
14.4
14.6
14.8
15.0
15.2
1.6
1.8
2.0
2.2
2.4
2.6
2.8
3.0
1/λ (μ⁻¹)

Figure 7.

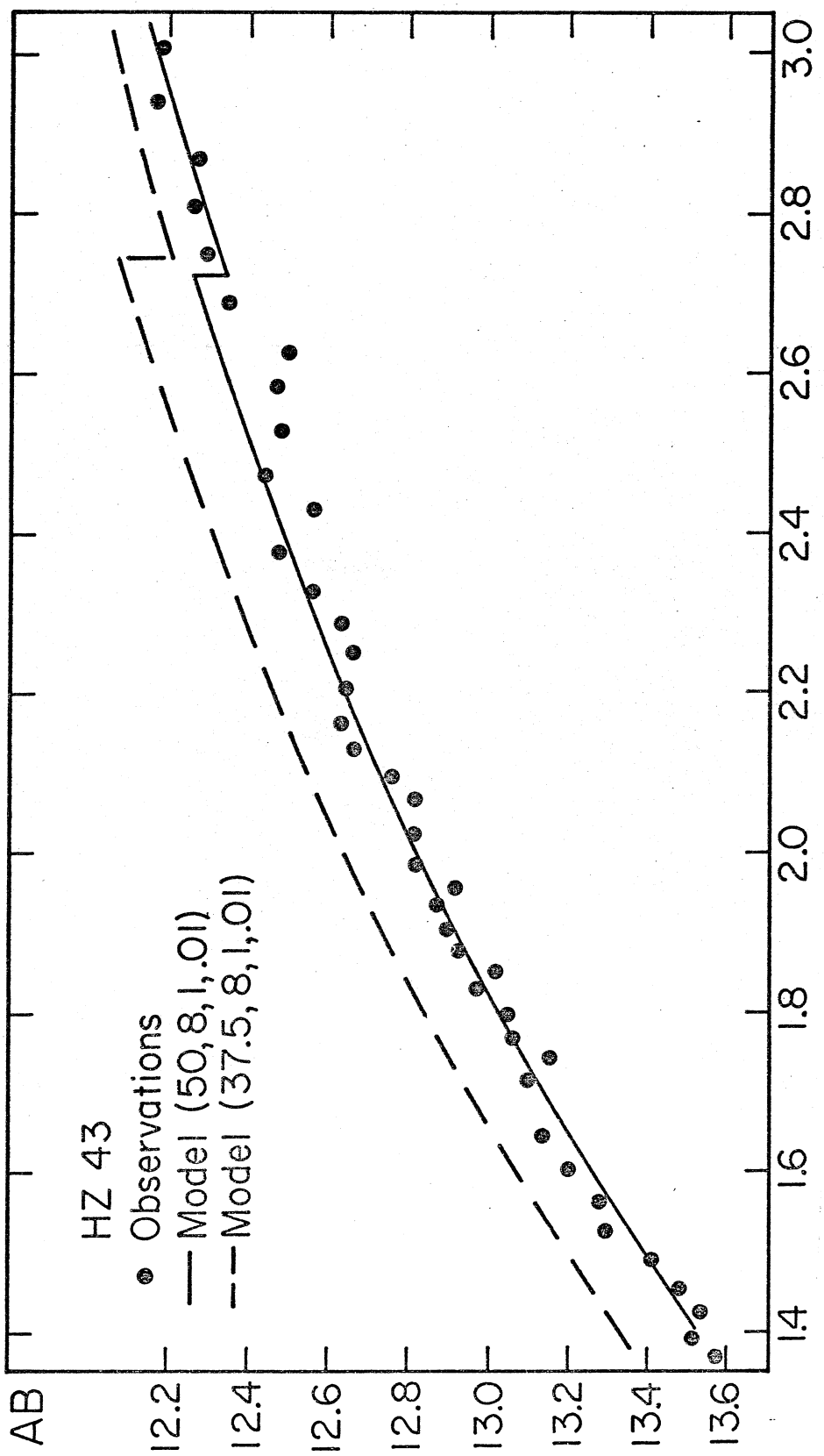
HZ 43
Observations
Model (50,8,1,.01)
Model (37.5,8,1,.01)
AB
12.2
12.4
12.6
12.8
13.0
13.2
13.4
13.6
1.4
1.6
1.8
2.0
2.2
2.4
2.6
2.8
3.0
1/λ (μ⁻¹)

Figure 8.

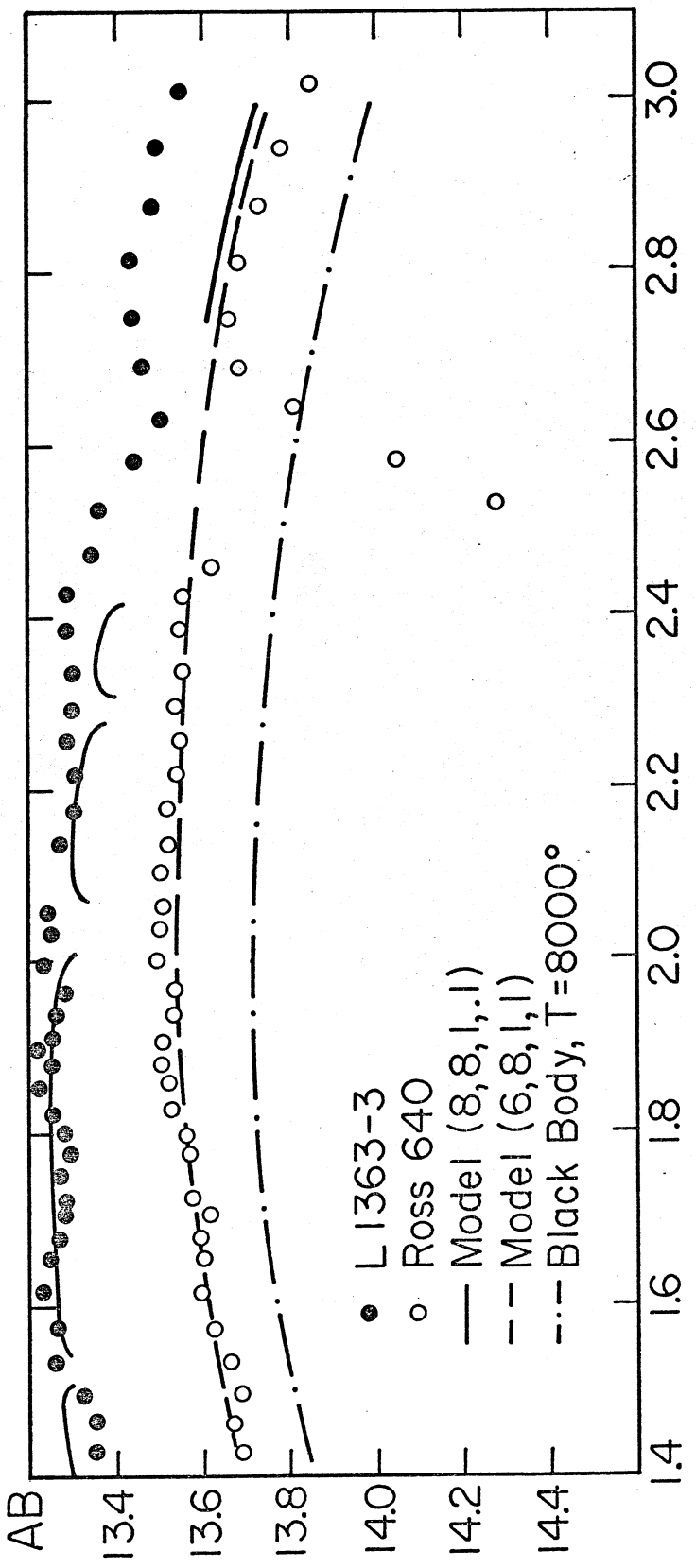
AB
13.4
13.6
13.8
14.0
14.2
14.4
1.4
1.6
1.8
2.0
2.2
2.4
2.6
2.8
3.0
1/λ (μ⁻¹)
● L 1363-3
○ Ross 640
— Model (8,8,1,.1)
– – Model (6,8,1,1)
–·– Black Body, T=8000°

Figure 9.

CHAPTER 5-

SIRIUS B

Summary

The spectrum of Sirius B photographed by Oke and Greenstein has been measured. Combining the hydrogen line profiles with the visual magnitude of Lindenblad (1970) yields T_{eff}=32,000°K, log g=8.70, R=.0078 $R_\odot$. A gravitational redshift of +88±16 km/sec has also been measured from the spectra, and this value is consistent with the radius determined from the hydrogen-line profiles.

Sirius B represents an unusual problem in the interpretation of white dwarfs, in that it is so hard to observe because of the proximity of Sirius A, which is 9.43 magnitudes brighter. The mass is fairly well-known from analysis of the orbit of the system to be 1.02 $M_\odot$ (van den Bos 1960); the only difficulty here being that there have been suggestions from time to time that the system is triple. The analysis by Lindenblad (1970) suggests a systematic pattern in the residuals from his observations, and consequently the mass of Sirius B is not completely well-determined from dynamical considerations.

The $H\gamma$ profile of Sirius B has been published by Oke (1963). Using conventional spectrophotometric techniques, I have measured the $H\alpha$ profile as well. Both profiles are presented in Figure 1, together with various models. The model with T_{eff}=33,000°, log g=8.8 was com-

puted for the purpose of trying to fit the profile; the fit is remarkably good. A profile interpolated from those presented in Chapter 2 with $T_{eff}=29,000^{o}$, log g=8.0 has a shape virtually identical to the ones plotted. A few line profiles from other models are shown in Figure 1 for comparison.

The fitting of hydrogen-line profiles thus defines a locus in the T_{eff}-log g plane, which is shown as the dot-dash line in Figure 2. The error bar represents an estimate of the probable error. Using the visual magnitude of Lindenblad, when combined with a parallax and the fluxes in Figure 1, Chapter 4 yields

$$2 \log R/R_{\odot}=x -1.3 \log T_4 -3.353. \qquad (5-1)$$

If we then use van den Bos' value for the mass, namely 1.02 $M_{\odot}$, I then obtain a second locus in the T_{eff}-log g plane, which is the solid line in Figure 2. These two lines yield $T_{eff}=32,000^{o} \pm 1,000^{o}$, log g=8.65, R=0.0078 $R_{\odot} \pm 0.002\ R_{\odot}$. These values place Sirius B on the mass-radius relation for degenerate configurations of He (see Figure 5 of Chapter 6).

From merely fitting the $H\gamma$ profile to the observations, it is also possible that the effective temperature is $9,300^{o}$K. At this temperature, the hydrogen line shapes are almost completely independent of surface gravity, owing to the similar n_e-dependence of the line and continuum absorption coefficients. Continuum absorption is almost entirely H^{-}. However, trying to fit both the $H\alpha$ and $H\gamma$ profiles to the

observations reveals significant discrepancies (see Figure 1). The $H\alpha/H\gamma$ ratio is too high at cooler temperatures. Furthermore, if the effective temperature is 9300°K, then the predicted radius will be .023 $R_\odot$, which, together with the mass of van den Bos, leads to an expected redshift of 28 km/sec, a result which can probably be, I believe, ruled out by the redshift measurements described below. In addition, with such a radius there would be a very large disagreement with the mass-radius relation. It would be helpful to have a measurement of color to settle the question; even a crude measurement would do, since the U-V color expected from the two temperatures, 9300° and 33,000°, differs by one magnitude. At this time, however, I feel that the data heavily favor the high-temperature interpretation.

Measuring the gravitational redshift of Sirius B is quite difficult. After some experimentation, it was found that the microphotometer was the most suitable instrument for this measurement. By means of a suitable combination of masks, a plate was traced so that the top and bottom halves of the comparison spectrum and the stellar spectrum entered the microphotometer slit simultaneously. Then the center of the hydrogen line in the stellar spectrum was found from the tracing, using only the part of the line within 20 Å of line center. Because

the tracings extended out to 100 Å from line center, the tilt of the background continuum could be taken into account.

Five plates were measured to determine the gravitational redshift; all of these were relatively uncontaminated with the spectrum of Sirius A. Because the lines were less well-exposed, the two measurements of Hβ were given half-weight, as was one of the Hα plates. The individual measurements are tabulated in Table 1. The mean redshift, determined from all of the plates, was +80 ± 16 km/sec, which, when combined with the measured radial velocity of Sirius A, yields a gravitational shift of +88±16 km/sec. The orbit of van den Bos indicates that in 1961 and 1962, when these plates were taken, the orbital motion along the line of sight was less than 1 km/sec. The radius found above predicts a redshift of +83 ± 3 km/sec. I regard this agreement as excellent.

It is also possible to test the accuracy of the dynamical mass. Using equation (5-1) together with the gravitational redshift yields another locus in the T_{eff}-log g plane, which is shown as the dashed line in Figure 2. This line does not assume a fixed value for the mass. Using this line in conjunction with the locus defined by the hydrogen line profiles (for the high temperature case) results in a mass of 1.20 ±.25 $M_{\odot}$, in agreement with van den Bos's value.

Because the surface gravity of Sirius B is so high, it is possible that Stark shifts may play a role. As is shown in Chapter 6, the role of Stark shifts is negligible for white dwarfs with log g=8. Wiese and Kelleher (1971) contend that Stark shifts may be responsible for a sizeable part of the redshift measured in white dwarf spectra. Using the electron densities in the $T_{eff}=33{,}000^{o}$, log g=8.8 model, and assuming that the line shift at a particular wavelength λ is the same as the line shift at $\tau_{\lambda}=1$, I find that the shift expected for Sirius B, from the Stark effect, is about 8 km/sec and may be somewhat less. Because the data of Wiese and Kelleher are somewhat noisy for such small shifts, and because of the complicated nature of the transfer problem, no more definitive statement can be made. At any rate, the Stark shift is considerably less than the errors of measurement.

CONCLUSION

The radius of Sirius B has been measured to be $(7.8 \pm 0.2) \times 10^{-3}$ $R_{\odot}$, assuming that the mass of 1.02 $M_{\odot}$ given by van den Bos (1960) is correct. This value is consistent with the measured value of the gravitational redshift of $+88 \pm 16$ km/sec. There are no indications from the present analysis of the existence of a third companion in the system.

TABLE 1 - MEASUREMENTS OF REDSHIFT

Plate	Line	Weight	$\underline{k}_i$
Pc 6281	Hϵ	1.0	+81 (km/sec)
Pc 7004	Hα	1.0	+99
Pc 7005	Hα	0.5	+73
Pc 6281	Hβ	0.5	+46
Pc 7004	Hβ	0.5	+85
Mean			+80 $\pm$16

FIGURE CAPTIONS

Figure 1. Hydrogen line profiles in Sirius B. Top: Hγ. Bottom: Hα . The notation corresponds to $T_{eff}/10^4$, log g, metal abundance/solar value, as usual.

Figure 2. Loci in the T_{eff}-log g plane. Solid line: Locus assuming that the visual magnitude of Lindenblad (1970) and the mass of van den Bos (1960) are constant. Dot-dash line: Locus from fitting hydrogen line profiles. Dashed line: Locus of constant visual magnitude and gravitational redshift, but varying mass.

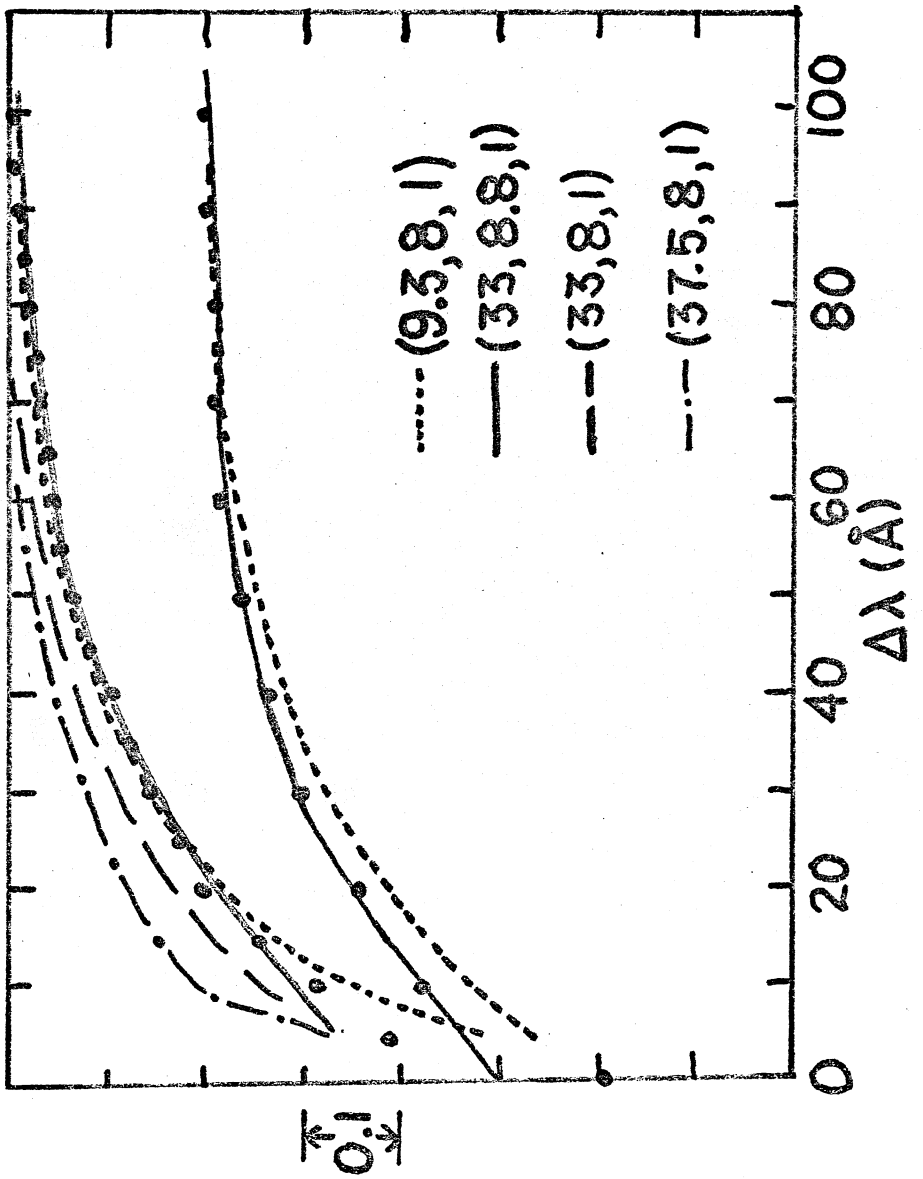

Figure 1.

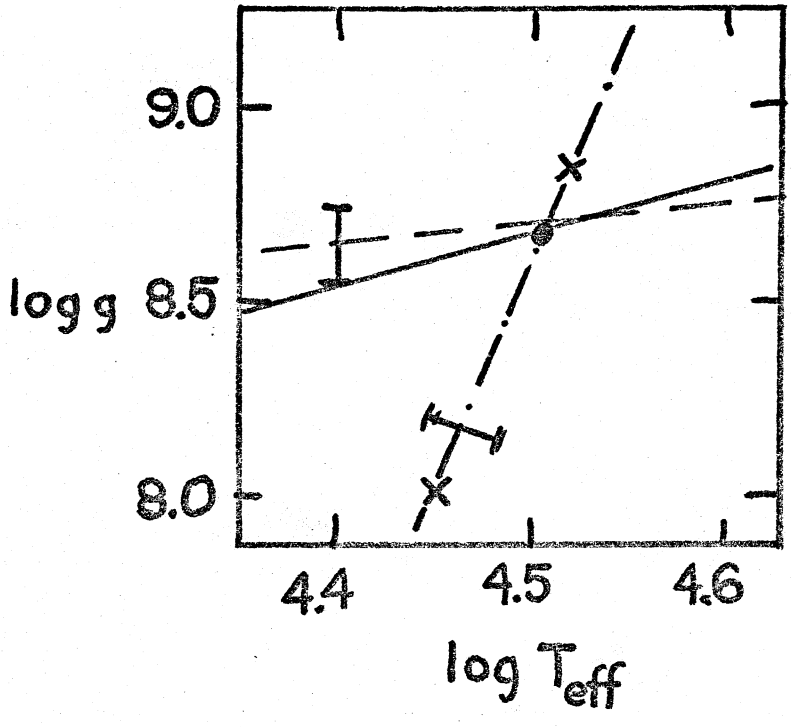

Figure 2.

CHAPTER 6

FURTHER APPLICATIONS

Summary

The stars analyzed in Chapter 4 are used to establish a T_{eff} - (U-V) relation for hydrogen-rich and helium-rich white dwarfs. These temperature scales are then used to derive luminosities, radii, and in some cases masses for white dwarfs with known distances. Spectroscopic masses and radii are then compared with the gravitational redshift results of Greenstein and the theoretical mass-radius relation; the agreement is satisfactory considering the substantial errors involved. I find a median mass of 0.52 $M_\odot$ and a median radius of 0.095 $R_\odot$.

The evolution of the white dwarfs through the H-R diagram is then discussed. I find that, given any reasonable supposition about the way white dwarfs evolve, the cool ($T_{eff} \leq 10{,}000^\circ$) DA and DA,F stars on the upper sequence cannot be the evolutes of hotter DA stars, confirming the suggestions of Chin and Stothers (1971). The existence and observed temperatures of the DB, DC, and λ4670 stars are then explained by a modification and extension of the convection-accretion hypothesis of Strittmatter and Wickramasinghe (1971).

I. INTRODUCTION

In Chapter 4 I derived temperatures, masses, radii, and luminosities for 37 white dwarfs from intermediate-band photoelectric scans. Broad-band photoelectric

observations are available for a much larger number of white dwarfs, and, in order to increase the statistical basis for any conclusion about the evolution of white dwarfs, it is helpful to use the results of Chapter 4 to calibrate the broad-band observations. The main difficulty with calculating, say, a U-V color index directly from a model atmosphere is that the transmission function and the zero point of the filters, particularly the U filter, are not known well enough. Errors as large as 0.05 magnitudes are possible. Consequently, using the bootstrap method which has played such an important role in the development of astronomy, it is possible to define a temperature scale using the well-observed stars of Chapter 4 and then make meaningful comments about a much larger statistical sample of stars.

II. TEMPERATURE SCALES: "AN ASTROPHYSICAL PUZZLE"REVISITED

Greenstein and Trimble (1967) have discussed the problem of determining temperature scales for the white dwarfs, and have labled the situation as an astrophysical puzzle in view of the large differences between the temperature scales then available. In figure 1,I have plotted the effective temperatures of the white dwarfs of type DA and DA,F analyzed in Chapter 4 against their U-V color (where, as usual, $\theta_{eff}=5040/T_{eff}$). The smooth curve defines the temperature scale for hydrogen-rich white dwarfs. The reason for the abrupt change of slope

at θ=0.35 is that at this point the Balmer jump becomes smaller with increasing θ_{eff} (or decreasing T_{eff}) and, consequently, the U-V color becomes redder more slowly. This behavior is also evident in the relation between the monochromatic color index ($m_{5560} - m_{3570}$) defined directly from the models in Chapter 4 (see Figure 2, Chapter 4). It would clearly be helpful to have a few more points in the range $-.45 \leq (U-V) \leq -.20$ to better define the temperature scale, but I believe that substantial errors are unlikely.

The other curves in Figure 1 represent the other temperature scales discussed by Greenstein and Trimble (1967, hereby referred to as GT). "TM" refers to the temperature scale of Terashita and Matsushima (1966; 1969, Matsushima and Terashita 1969a,b) who computed UBV colors directly from the models. Their scale suffers from the difficulties mentioned above. "W" refers to the temperature scale of Weidemann (1963), who determined the effective temperatures of several DA stars from the central depths of the hydrogen line profiles and approximate model atmospheres. "GT" refers to the scale originally defined by Eggen and Greenstein (1965, hereafter EG I) which was established by interpolating between the main-sequence and the black-body line in the two-color U-B vs. B-V diagram. Clearly the present temperature scale represents an improvement.

I have also attempted to define a U-V vs. T_{eff}

relation for the DB and DC stars. Not as many photoelectric observations for these stars are available; furthermore, the model atmospheres used to define this temperature scale are much more uncertain because of the difficulties with convection, the uncertainties in metal abundance, and the uncertainties in the He^- absorption coefficient. The temperature scale is presented in Figure 2. The two points marked "F" represent the DF stars L 745-46A and Ross 640;"mag" is Grw+70°8247, a star with circular polarization, and "4670" is G47-18, a star with carbon bands, and"C" is L 1363-3. The dots are DB stars. The temperature scale is drawn on the assumption that DC stars are cool versions of DB stars (see below). Clearly, the effective temperatures of these stars are well-defined only for $T_{eff} > 12{,}000^{\circ}$ ($\theta_{eff} < 0.43$) - the extension of the scale to cooler temperatures may be regarded as a preliminary attempt. In extending the scale to the DC stars, it was not assumed that the λ4670 and λ4135 stars belonged on the scale; they are merely plotted for comparison. The DF stars may well be helium-rich stars with some Ca in their envelopes (see Chapter 4).

III. LUMINOSITIES AND RADII

Using the temperature scales in Figures 1 and 2, it is possible to calculate masses and radii for white dwarfs of known distances. The absolute magnitudes of white dwarfs have been discussed by Eggen (1969), and the reader is referred to that paper for the parallaxes used here.

I have amalgamated Eggen's lists into two sets of parallax determinations: first class distances based on large parallaxes measured at more than one observatory, (Eggen's Table 1), common proper motion pairs with the non-white dwarfs member a main sequence star bluer than B-V=1.2 mag (Eggen's Table 2), and members of the Hyades and Praesepe (Eggen's Table 3, and Table 4 of EG I). The white-dwarf member of the Pleiades was not included here, as the temperature scale of Figure 1 does not extend to U-V=-1.30. The distance modulus of the Hyades was assumed to be m-M=+3.03 (Chapter 4). The first-class determinations of distance lead to errors in the radii of less than 0.08 in the logarithm.

The second-class distance determinations (Eggen's Tables 4 and 6) are based on trigonometric parallaxes greater than 0".03, many of which have only been determined at one observatory, and common motion pairs containing a very red dwarf. In the trigonometric parallax cases, the estimated errors in the radii are smaller than 0.15 in the log. It is difficult to guess the errors arising from the proper-motion pair determinations, but an error of 0.15 dex in the radius corresponds to an error of 0.75 in the absolute magnitude. I feel that this is an upper limit to the uncertainty in the luminosity of the pairs in Eggen's Table 6. The third-class determinations listed in Table 1 are from Eggen's Table 7, where I have included only those stars with $\pi \geq 0".01$. They are extremely

uncertain, with the deduced radii having errors of as much as a factor of 2. I have also included, where applicable, the parallaxes of Riddle (1970).

Radii were computed from the colors and magnitudes following the same procedures as in Chapter 4. The photometry was taken from the papers of Eggen and Greenstein (EG I, Eggen and Greenstein 1967a,b; hereafter EG II, III), or from Eggen (1969) if the star was not listed in EG. If the spectral type was unavailable, the star was assumed to be of type DA.

A Hertzsprung-Russell diagram compiled from the first and second-class determinations is shown in Figure 3. Some of the points were taken from Chapter 4, and the first-class determinations (uncircled points) were those in parallax classes A and B of that chapter, and the second-class determinations (circled points) were those in parallax class C. The third-class determinations of Table 1 and the D-class parallaxes of Chapter 4 were not plotted. Also shown are the upper sequence of Eggen and the two crystallization sequences of Van Horn (1968). The appearance of Figure 2 demonstrates that there is probably some validity to the two sequence hypothesis, although the lower sequence is somewhat diffuse.

The one thing that is clear from Figure 3 is that the white dwarfs on the red end of the upper sequence have radii that are considerably greater than those on the blue end. It is not possible to account for this difference

by an error in the temperature scale; for the well-determined temperatures of L 870-2 and Ross 627 would have to be in error by as much as a factor of 2. I believe that such errors can definitely be ruled out. The evolutionary significance of this fact will be discussed in section V below.

IV. MASSES

It is possible also to compute masses for a few more stars than were treated in Chapter 4. Graham (1969 and unpublished) has done Stromgren uvby photometry on a large number of white dwarfs. The m_1-index, defined by

$$m_1=(v_{4100} - b_{4670}) - (b_{4670} - y_{5500}) \quad (6\text{-}1)$$

where the subscripts indicate the central wavelength of the relevant filter, is a useful indicator of Hδ strength in white dwarfs, although it was originally established as a metallicity index. In the same way as for the temperature scales, the m_1-index was calibrated using the stars analyzed in Chapter 4. The effective temperature and surface gravity of each star was used to compute a theoretical Hγ equivalent width from the model atmospheres of Chapter 2. This theoretical width was used instead of the observationally measured Hγ strength so that the uncertainties of measuring line profiles near line center with 20 Å filters did not enter the reduction procedure. A plot of these theoretical widths versus the m_1-index for each star

(Figure 4) defines a calibration curve for the m_1-index. The dashed portion of the curve is less certain, but was not used in the computation of masses. Then, for the stars in Table 2, this relation was used to compute an Hγ equivalent width for each star, and use of the model atmospheres provided a surface gravity and hence a mass. The masses listed in Table 2 have been adjusted by +0.1 in the logarithm to account for the low helium abundance in white dwarfs (cf. Chapter 4). The uncertainties in this procedure are considerable, so that the derived masses are uncertain by about 0.4 in the logarithm. Unfortunately it was not possible to compute masses for the cooler stars, since the hydrogen line strengths are almost independent of surface gravity. The star LDS 678B has extremely weak hydrogen lines for its color - the m_1-index gives W(Hγ) = 5.1 Å, while log g=8 at the same temperature gives W(Hγ)= 33 Å. This star is probably underabundant in hydrogen, since its luminosity is well-determined by the first-class parallax, and deserves detailed study.

Given the masses in Table 2, and those derived in Chapter 4, it is possible to compare "atmospheric" masses with those derived from gravitational redshifts. The excellent agreement between the atmospheric mass of 40 Eri B and the mass determined from the redshift of Popper (1954) has been mentioned in Chapter 4. Other gravitational redshifts have been measured by Greenstein and Trimble

(1967), and a comparison of the redshifts they measure and the redshift predicted from the model-atmosphere results using the familiar equation

$$\underline{k}=0.635\ (M/M_\odot)\ (R/R_\odot)^{-1}\ \text{km/sec} \qquad (6\text{-}2)$$

is shown in Table 3. It is evident that the atmospheric redshifts are somewhat smaller than those measured by Greenstein and Trimble. The mean value of $\underline{k}$ (atmospheric) - $\underline{k}$ (observed) is -19 km/sec. From the discussion of GT, however, it is evident that such a systematic effect is not out of the question. The difference of 19 km/sec corresponds to a wavelength shift of 0.3 Å at Hγ, and is less than 1% of the half-width of the line in a typical white dwarf spectrum.

It is also possible to compare mean values of the masses from both atmospheres and redshifts. The mean mass from Table 2 and the data in Chapter 4 is 0.54 $M_\odot$. Using the temperature scale of Figure 1, the GT mean value of $\underline{k}$=+65.6 km/sec corresponds to a mass of 0.98 $M_\odot$. A mean radius of 0.0095 $R_\odot$ was taken from the data in Table 1 and Chapter 4. If one assumes that the redshifts of GT are all 19 km/sec too high, the mean mass becomes 0.70 $M_\odot$. It is interesting that this last value for the mean mass, when combined with the mean radius of 0.0095 $R_\odot$, falls exactly on the mass-radius relation for degenerate configurations of Mg. It is possible, of course, that the atmospheric

masses are systematically in error, although the excellent agreement in the case of 40 Eri B would seem to indicate that there are no serious problems with the atmospheric results. Clearly more observational work on gravitational redshifts is needed. It is interesting that the mass of the horizontal branch stars is 0.5-0.6 $M_\odot$ (Demarque and Mengel 1971; Newell 1970; Newell, Rodgers and Searle 1966a,b), which is very close to the median atmospheric mass of 0.54 $M_\odot$ for white dwarfs.

Wiese and Kelleher (1971) have suggested that a sizeable part of the gravitational redshift is due to a pressure shift. Such an effect would cast doubt on the well-determined agreement between model-atmosphere and gravitational-redshift results for 40 Eri B. However, my model-atmosphere work indicates that for log g=8 the electron densities at $\tau_\nu=1$ are less than 10^{16} cm^{-3} for wavelengths within 30 Å of line center. According to the laboratory measurements of Wiese and Kelleher, such densities correspond to a negligible pressure shift (<0.1 Å, or <6 km/sec for Hγ).

The reason that the electron densities are so surprisingly low (the electron densities at $\tau_{5000}=1$ are almost an order of magnitude higher) is the peculiar nature of the transfer problem. What determines the emergent flux in a spectrum line is the value of the source function S at $\tau_\nu \approx 1$. For the line intensity to be, for

instance, 75% of the continuum intensity means that $S(\tau_{line}=1) = S(\tau_{continuum}=1)$. However, the source function is not a linear function of optical depth, and the above relation does not mean that $\tau_{line}=1$ refers to the same point in the atmosphere as $\tau_{continuum}=0.75$; in fact, for the Hα profile of a $T_{eff}=25{,}000^{o}$, log g=8 model, the above condition means that $\tau_{line}=1$ corresponds to $\tau_{continuum}=0.0089$. Since the electron density varies as the square root of the optical depth in a fully ionized atmosphere, for the $25{,}000^{o}$ log g=8 model the part of the Hα profile where the line depth=0.25 ($\Delta\lambda$ =5 Å) corresponds to an electron density of 10^{15} cm^{-3}, about 1/10 of the density at $\tau_{continuum}=1$. Far out in the line wings, of course, there may well be a line shift, but the measurements of gravitational redshifts are made in the line center. For higher surface gravities, the Stark shifts are more important (although they are still, in general, less than the observational errors; see Chapter 5). The model-atmosphere results, however, indicate that log g 8 for most white dwarfs.

One can also compare the atmospheric masses and radii with the mass-radius relation for degenerate configurations. The mass-radius relation itself is somewhat indeterminate, owing to the lack of knowledge of the coupling between the electrons and ions in a degenerate star. While the degeneracy pressure is known fairly

accurately, the problem is that the electrons contribute the pressure and the ions contribute the mass, so that if the coupling between them is less than perfect, the modifications to the equation of state are appreciable. However, this effect, and thermal effects owing to the fact that white dwarfs are not at zero temperature, are most serious at low masses. The mass-radius relations computed by Hamada and Salpeter (1961) for zero-temperature stars and by Hubbard and Wagner (1970) for stars with $L=10^{-2}L_{\odot}$ are plotted in Figure 5. The effects of rotation discussed by Ostriker and Bodenheimer (1968; see also Tassoul and Ostriker 1968; Ostriker and Tassoul 1970) are also indicated in the diagram. The observed masses and radii are from Chapter 4 and Table 2.

Highly accurate masses from binary-star orbits are only available for 40 Eri B, Sirius B, and Procyon B. The radius of Procyon B is unknown, because spectroscopic observation of it is impossible, and the mass of Sirius B may be in error because the system may be triple (see Chapter 5). For other stars, it would clearly be premature to make any conclusions about their compositions on the basis of this diagram. The two stars with very high masses (W 485 A and HZ 43) should not, at this time, be regarded as evidence for the existence of rapidly rotating white dwarfs with masses above the Chandresekhar limit. Although rotation would explain their high masses, a more probable explanation is that the mass is in error; the uncertainties

in the mass determinations of these two stars are considerable.

V. EVOLUTION OF WHITE DWARFS

Chin and Stothers (1971) have suggested that the white dwarfs are divided into two groups - the hotter ones, which are fairly massive ($\sim 1\ M_\odot$) and which occupy the blue half of the H-R diagram, and the red white dwarfs, which, they contend, are low-mass ($\sim 0.1\ M_\odot$) and have not passed through the Harman-Seaton (1964) evolutionary track for planetary nuclei or any similar track in the high-temperature part of the H-R diagram. The appearance of Figure 3 and the analysis in Chapter 4 make it clear that, for $T_{eff} < 10{,}000^\circ$, there exists a sizeable number of white dwarfs with radii substantially greater than 0.01 $R_\odot$ - a typical radius for DA stars with $T_{eff} \geq 12{,}000^\circ$K. This suggestion was advanced earlier by Eggen and Greenstein (EG III) for the extremely red ($U-V \sim +1.2$) subluminous stars. It is unreasonable to suppose that in the course of cooling off into the black dwarf state, a white dwarf could <u>increase</u> its radius. There is also weak evidence for an increase of radius along the upper sequence as one progresses towards cooler temperatures, even for $T_{eff} \geq 10{,}000^\circ$K (see Figure 3).

Consequently one probably must abandon the thought of the upper sequence as an evolutionary track, and a very attractive alternative interpretation is that the

region of the upper sequence represents a region in the H-R diagram in which the evolution takes place more slowly than in the other regions. In other words, when a white dwarf reaches the region of the upper sequence, no matter what its previous evolutionary history has been, it will remain on the upper sequence for an appreciable amount of time. This is a generalization of the suggestion of van Horn (1968) that the upper and lower sequences represent crystallization sequences, where the white dwarf can cool for a long time without appreciably changing its internal temperature. His conclusion is based on the assumption that the solidification of white-dwarf matter is a first-order phase change, an assumption which has been questioned by Mestel and Ruderman (1967). Consequently, one can accept the suggestion of Chin and Stothers without dropping the idea of two sequences of white dwarfs in the red as well as the blue region of the H-R diagram. What may happen is that as a low-mass white dwarf follows the evolutionary track of Chin and Stothers, it reaches a point where it evolves at a much slower pace. Consequently there exists a sequence at that point.

One other major problem exists in the interpretation of the evolution of white dwarfs - the existence of separate groups of white dwarfs with different atmospheric compositions. A suggestion has been put forward by Strittmatter and Wickramasinghe (1971, hereafter SW) to try to explain the existence of the DB stars. They note that the DB stars are concentrated in a region where

their atmospheres are convectively unstable. They also note that the existence of DB stars is impossible unless some mechanism can be found for eliminating accreted interstellar material. They then propose that a star cools as a DA until it reaches the region of the H-R diagram in which the DBs are convectively unstable, and then the establishment of a convection zone causes the presumably helium-rich interior to be mixed to the surface. At this point, the star becomes a DB, until the convection ceases. Then the star cools as a DA again.

The main observational consequence of the SW hypothesis is that there will be a deficiency of DA stars in the region $15{,}000^{\circ} \leq T_{eff} \leq 18{,}000^{\circ}$, in which they claim the atmospheres of the DBs are convective. There are several difficulties with this hypothesis, and the principal one is illustrated in Figure 6. I have calculated effective temperatures for all the stars for which $\theta_{eff} < 0.8$ in the EG lists (EG I, II, III, Greenstein 1969a,b, 1970) from the temperature scales of Figures 1 and 2. I have not plotted HZ 29, which may not be a white dwarf. The region for which SW predict no DA stars is indicated "SW DB". There is no evidence of a shortage of DA stars in this temperature region. Furthermore, of the stars analyzed in Chapter 4, for which the effective temperatures are highly reliable because they are determined from intermediate-band scans, there are 6 stars in this temperature range (out of a total sample of 18 DA stars). Another difficulty with the hypothesis of SW is that a subsurface convection zone

present in DB stars cooler than T_{eff}=15,000°K will be sufficient to remove accreted material.(see below).

However, it is possible to regard the SW hypothesis as viable if it is modified a bit. It can also be extended to explain a few other features, such as the DC stars and tentatively the λ4670 stars, which show C^2 bands. The revision of the SW theory that I propose is this:

(i) A star entering the white dwarf phase begins to accrete hydrogen and exists as a DA star, just as SW propose. However, it remains as a DA until $T_{eff} \approx$ 13,000°K, where the atmosphere of a DA star becomes convectively unstable due to the recombination of hydrogen. At this point, either the convective layer does not extend to the region of the star where heavy elements predominate, in which case the star continues to cool as a DA, or

(ii) the mixing process is sufficiently efficient that the interior is mixed with the surface layers. At this point, the stellar surface becomes hotter as the opacity of its outer layers is decreased, because the composition of the outer layers is changed from hydrogen to helium. Consequently the temperature gradient is lowered. At this point, the star becomes a DB. Convection occurs, and is sufficiently efficient so as to remove accreted material from the surface, so that the star continues to cool as a DB star. When it gets cool enough so that the helium lines disappear, (at $T_{eff} \approx$

11,000°K) it becomes a DC. Or alternatively, if the interior is made of carbon,

(iii) the atmosphere of the star becomes carbon-rich and the star becomes a λ4670 star. This last is quite speculative, because little work has been done on the λ4670 stars. It is significant that the bluest λ4670 star, which was analyzed in Chapter 4, has an effective temperature probably between 10,000 and 12,000°K.

There are two basic points about the above hypothesis which need to be checked quantitatively: (1) is the increase in effective temperature expected under (ii) sufficient to explain the observed effective temperatures of DB stars, and (2) when the DB cools and becomes (as I propose) a DC, is the convective mechanism still sufficiently effective to remove material from the surface.

As to (1), it is possible to estimate very crudely the rise in surface temperature from a stellar-interior type of calculation. Starting with the standard stellar-interior equation for radiative energy transport

$$\frac{dT}{dr} = -\frac{3}{4ac}\,\frac{\kappa\rho}{T^3}\,L_r \qquad (6\text{-}3)$$

one can integrate this equation inwards from the surface of the star, and let $L_r = 4\pi R^2 \sigma T_{eff}^4$ to find

$$\int_{inside}^{outside} dT = -\frac{3}{4ac}\left(\overline{\frac{\kappa}{T^3}}\right)\sigma T_{eff}^4 \int 4\pi R^2 \rho\, dr \qquad (6\text{-}4)$$

Now set the surface temperature equal to T_{eff} and the interior temperature be T_i, let $M_r = \int 4\pi R^2 \rho\, dr$ be the mass

of the surface layer, and let $\overline{T^3} = [(T_i - T_{eff})/2]^3$. Then, after some algebra

$$\left(\frac{T_i - T_{eff}}{T_{eff}}\right)^4 = \frac{3}{4ac}\bar{\kappa} M_r \qquad (6\text{-}5)$$

If the opacity is changed, and T_i is kept constant, T_{eff} will change. If $T_i \gg T_{eff}$, then

$$T_{eff} \approx T_i \left(\frac{4ac}{3\bar{\kappa} M_r}\right)^{1/4} \qquad (6\text{-}6)$$

Comparing typical values of the Rosseland mean opacity from the stellar atmospheres of Chapter 2, I find that $\bar{\kappa}(X=1) \approx 5\bar{\kappa}(Y=1)$ for typical temperatures and densities at $\tau=1$. If, then, during the course of the evolution from a DA star to a DB star, T_i remains constant, then T_{eff} will increase by a factor of $5^{1/4}$ because $\bar{\kappa}$ decreases by a factor of 5. If the change sets in at $T_{eff}=13{,}000^\circ$, which is where the DA stars become convective, then the temperature of the resulting DB star is $19{,}500^\circ$K, or $\theta_{eff}=0.26$. This temperature is almost exactly that of the hottest DB stars (with the exception of HZ 29), as can be seen from Figure 6.

The above treatment assumes that in most of the zone between T_i and the surface, radiative energy transport operates. This is the case for DA stars with $13{,}000 < T_{eff} < 19{,}000$; in a DB star convection is important in this temperature range. For intermediate chemical compositions, it is impossible in the absence of a

detailed calculation to tell which energy transport mechanism is relevant. At any rate, if convection applies, the temperature gradient would be less steep than in the radiative case that was considered above, and the rise in surface temperature would be greater.

I also attempted to estimate the magnitude of the surface temperature change by comparing the temperature and pressure at the top of the convective zone in a T_{eff}= 12,000°, log g=8 model with the temperature and pressure at a corresponding mass shell in various DB models. The same mass shell was at a much lower optical depth in the DB model, because of the increased density and decreased opacity. Because the models are so radically different, it was difficult to make any good comparisons; however, if the mass element at the top of the convective zone is followed along an adiabat in the T-P plane, it intersects the locus in the T-P plane of the corresponding mass shell in a DB model atmosphere with T_{eff}=21,000°. This temperature change is in reasonable agreement with the previous result. Clearly, in order to determine the magnitude of this temperature change, it would be necessary to construct a series of models for intermediate values of the helium abundance and try to make up an evolutionary sequence.

It is also important to investigate the time scale of the convective-mixing process. The time scale for

convection is very short, since the convective velocities are on the order of 10^7 cm/sec and the scale height is 10^3 cm. Thus the eddy time is 10^{-4} sec. If the convective mixing is treated as a random-walk process, then the time for mixing to take place over a length of 30 km (about 300 times the geometrical height from τ=1.0 to the surface) is 10 sec. Bohm and Cassinelli (1971) have indicated that 30 km is the maximum height of the convective zone in helium-rich atmospheres. Clearly, if the accreted interstellar matter can be transported to a convective zone that reaches to any appreciable depth, it will be mixed very rapidly with the material in the convective zone, and the whole convective zone will assume the composition of whatever lies beneath it.

The only problem now is that the convective zone never extends all the way to the stellar surface. Consequently, accreted matter may not reach the top of the convective zone fast enough to be sufficiently diluted. I propose that ordinary diffusion will suffice to mix the material of the top of the atmosphere with the top of the convective zone. As long as diffusion proceeds much faster than accretion, the accreted material will be removed from the atmosphere and will not appear in the stellar spectrum.

The time scale for ordinary diffusion is given by, for example, Reif (1965, p. 485):

$$t_D = L^2 n \sigma \sqrt{\frac{m}{kT}} \qquad (6\text{-}7)$$

where n is the particle density, σ the cross section, and L the length over which diffusion occurs. Adopting $\sigma \approx 10^{-15}$ cm^2 (since, in the cool DB stars that we are concerned with, most of the material is unionized),

$$t_D = \frac{3L^2\rho_{-6}}{T_4^{1/2}} \text{ sec} \qquad (6\text{-}8)$$

where $T_4 = T/10^4$ °K, $\rho_{-6} = \rho \times 10^6$ gm/cm^3, and L is expressed in km. For a 10,000°, log g=8, helium-rich model atmosphere, a typical density of 10^{-3} leads to a diffusion time of 10^4 sec from the top of the atmosphere to the top of the convective zone (a distance of 0.4 km). In a similar model with T_{eff}=6,000°, the corresponding time is 6 x 10^4 sec. In the hotter DB stars, diffusion times are considerably less than these because the top of the convective zone is very near the surface.

These times have to be compared to the rate at which a star accretes material. If mixing is to work, the mixing must proceed much faster than the accretion. The rate at which a star of mass M moving with velocity v (in km/sec) through a medium of particle density n accretes matter is given by (Bondi and Hoyle 1944):

$$\frac{dM}{dt} = 3 \times 10^{21} \frac{M^2 n}{v^3} \text{ gms/year.} \qquad (6\text{-}9)$$

Setting n=1, and v=10 (for the purpose of maximizing the accretion rate; in fact, velocities of DB and DC stars are generally higher than 10 km/sec and accretion is

correspondingly slower), and letting the radius of the star be 0.01 solar radii, a star will accrete a spherical layer with column density $\tilde{\rho}$ (in gm/cm^2) in

$$t_{acc} \approx 0.6\,\tilde{\rho} \text{ years.} \qquad (6\text{-}10)$$

Applying the column densities from the model atmospheres leads to times of 0.3 and 1 year for the 10,000° and 6,000° He-rich models to accrete the material that lies above the convective layer, respectively, for v=10 km/sec. The proportion of interstellar matter (primarily hydrogen) in the surface layer is about equal to $t_{dilution}/t_{acc}$, or about 2×10^{-3} in both cases.

The accretion rate given by Eq. (6-9) may well be too rapid. In such a case, the problems of diluting the accreted material sufficiently rapidly are lessened, and the whole convection-accretion hypothesis is still viable as long as the accretion proceeds fast enough so that a DA star can accrete an optically thick hydrogen layer in a time short compared to its lifetime as a white dwarf. Even if the accretion rate is 10^{-5} of that given by Eq. (6-10), the hypothesis is still viable, and the results of Appendix A indicate that the rate is at least that high.

One complication that I have neglected so far is the problem of gravitational settling. In its crudest form, the velocity with which a heavy particle will settle towards the bottom of a fluid is (Greenstein et. al. 1967):

$$v_S = \tfrac{1}{2}\, g\, t_{coll} \qquad (6\text{-}11)$$

If settling takes place faster than diffusion, then the hydrogen accreted from the interstellar medium will form a stable layer on the surface of the star. Using the collision time for unionized matter given by Reif (1965), the settling time is given by

$$t_S = \frac{L}{v_S} = \frac{2L}{g t_{coll}} = \frac{2Ln\sigma}{g}\left(\frac{2kT}{m}\right)^{1/2} . \qquad (6\text{-}12)$$

Putting in typical parameters for a DB star, I find that t_S=100 years. Thus it would seem that over lengths comparable to the distance between the stellar surface and the top of the convective zone ($\sim$0.4 km), gravitational settling is unimportant. Schatzman (1958, pp. 107 ff.) has made a much more elaborate calculation, and finds that over a few tenths of a kilometer, gravitational sorting of the elements is unimportant, even for $g=10^9$. For typical white dwarfs ($g=10^8$) the length scale of gravitational sorting is even greater, and thus Schatzman's result agrees with mine. Over larger distances, such as those considered important by Schatzman, gravitational settling would become much more important than diffusion, as the time-scale for diffusion varies as L^2, while the settling time varies as L.

Van Horn (1970) has shown that as long as there is any partially ionized or unionized matter on the surface of a star, there will be a sizeable convection zone that will, in some cases, extend to the degeneracy transition

layer. This conclusion has also been reached for helium-rich stars by Bohm and Cassinelli (1971). Hence there will be a convection zone that will be able to dilute the accreted matter for a DC star or a DB star.

Thus, in the present picture, the magnitude of the temperature change is in rough agreement with the observed temperature change that takes place when a DA star of T_{eff}= 13,000°K changes into a DB star. Furthermore, the time scales for convection and diffusion, which remove accreted matter from the surface of a DB star, are shorter than the time scales for gravitational settling and accretion, which would bring hydrogen to the surface. Thus convection and diffusion can keep the outer layers of a DB or DC star well-mixed, as is required under the present hypothesis.

VI. OBSERVATIONAL TESTS OF THE THEORY

There are two main aspects in which the observational evidence supports the theory. One is the temperature ranges in which various types of stars are observed. The DB stars fall in the appropriate range ($T_{eff} < 19,000°K$), and, as is pointed out by SW, this effect explains why the helium line strengths observed in DB stars are so much weaker than the maximum strength calculated from the models. There is a slight drop in the number of DA stars per unit θ-interval at $T_{eff} \approx 12,000°K$, which would be expected as DA stars became DB stars. It is difficult to

assess the reality of this decrease since it may well be a result of observational selection, in that many white dwarfs have been found by virtue of their blue color. However, it is at least consistent with the idea that many DA stars evolve into hotter DB stars when their surface layers become convectively unstable. The fact that the DC stars are all quite cool (with one exception, G 64-43, also known as EG 272) supports the present hypothesis; they would correspond to the DB stars which have coded off.

There are a number of features of white dwarf spectra which are unexplained by this model. In general, these features were not explained by the SW convection-accretion hypothesis either. First, one has to explain the absence of helium in the surface layers of DA stars. Simple theories of gravitational settling (e.g., Greenstein, Truran, and Cameron 1967) lead to a time scale for gravitational settling which is about the same order of magnitude as the time scale for accretion. It may be that the time scale quoted above for accretion is too fast, since I adopted a low space velocity for the white dwarfs, for the purposes of maximizing the accretion rate. A slower time scale, such as that suggested by the calculation in Appendix A, would make gravitational settling feasible. A more complex theory of gravitational settling is

needed here to determine whether gravitational settling will indeed remove helium from the DA atmospheres.

The second difficulty is the problem of explaining why some DA stars mix helium up from their interiors and why some do not. There are quite a few DA stars with T_{eff} $<10{,}000^{\circ}K$, and apparently they have not evolved into DB stars at the time they have become convective. It is possible that in these stars the surface layer of hydrogen, which has been accreted from the interstellar medium, is sufficiently thick so that the convection zone is confined to the hydrogen layer. It may be that these stars entered the white-dwarf stage with a surface layer of hydrogen. The existence of O subdwarfs with a variety of helium abundances supports this last idea; it may be that the O subdwarfs with a very small quantity of surface He have a fairly thick envelope of hydrogen, in which case when they become convective, the convective mixing process did not extend below the hydrogen layer. The helium-rich subdwarfs would then become DBs at the appropriate time.

Another difficulty with the theory, which is also a problem with the SW theory, is explaining the very low metal abundance of DB and DC stars. In the present picture, this observation would mean that the subsurface helium layer contains a very small amount of metals. The main problem is that if the subsurface layer has been processed through normal hydrogen-burning, one would expect

that the original metal abundance (expressed by metals/ total number of atoms)would remain. It would seem that any theory of the origin of the DB stars would have to cope with that difficulty. It is also possible that gravitational settling may operate here, although this process is not too efficient in DB stars because of their higher density.

I do not regard any one of the above three problems as insuperable. Most of them relate to questions which are unanswerable until more is known about the late stages of stellar evolution which immediately precede the white dwarf phase.

VII. CONCLUSION

Using the results of Chapter 4, I have determined radii for stars with known distances, and masses for stars whose m_1 indices have been measured by Graham. Comparison of the results with gravitational-redshift measurements and mass-radius relations reveal no bad conflicts. Modifying the convection-accretion theory of Strittmatter and Wickramasinghe (1971) has sucessfully explained the temperature distribution of the DB and DC stars, and possibly the λ4670 stars. What happens is that a DA star cools as a DA until its survace layers become convective, at which point it may convectively mix up helium from its subsurface layers and become a DB or possibly a λ4670 if its subsurface layers are composed of carbon. It will then cool towards the black

dwarf state, and if it is a DB it will become a DC when its effective temperature drops below 11,000°K.

TABLE 1 - LUMINOSITIES AND RADII

Star	Spec.	EG	M_V	θ_{eff}	log R/R⊙	log L/L⊙
First-Class Determinations						
LDS 678B#	DAwk	131	+12.2	.267	-2.14	-2.26
L 997-21	DAs	135	+13.5	.500	-2.20	-3.22
L 326-81	DAs	165	+13.4	.262	-2.36	-2.69
G 94-B5B	DAn	18	+12.5	.295	-2.17	-2.48
G 102-39	DC	44	+12.9	.63	-1.83	-3.10
G116-16	DAs	64	+11.7	.57	-1.64	-2.56
-37°6571	DAs	114	+12.2	.90	-1.85	-2.76
G 140-B1B	DC	124	+12.9	.66	-1.77	-3.08
G 165-B5B	DA	173	+12.0	.305	-2.06	-2.30
G 156-64	DA,F	178	+14.2	.93	-1.70	-3.54
LDS 157C	--	--	+12.2	.200	-2.23	-1.97
HZ 10	DA	30	+10.7	.440	-1.69	-2.21
VR 7	DA	36	+11.1	.250	-2.02	-2.80
VR 16	DA	37	+10.5	.200	-1.98	-1.42
LP 475-242	--	--	+11.9	.205	-2.16	-1.82
LB 390	--	59	+12.2	.300	-2.11	-2.36
LB 1847	--	60	+12.6	.375	-2.11	-2.76
LB 393	--	61	+12.1	.320	-2.07	-2.39
Second-Class Determinations						
LP 9-231*#	DAss	199	+12.9	.72	-1.66	-3.06
R 198	DA	143	+13.4	.335	-2.32	-2.97
+82°3818	DA	147	+13.7	.275	-2.01	-2.05
-51°13128B	--	---	+13.7	.290	-2.42	-2.94
G 130-49	--	1	+13.4	.375	-2.27	-3.08
G 71-B5B	--	14	+13.0	.308	-2.25	-2.70
G 86-B1B	DA	43	+12.8	.525	-1.94	-2.85
G 105-B2B	--	47	+13.3	.345	-2.28	-2.96
G 148-7	DAn	83	+11.1	.295	-1.89	-1.92
LDS 455B	DA	101	+12.0	.242	-2.13	-2.04
G 152-B4B	DAs	174	+11.2	.330	-1.88	-2.08
G 154-B5B	DA	175	+11.2	.82	-1.25	-2.39
G 148-7	DAs	185	+11.1	.305	-1.92	-2.08
Second-Class determinations from Riddle (1970)						
W 1516	DC	9	+12.7	.630	-1.80	-3.02
G 93-48	DA	150	+10.7	.265	-1.76	-1.47
G 29-38	DA	159	+12.4	.500	-1.88	-2.82
Third-Class	Spec.	EG	π(".001)	θ_{eff}	log R/R⊙	log L/L⊙
+25°6725#	DA	15	024	.240	-1.76	-1.30
h Per 1166	DA	17	025	.205	-1.91	-1.32
R 808	DA	115	022	.44	-1.72	-2.26

TABLE 1 - LUMINOSOTIES AND RADII (continued)

Third-Class Determinations

Star	Spec.	EG	π(".001)	θ_{eff}	log $R/R_\odot$	log $L/L_\odot$
C 2	DA	116	022	.355	-1.76	-1.99
R 137#	DA	125	017	.245	-1.63	-1.08

Notes

* LP 9-231: The colors are from Eggen (1969). The colors in EG III lead to θ_{eff}=.90, log $R/R_\odot$=-1.42, and log $L/L_\odot$=-2.90, but the more recent colors were adopted here.

LDS 678B,LP 9-231, +25°6725, R 137: In addition to the parallaxes quoted by Eggen, the work of Riddle (1970) was also used for distance determinations.

TABLE 2-MASSES

Star	m_1	log g	log $M/M_\odot$
G165-B5B	+.317	7.9±.4	-.56±.4
HZ 10	.358	8.0±.4	+.01±.4
VR 7	.275	7.6±.4	-.70±.4
VR 16	.245	7.7±.4	-.52±.4
+82°3818	.290	7.6±.4	-.76±.4
G 148-7	.347	7.9±.4	-.22±.4
G 152-B4B	.312	7.65±.4	-.46±.4
R 808	.312	7.65±.4	-.13±.5
C 2	.344	7.85±.4	-.02±.5

TABLE 3-REDSHIFTS

Star	EG	K(atmosphere)	K(GT)	$K_{at}-K_{gt}$
HZ 4	26	48(+40,-20)	+69±20	-21
LB 1240	28	20(+20,-10	+52	-32
HZ 10	30	48(+50,-25)	+43	+5
HZ 2	31	36(+12,-9)	+27	+9
HZ 7	39	25(+12,-9)	+79	-54
HZ 14	42	55(+90,-32)	+65	-10
W 1346	139	7(+3,-2)	+38	-31

FIGURE CAPTIONS

Figure 1 - Temperature scales for DA stars. The dots are from Chapter 4. The other temperature scales referred to are described in the text.

Figure 2 - Temperature scales for DB and DC stars. The points all refer to DB stars unless marked with another spectral type. The cross is HZ 29, which may not be a white dwarf. Only the filled circles were used to determine the temperature scale (solid line); below $\theta_{eff} = .40$, it is very uncertain. The black-body line is taken from Matthews and Sandage (1963).

Figure 3 - A Hertzsprung-Russell diagram. The circled and uncircled points correspond to the two error classes described in the text; the error bars indicate the maximum error for each group. The shaded lines represent the crystallization sequence of Van Horn (1968)-the top line is the sequence for S^{32} and the bottom for C^{12}.

Figure 4 - Calibration of the m_1-index. The errors in the abcissa are not indicated.

Figure 5 - Mass-radius relations. The three symbols represent various error classes; the error bars indicate the maximum uncertainty for each group. The dot with error bars is 40 Eri B; the square with error bars is Sirius B. The two large circles are from the gravitational redshifts of Greenstein and Trimble; the crossed circle represents a reduction of their mean redshift by 19 km/sec.

"HS" refers to the zero-temperature relation of Hamada and Salpeter (1961), "HW" refers to the thermal modification of Hubbard and Wagner (1970), the top HW curve includes hydrogen envelopes. "OBA","OBB", and"OBC" refer to Series A, B, and C, of the rotating white-dwarf models of Ostriker and Bodenheimer (1968).

Figure 6 - Histogram of effective temperature for various types of stars. The column on the extreme left represents all stars in the EG lists with $\theta_{eff} < 0.1$. "SW DB" marks the temperature region where SW predict a shortage of DA stars, and "DA convc." marks the onset of convection in DA stars. The dotted line refers to the DB and DC stars taken as a group; under this line the shaded areas represent DC stars. The interval used in counting the DB and DC stars was twice as large as the interval used in counting DA stars.

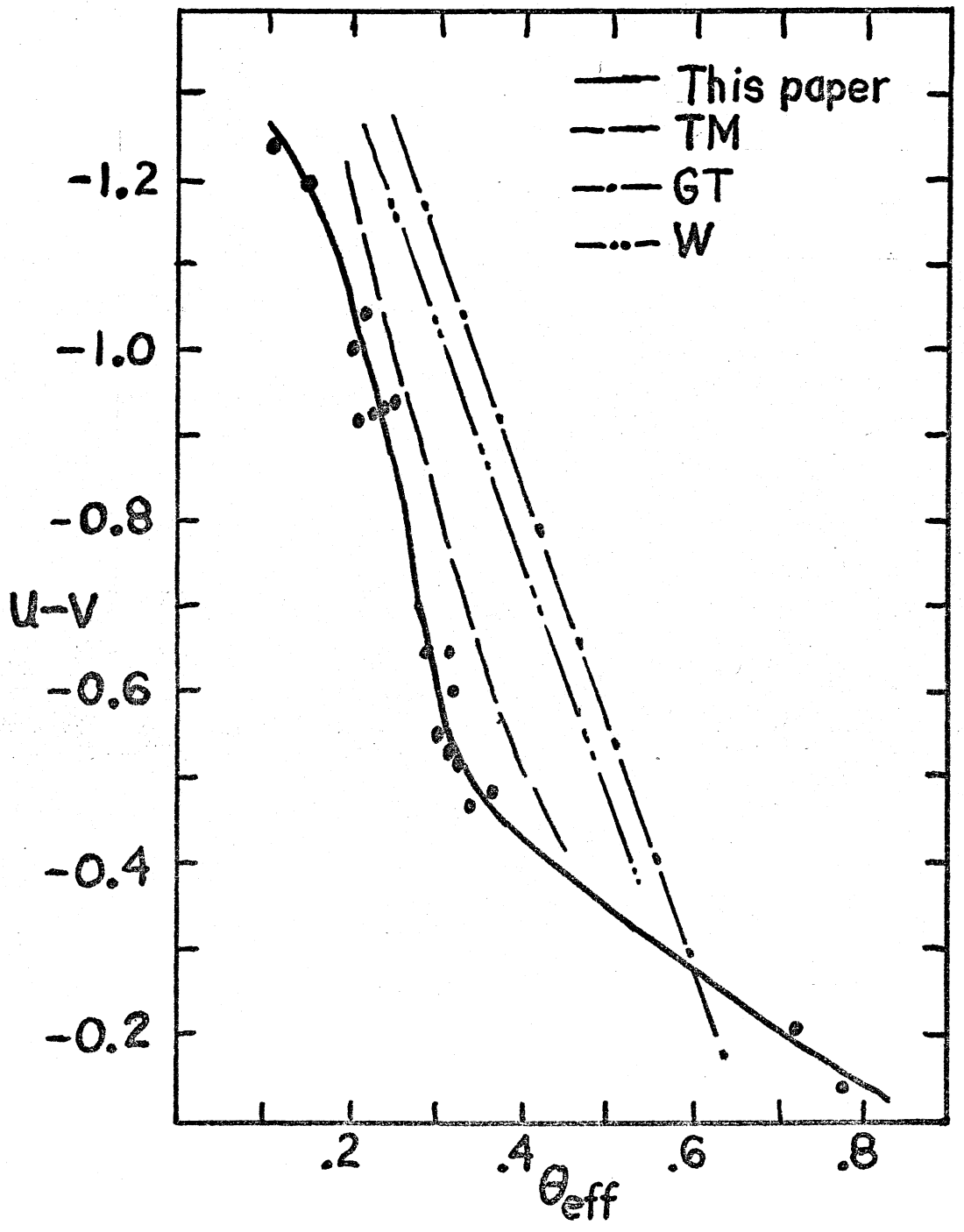

Figure 1.

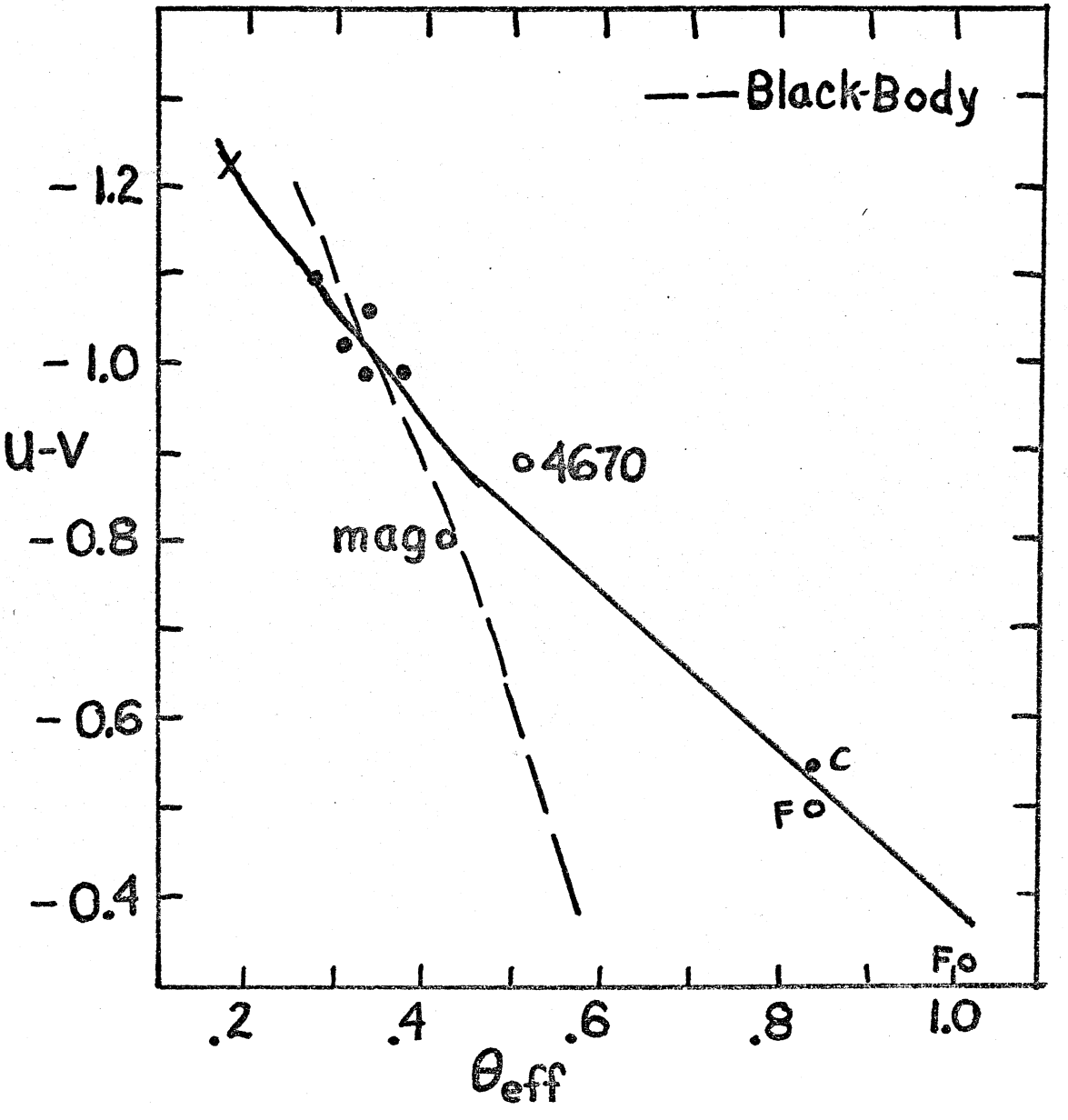

Figure 2.

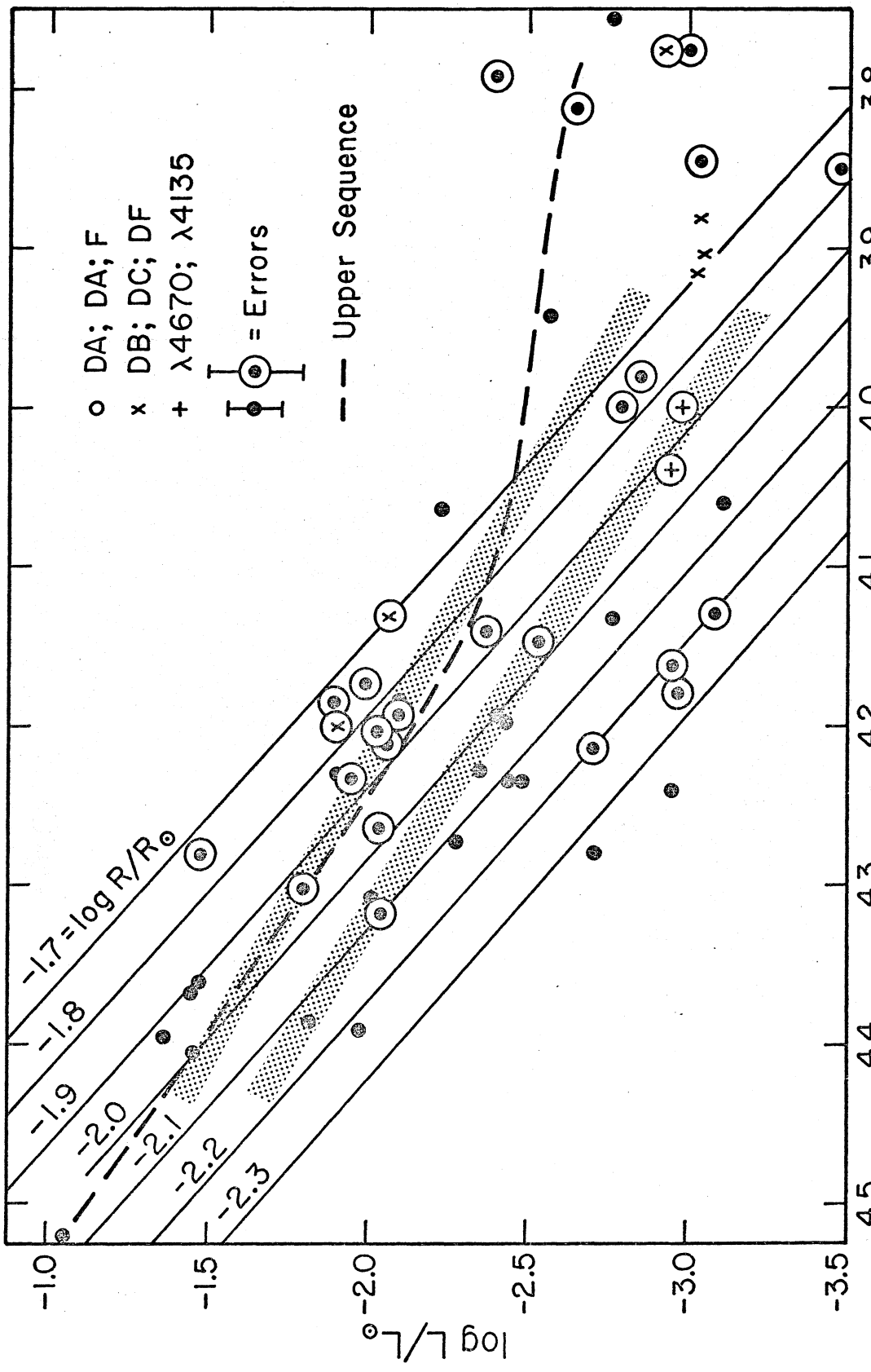
o DA; DA; F
x DB; DC; DF
+ λ4670; λ4135
= Errors
Upper Sequence
-1.7=log R/R⊙
-1.8
-1.9
-2.0
-2.1
-2.2
-2.3
log L/L⊙
log Teff
-1.0
-1.5
-2.0
-2.5
-3.0
-3.5
4.5
4.4
4.3
4.2
4.1
4.0
3.9
3.8

Figure 3.

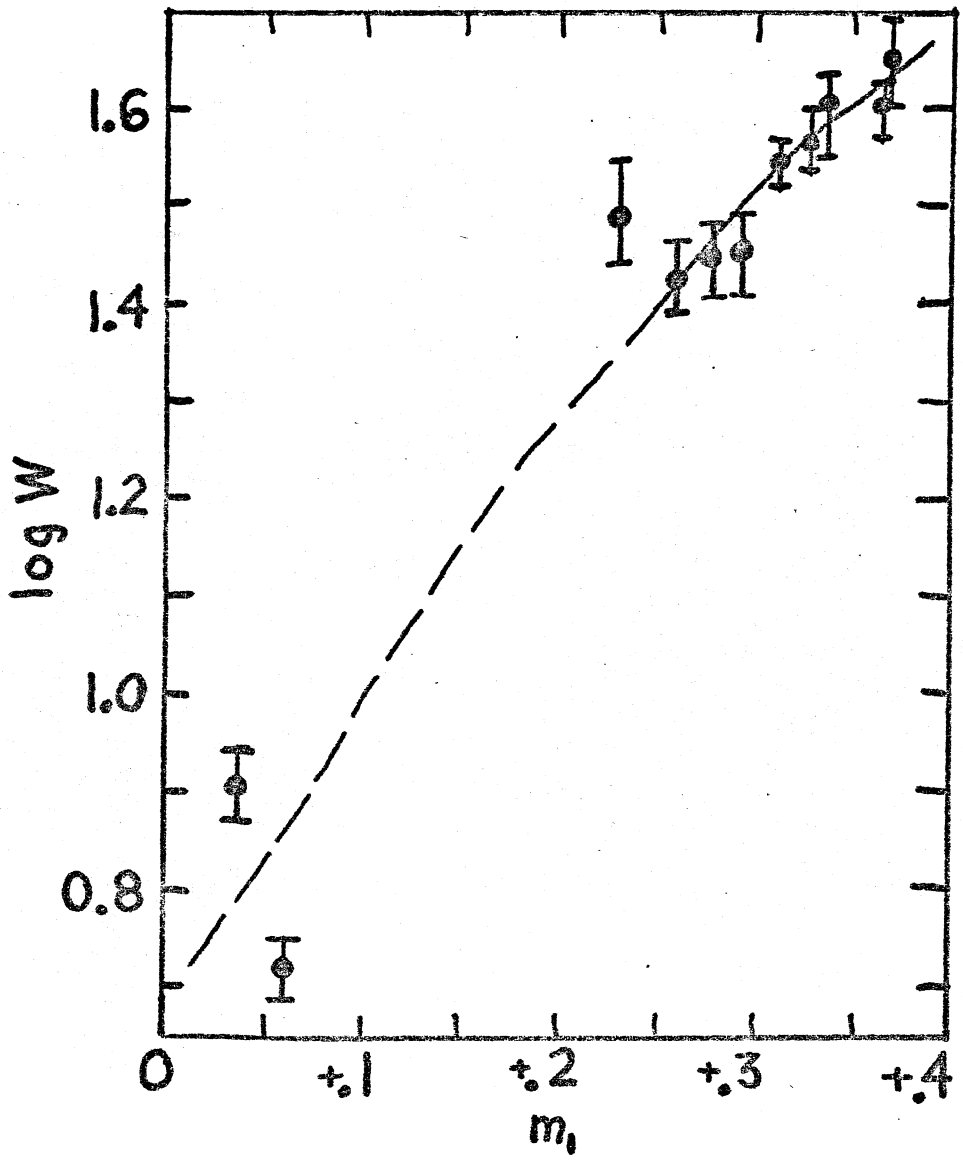

Figure 4.

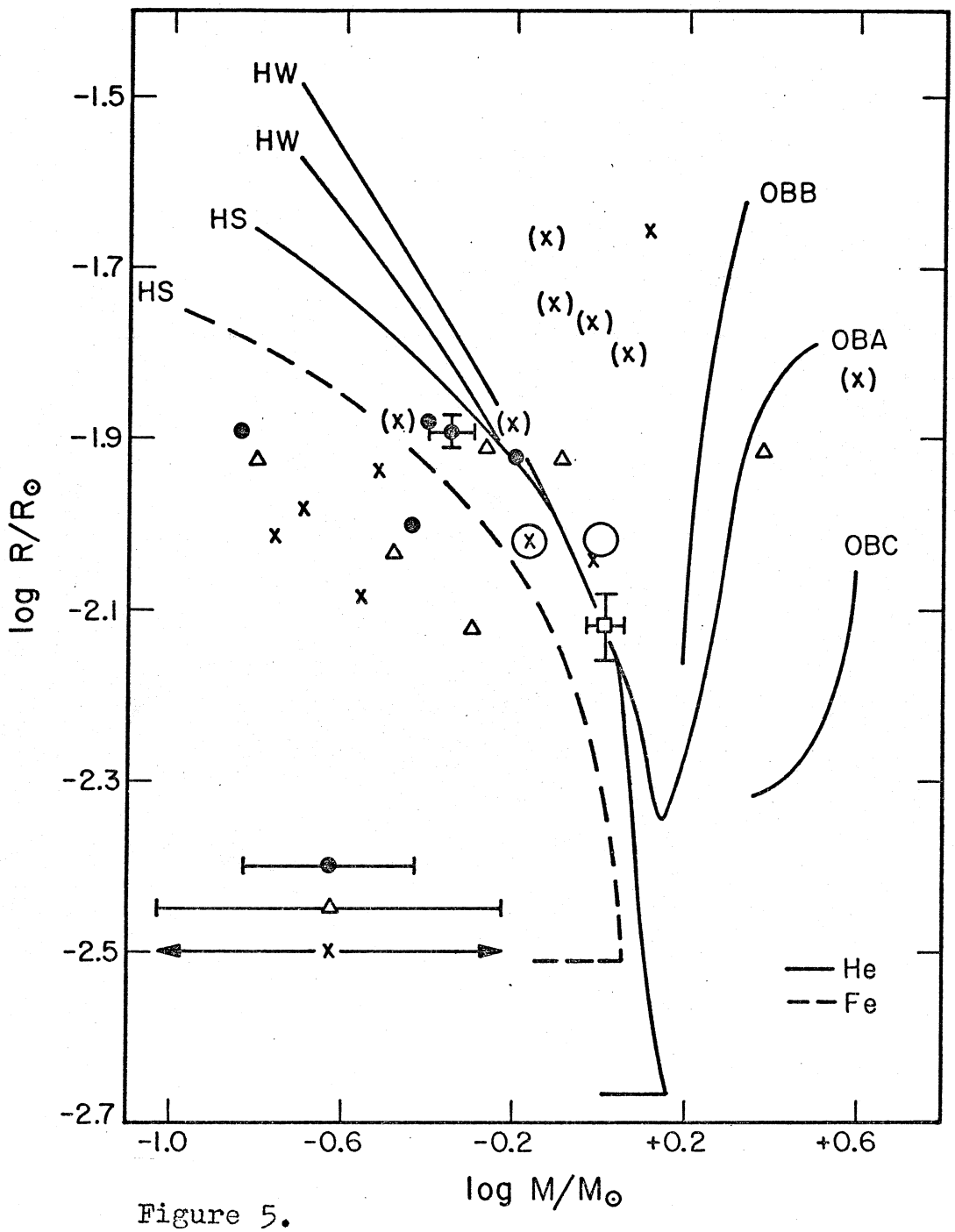
HW
HW
HS
HS
OBB
OBA
OBC
(x)
(x)
(x)
(x)
(x)
(x)
(x)
-1.5
-1.7
-1.9
-2.1
-2.3
-2.5
-2.7
log R/R⊙
-1.0
-0.6
-0.2
+0.2
+0.6
log M/M⊙
He
Fe

Figure 5.

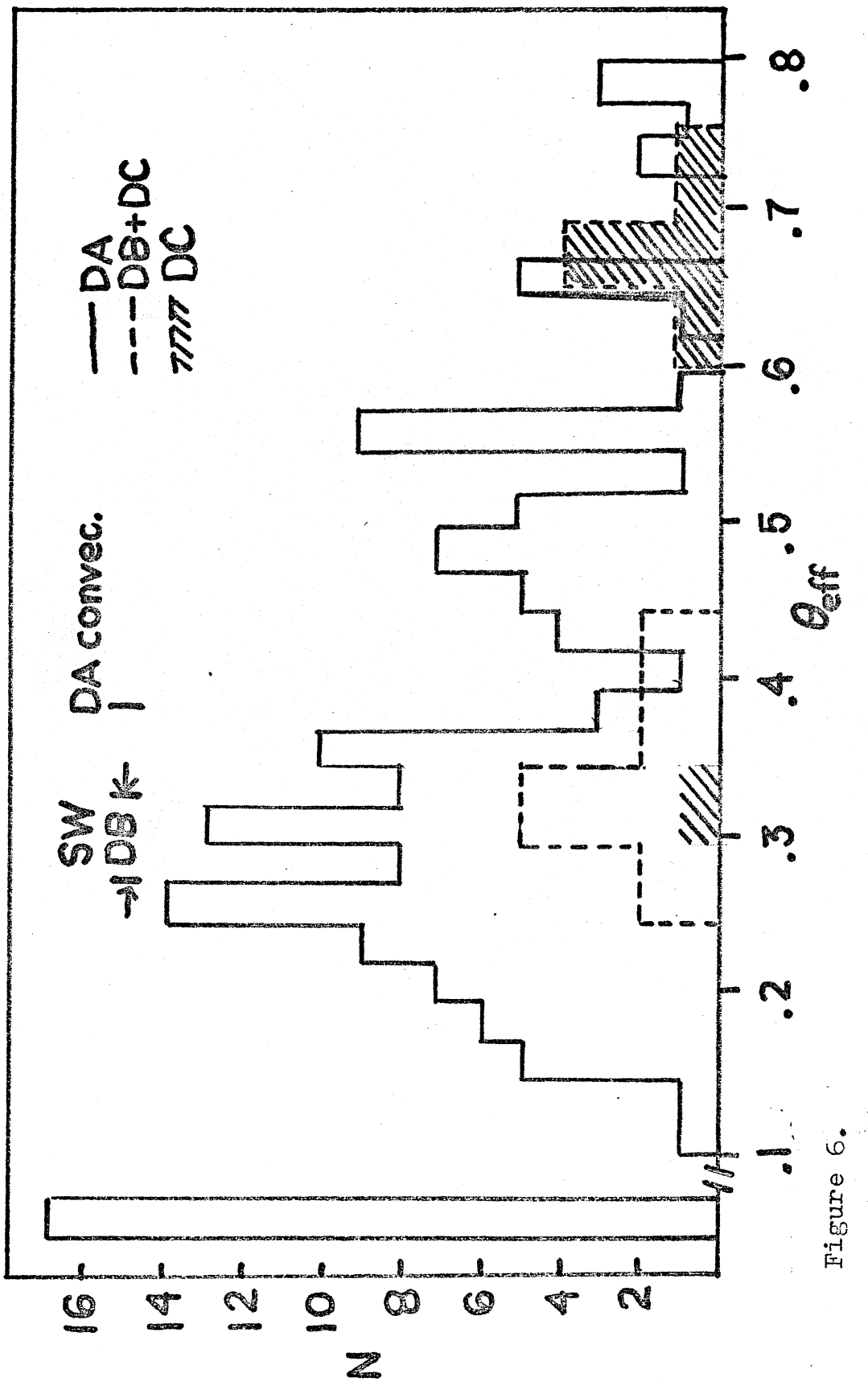

Figure 6.

CHAPTER 6

Appendix A - Another Accretion Formula

Here I will derive a pessimistic estimate of the rate at which a star of mass M and radius R accretes matter from the interstellar medium. I shall assume that the interstellar atoms are in Keplerian orbits around the star, and that only those atoms whose orbits intersect the stellar surface are accreted. Thus I shall treat the problem as a single-particle problem, instead of as a gas as Bondi and Hoyle did. The rate I derive is of a different functional form than that of Bondi and Hoyle, and is less than the Bondi-Hoyle rate by a factor of 3×10^5.

Consider an atom in interstellar space approached by a star. This atom will describe a Keplerian orbit around the star. Here I neglect collisions, which occur in interstellar space about once every 400 years for a single atom. Let x_0 be the distance of closest approach of atom and star, v_0 be the atom's velocity at the point of closest approach, b be the impact parameter, and v_S be the velocity of the star through the medium, which is the velocity of the atom with respect to the star. Then by Kepler's law of areas

$$v_S b = v_0 x_0 . \qquad (6A\text{-}1)$$

But conservation of energy gives

$$\frac{m v_S^2}{2} = \frac{m v_0^2}{2} - \frac{GMm}{x_0} \qquad (6\text{-}A2)$$

where m is the mass of the interstellar atom. Substituting (6-A2) in (6-A1), and after some algebra, one can find

$$b^2 = x_0^2 + \frac{2GM}{v_S^2} x_0. \qquad (6\text{-}A3)$$

Now assume that the star will accrete an atom only if the atom hits the stellar surface. This means that if I let $x_0=R$, then only those atoms with impact parameters less than the resulting value of b from (6-A3) will be accreted. Thus there is an accretion cross section

$$\sigma_{acc} = \pi b^2 = \pi \left[R^2 + \frac{2GM}{v_S^2} R \right] \qquad (6\text{-}A4)$$

and the star will accrete an amount of mass given by

$$\frac{dM}{dt} = \sigma_{acc} nmv_S \left[R^2 + \frac{2GM}{v_S^2} R \right]. \qquad (6\text{-}A5)$$

To estimate the rate at which a star will accrete a layer of column density $\tilde{\rho}$ in gms/cm^2, divide (6-A5) by $4\pi R^2$, and note that the second term in brackets dominates. Numerically, using $t_{acc} = \tilde{\rho} (d\tilde{\rho}/dt)^{-1}$,

$$t_{acc} = 2 \times 10^5 \frac{n\ M/M_\odot}{(v/10)(R/10^{-2}R_\odot)} \text{ years.} \qquad (6\text{-}A6)$$

This time is much longer than that given by Bondi and Hoyle (1944).

The time scale for a DA star with velocity v=100 km/sec to acquire an outer layer of $\tilde{\rho} = 2 \times 10^{-3}$ gm cm^{-2} is thus some 4000 years. This column density is approximately the column density above $\tau = 1$ in a $T_{eff}=25{,}000^\circ$, log

g=8 atmosphere. The lifetimes of white dwarfs are considerably longer than this value; consequently, accretion does make it possible for a core of non-hydrogen to accrete a surface layer of hydrogen and thus look like a DA. Of course, the star would have to accrete considerably more than the column density referred to above, for with only one atmosphere of hydrogen on top of the core, diffusion will take place. Although this analysis of accretion is very much oversimplified, the fact that the convection-accretion hypothesis is viable with an accretion rate 3×10^5 slower than that of Bondi and Hoyle is encouraging. Clearly, more work needs to be done in this area.

CHAPTER 7-POLARIZATION OF GRW +70°8247: THE TRANSFER PROBLEM

SUMMARY

The gray-body magneto-emission theory of Kemp (1970) is applied to white dwarf atmospheres appropriate for GRW +70°8247. The wavelength dependence of the circular polarization is explained for $3000 \leq \lambda \leq 9000$ Å with a derived magnetic field (projected along the line of sight) of 1×10^7 gauss if the star is helium-rich and 0.6×10^7 gauss if the star is hydrogen-rich.

The discovery of circular polarization of the peculiar white dwarf GRW +70°8247 by Kemp et.al. (1970) was prompted by Kemp's (1970a) proposal of a gray-body magneto-emission theory for optically thin objects. However, Kemp's prediction that the circular polarization increases linearly with wavelength clearly contradicts the observations. This paper shows that combining Kemp's weak-field theory with the solution to the radiative transfer problem leads to a wavelength dependence of the polarization quite different from the one Kemp proposes. The polarization predicted in this paper is in general agreement with observation except in the infrared, where the cyclotron frequency becomes comparable to the emitted frequency, and Kemp's first-order theory is not valid.

I shall first derive an analytic approximation to the polarization expected from an optically thick atmosphere and then present the results of detailed computed calculations for model atmospheres hopefully representative of GRW $+70^{\circ}8247$.

Kemp states that the bremsstrahlung from an ionized, optically thin gas will be circularly polarized with

$$q = \frac{j_{RH} - j_{LH}}{j_{RH} + j_{LH}} \approx \frac{8\Omega}{\omega} \qquad (7\text{-}1)$$

where j is the intensity and $\Omega = eB\cos\theta/mc$ with θ the angle between the magnetic field direction and the line of sight. Since, by Kirchhoff's law, $j_\nu = B_\nu$ (in LTE), one can represent the magneto-emission phenomenon by a difference in the absorption coefficients for the two senses of circular polarization (κ_{LH} and κ_{RH}):

$$\frac{\Delta\kappa}{2\kappa} = \frac{\kappa_{RH} - \kappa_{LH}}{\kappa_{RH} + \kappa_{LH}} \approx \frac{8\Omega}{\omega} \qquad (7\text{-}2)$$

Equations (7-1) and (7-2) are correct only to first order in Ω/ω.

In radiative transfer theory one can write the emergent flux from an optically thick body as

$$H_\nu = \int E_2(t) S_\nu(t)\, dt \qquad (7\text{-}3)$$

where $E_2(x) = \int e^{-xy}/y^2\, dy$ is the second exponential integral and S_ν is the source function. As a zero-order

approximation, one can greatly simplify the calculation of the emergent flux by replacing the exponential integral by the delta function $\delta(t-2/3)$. One thus assumes that all the emergent flux comes from optical depth 2/3 and $H_\nu = S_\nu(\tau = 2/3)$. If the optical depth scale is different in the two senses of circular polarization, $\tau_{RH} = \tau_{LH} + \Delta\tau$, then $H_{RH} = S_{RH}(\tau_{RH}=2/3)$ and $H_{LH} = S(\tau_{LH}=2/3)$ and $S(\tau_{RH}=2/3+\Delta\tau)$. Therefore

$$q = \frac{H_{LH} - H_{RH}}{H_{LH}+H_{RH}} \approx \frac{S(2/3+\Delta\tau)-S(2/3)}{2S(2/3)} = \frac{1}{2S_\nu}\left(\frac{dS_\nu}{d\tau_\nu}\Delta\tau_\nu\right)_{\tau_\nu = 2/3} \quad (7\text{-}4)$$

where $\Delta\tau_\nu = \Delta\int k_\rho\, dx = (\Delta k/k)\tau$ if $\Delta\tau/\tau \ll 1$.*

The magneto-emission phenomenon produces an observable polarization because the atmosphere is more transparent in one sense of circular polarization than in the other. Hence the emergent flux in the two senses of polarization effectively comes from different layers in the atmosphere, and thus the observed polarization is related to the derivative of the source function.

If I assume $S_\nu = B_\nu$, the Planck function (which is quite valid in white dwarf atmospheres, where scattering is unimportant), then with some algebra and equation (7-2) I obtain

$$q \approx \left(\frac{8\Omega}{\omega}\frac{h\nu}{kT^2}\frac{1}{(1-e^{-h\nu/kT})}\tau_\nu\frac{dT}{d\tau_\nu}\right)_{\tau_\nu = 2/3} \quad (7\text{-}5)$$

*Dr. Jesse Greenstein has informed me that this simplification of the transfer problem is not altogether new. (cf. Unsold 1955).

Using the Eddington-approximation temperature-optical depth relation

$$T^4 = T_0^4 \left(1 + \frac{3}{2}\tau_{std}\right) \tag{7-6}$$

where τ_{std} is a mean optical depth (such as the Rosseland depth), it follows that

$$q \approx \frac{h\Omega}{2\pi k}\left[\frac{\tau_\nu}{(1-e^{-h\nu/kT})}\cdot\frac{3}{8T}\cdot\frac{K_{std}}{\left(1+\frac{3}{2}\tau_\nu\frac{K_{std}}{K_\nu}\right)K_\nu}\right]_{\tau_\nu=2/3} \tag{7-7}$$

or, if $(1-e^{-h\nu/kT}) \ll 1$ (neglecting stimulated emission),

$$q \approx 2.16\times10^{-1}\,\frac{B_7\cos\theta}{T_4}\,\frac{K_{std}}{K_\nu+K_{std}} \tag{7-8}$$

if $B_7 = B/10^7$ gauss and $T_4 = T(\tau_\nu=2/3)/10^4\ ^\circ K$.

To evaluate the polarization more accurately and to test the validity of the above approximate result, I have used the model atmosphere program ATLAS, kindly supplied by R. Kurucz (1969b) to calculate expected polarizations from white dwarf models representative of GRW $+70^\circ 8247$. I estimate the effective temperature to be about $12{,}000^\circ$ from unpublished scans by J.B.Oke and have calculated polarizations for models with [$T_{eff}=12.000^\circ$, log g=8, (H=0.9, He=0.1)] and [$T_{eff}=14{,}000^\circ$, log g=8, (H=0,He=1)].* Both models are in LTE, in radiative equilibrium, and have solar metal content (relative to the total number of atoms).

*I have subsequently calculated polarizations for the other DB models; there is no substantial difference from the results presented here.

At each frequency the emergent flux was determined twice, once with the unperturbed, zero-magnetic field opacity and once with the opacity increased by a factor $(1+8\,\Omega/\omega)$ to account for the change produced by the magnetic field according to equation (7-2). The emergent flux was calculated using equation (7-3). The difference between the two emergent fluxes determined the net polarization.

These detailed calculations confirm the semi-intuitive expectations of equation (7-8). The results are shown in figure 1, where I plot both the opacities and the expected polarization. The opacity in the hydrogen-rich model is almost all bound-free, and free-free H I, and in the helium model is almost all free-free He^-. It is interesting that both models predict approximately the same wavelength dependence as the observations. I do not expect that changing the assumptions used in constructing the models (by, for instance, changing the metal abundance, including convection, or changing the effective temperature a little) will radically affect the wavelength dependence of the polarization, which arises solely from the wavelength dependence of the opacity (cf. equation (7-8). The opacity is only slowly dependent on temperature. The magnetic fields were determined by fitting models to observations at λ=5000 Å. I find that for the hydrogen-rich model $B \cos\theta = 0.6 \times 10^7$ gauss and

and in the helium-rich model, B cos θ=1 x 10^7 gauss. If $\theta \neq 0$, it can be shown that the magneto-emission phenomenon produces a combination of linear and circular polarization, with the linear polarization having the same wavelength dependence as the circular polarization (Kemp 1970b). This result is in general agreement with the observations (Angel and Landstreet 1970).

There are two discrepancies between these models and the observations - in the ultraviolet, the observed drop in polarization is a little greater than that predicted theoretically, and in the infrared the great increase in polarization observed by Kemp and Swedlund (1970) is not predicted. The small discrepancy in the ultraviolet may be due to observational problems, a different temperature gradient in the atmosphere from that in the models because of convection, or in the inapplicability of the magneto-emission theory to bound-free transitions.

One can guess about the behavior of the circular polarization of bound-free emission by comparing the bremsstrahlung results with the harmonic oscillator model of Kemp. He predicts that the circular polarization of radiation from a group of harmonic oscillators will be $q \approx \omega/\omega_0$ less than that from bremsstrahlung by a factor of 8. The drop in polarization for $\lambda \leq 3600$ Å in both models is due to the abrupt increase in absorption caused by the Balmer continuum in hydrogen, and the continua from the 2^3p and 2^1p levels in helium. Consequently,

a sizeable fraction of the radiation shortward of these edges is bound-free emission, whereas virtually all of the radiation longward of these edges is free-free. In the above calculations all of the radiation was assumed to be polarized according to equation (7-1) - the bremsstrahlung model. If bound-free emission is described by the harmonic oscillator model rather than the bremsstrahlung model, the circular polarization for $\lambda \leq 3600$ Å will be considerably lower than that predicted above, while the polarization for $\lambda \geq 3600$ Å will be unaffected. This reduction in polarization in the ultraviolet is about 20% for the helium-rich model and 70% for the hydrogen-rich model. These considerations may very well explain the ultraviolet problem without affecting the sucessful explanation of the polarization in the visual region of the spectrum.

The results of this paper do not account for the steep increase in polarization in the infrared. However, Kemp's assumption that $\Omega/\omega \ll 1$ clearly breaks down for $\lambda \sim 1$ μm, and the present calculations are invalid. Even though q probably increases with wavelength in the infrared, if the increase is no steeper than linear it is cancelled by the $1/\lambda$ decrease in dB/dT (equation 7-5). Hence some other mechanism for the abrupt increase in polarization must be sought, and better observations in the infrared would be helpful. There is no known opacity source with a sufficient increase in opacity at the

correct wavelength (with no B field), and so it is probable that the existence of such a large magnetic field is responsible for a radical change in the absorption properties of matter at $\lambda \sim 1$ μm, as noted by Kemp (1970b). More detailed quantum-mechanical calculations are needed here. It is unlikely that plasma effects are important as the electron density at $\tau = 1$ is 1.4×10^{7} cm^{-3} and the plasma frequency is 1/100 of the frequency of the emitted radiation.

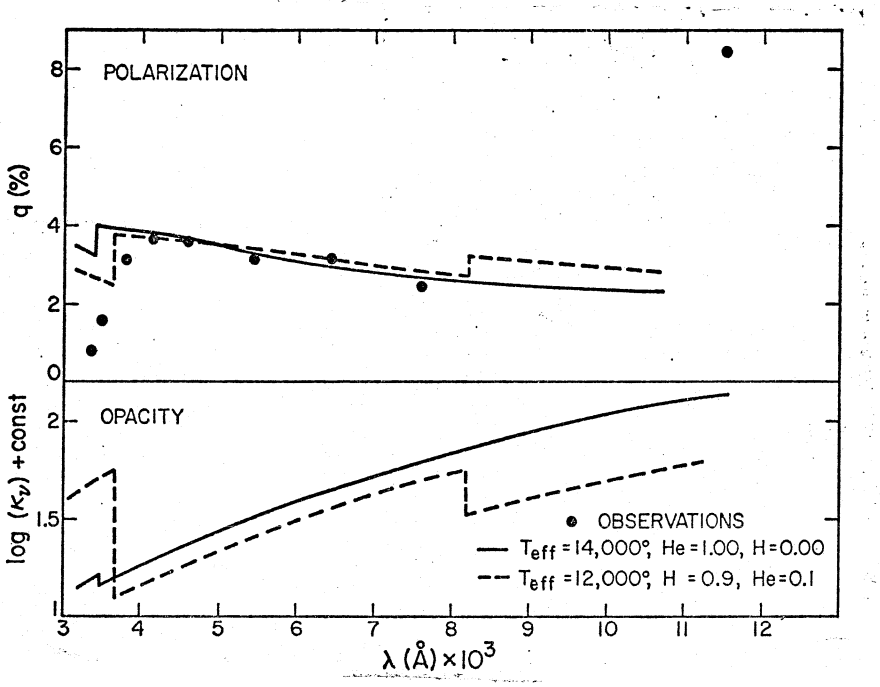

Figure 1.- Wavelength dependence of the opacities, and predicted and observed polarizations (the observations are from Angel and Landstreet 1970, Kemp and Swedlund 1970). The bottom curves are the opacities (at $\tau_{5000}=1$) and the top curves are the circular polarizations.

BIBLIOGRAPHY

Allen, C.W. 1963. Astrophysical Quantities, 2nd ed. London: Athlone Press.

Angel, J.R.P., and Landstreet, J.D. 1970. Ap. J. (Letters), 162,L61.

_____ 1971. (preprint).

Barnard, A.J., Cooper, J., and Shamey, L.J. 1969. Astron. and Astrophys. 1,28

Bohm, K.-H., and Cassinelli, J. 1971 (preprint).

_____, and Stuckl, E. Zs. f. Ap. 66,487.

Bondi, H., and Hoyle, F. 1944. Monthly Not. R.A.S.104,273.

Bues, I. 1969. Thesis, Christian Albrechts Universitat, Kiel, Germany.

Bues, I. 1970. Astron, and Astrophys. 7,91.

Carbon, D., Gingerich, O., and Kurucz, R. 1969. Theory and Observation of Normal Stellar Atmsopheres, ed. O. Gingerich (Cambridge: M.I.T.Press), p. 382.

Chandresekhar, S. 1939. An Introduction to Stellar Structure.(Chicago: University Press).

Chin, C.-W., and Stothers, R. 1971. Ap. J. 163,555.

Demarque, P., and Mengel, J. 1971. Ap, J. 164,469.

Edmonds, F.N. jr., Schluter, H., and Wells, D.C. III. 1967. Memoirs of the R.A.S. 71,271.

Eggen, O.J. 1969. Ap. J. 157,287.

_____, and Greenstein, J.L. 1965a. Ap. J. 141,83 (EG I).

_____ 1965b. Ap. J. 142,925 (EG II).

_____ 1967. Ap. J. 150,927(EG III).

Fowler, R.H. 1926. Monthly Not. R.A.S. 87,114.

Gieske, H.A., and Griem, H.R. 1969. Ap. J. 157,963.

Gingerich, O., Latham, D.W., Linsky, J.L., and Kumar, S.S. 1966. in M. Hack (ed). Colloquium on Late-Type Stars, (Trieste: Observatorio Astronomico di Triests), p. 291.

Gliese, W. 1969. Catalogue of Nearby Stars, Heidelberg Publications No. 22.

Goldberg, L., Muller, E.A., Aller, L.H. 1960. Ap. J. Suppl. 5,1.

Graham, J.A. 1969. Proceedings of the Symposium on Low-Luminosity Stars, (New York: Gordon and Breach), p. 139.

Greenstein, J.L. 1958. Encyclopedia of Physics 50,161.

_____ 1960. Stars and Stellar Systems, vol. VI, (Chicago: University Press), p. 676.

_____ 1969a. Ap. J. 158,281.

_____ 1969b. Comments on Astrophys. and Space Phys. 1,62.

_____ 1970. Ap. J. 162,L55.

_____ and Trimble, V.L. 1967. Ap. J. 149,283.

Greenstein, G.S., Truran, J.W. and Cameron, A.G.W. 1967. Nature 213, 871.

Griem, H.R. 1964. Plasma Spectroscopy, (New York: McGraw-

Hill).

Griem, H.R, 1968. Ap. J. 154,1111.

Hamada, T., and Salpeter, E.E. 1961. Ap. J. 134,683.

Harmon, R.J., and Seaton, M.J. 1964. Ap. J. 140,824.

Harris, D.L., III. 1956. Ap. J. 124,665.

Hubbard, W.B., and Wagner, R.L. 1970. Ap. J. 159,93.

Jenkins, L. F. 1963. General Catalogue of Trigonometric Stellar Parallaxes, (New Haven: Yale University Observatory).

Jones, E.M. 1970. Ap. J. 159,101.

Kemp, J.C. 1970a. Ap. J. 162,169.

1970b. Ap. J. (Letters) 162,L69.

Kemp, J.C., and Swedlund, J.B.1970. Ap. J.(Letters)162,L67.

Kemp, J.C., Swedlund, J.B., Landstreet, J.D., and Angel, J.R.P. 1970. Ap. J. (Letters) 161,L77.

Kolesov, A.K. 1964. Astron. Zhur. 41,485 (translated in Soviet Astronomy-AJ 8,387).

Kurucz, R.L. 1969a. Ap. J. 156,235.

Kurucz, R.L. 1969b. Theory and Observation of Normal Stellar Atmospheres, ed. O. Gingerich (Cambridge, M.I.T. Press), p. 375.

Lasker, B. M., and Hesser, J. E. 1971. Ap. J. (Letters) 163,L89.

Lindenblad, I.W. 1970. A.J. 75,841.

Matsushima, S., and Terashita, Y. 1969a. Ap. J. 156,183.

Matsushima, S., and Terashita, Y. 1969b. Ap. J. 156,219.

Matthews, T.A., and Sandage, A.R. 1963. Ap. J. 138,30.

Mestel, L. 1965. Stars and Stellar Systems, vol. VIII, L.H. Aller and D.B. McLaughlin, eds. (Chicago: University Press), p. 297.

Mestel, L., and Ruderman,M. 1967. Monthly Not. R.A.S.136,27.

Minkowski, R. L. 1937. Ann. Rept. Mt. Wilson Obs., p. 28.

Newell, E. B. III. 1970. Ap. J. 159,443.

_____, Rodgers, A.W., and Searle, L. 1969a. Ap. J. 156,597.

_____ 1969b. Ap. J. 158,699.

Oke, J.B. 1963. Paper presented at the Cleveland meeting of the A.A.S.

Oke, J.B. 1969. Publ. A.S.P. 81,11

_____, and Schild, R.E. 1970. Ap. J. 151,1015.

Ostriker, J.P., and Bodenheimer, P. 1968. Ap. J. 151, 1089.

_____, and Tassoul, J.-L. 1970. Ap. J. 155,987.

Parenago, P.P. 1946. Astr. Zhur. 23,31.

Peterson, A.V. 1969. Thesis, California Institute of Technology.

Peterson, D.M., and Scholz, M. 1971. Ap. J. 163,51.

Popper, D.M. 1954. Ap. J. 120,316.

Preston, G.W. 1970. Ap. J. (Letters) 160,L43.

Reif, F. 1965. Fundamentals of Statistical and Thermal Physics, (New York: McGraw-Hill).

Riddle, R.K. 1970. Publications of the United States Naval Observatory, vol. 20.

Schatzman, E. 1958. White Dwarfs. (Amsterdam: North-Holland),

Schild, R. Peterson, D.M., and Oke, J.B. 1971. Ap. J. (to be published).

Schwarzschild, M. 1958. Structure and Evolution of the Stars, (Princeton: Princeton University Press).

Searle, L. and Rodgers, A.W. 1969. Ap. J. 143,809.

Strittmatter, P.A., and Wickramasinghe, N. 1971 (preprint).

Strom, S.E., and Strom, K.M., 1970. Ap. J. 162,523.

Tassoul, J.-L., and Ostriker, J.P. 1968. Ap. J. 154,613.

Terashita, Y., and Matsushima, S. 1966. Ap. J. Suppl. 13, 471.

_____ 1969. Ap. J. 156,203.

Unsold, A. 1955. Physik der Sternatmospharen, (New York: Springer-Verlag).

van Altena, W.F. 1969. A.J. 74,2.

_____ 1971. Ap. J. (Letters) (submitted).

van den Bos, W.H. 1960. J. des Observateurs 43,145.

van Horn, H.M. 1968. Ap. J. 151,227.

van Horn, H.M. 1970. Ap. J. 160,L53.

Vila, S.C. 1971. Ap. J. 163,143.

Wagman, N.E. A.J. 72,957. (1970).

Wayman, P.A. 1967. Publ. A.S.P. 79,156.

Wayman, P.A., Symms, L.S.T., and Blackwell, K.C. 1965.

Roy. Obs. Bull No. 98.

Weidemann, V. 1963. Zs. f. Ap. 57,87.

Weidemann, V. 1968. Ann. Rev. Astron. Astrophys. 6,351.

Wickramasinghe, N., and Strittmatter, P.A. 1971. Monthly Not. R.A.S. 151, (to be published).

Wiese, W.L., and Kelleher, E. 1971. Ap. J. (Letters), to be published.

Wright, K.O., Lee, E.K., Jacobson, T.L., and Greenstein, J.L. 1964. Publications of the Dominion Astrophysical Observatory, 12,173.